Leveraging Rehabilitation and Implantable Strain Sensors to Improve Bone Healing After Traumatic Femur Fractures

by

Kylie Elizabeth Williams

A dissertation accepted and approved in partial fulfillment of the

requirements for the degree of

Doctor of Philosophy

In Bioengineering

Dissertation Committee:

Nick J Willett, Chair

Robert E Guldberg, Advisor

Keat Ghee Ong, Core Member

Mike Hahn, Institutional Representative

Morgan Giers, Core Member

University of Oregon
&
Oregon State University

Fall 2024

DISSERTATION ABSTRACT

Kylie Elizabeth Williams

Doctor of Philosophy in Bioengineering

Title: Leveraging Rehabilitation and Implantable Strain Sensors to Improve Bone Healing After Traumatic Femur Fractures

The primary objective of this thesis was to quantify patient-specific loading and rehabilitation parameters to elucidate how specific rehabilitation conditions impact bone healing after traumatic bone injuries. Our overall hypothesis was that parameters of mechanical loading and exercise will impact bone healing. To test this hypothesis, we utilized three rehabilitation platforms that enabled investigation of distinct rehabilitation parameters. These platforms including (1) a rodent running wheel with engineered resistance brakes or on/off brakes to enable running of different intensities or durations, respectively, (2) a treadwheel with an adapted on/off brake as a scalable platform, and (3) altered treadmill with speeds conducive to rodent needs. These platforms allowed for the investigate of distinct rehabilitation platforms and their relationship to bone healing. We also used implantable wireless strain sensors that enabled real-time non-invasive monitoring of mechanical cues as a function of time, rehabilitation conditions, and healing status. In collaboration with University of Utah, we used these sensors and *in vivo* microCT scans to develop subject-specific finite element models to quantify niche mechanical cues during different rehabilitation conditions. We discovered that higher intensity rehabilitation, relative to rehabilitation of lower intensity, increased early-stage strain magnitudes and significantly improved bone healing, with explant femurs matching intact strength. Beyond loading magnitude, we also discovered the importance of both long term and short term on bone healing. Nonlinear multivariate analyses revealed that rehabilitation must balance activity and

rest to improve bone healing, where rehabilitation with longer running distance and shorter daily rest periods resulted in 100% union after 3 mm bone injuries. These results further found that the necessary balance of rehabilitation and rest depends on subject-specific factors such as injury size since the same rehabilitation conditions resulted in only 20% union after a 2 mm bone injury but 100% nonunion after a 3 mm bone injury. Using previous studies to inform a rehabilitation regimen predicted to improve bone healing, we also found the importance of short-term rest between exercise loading bouts. Rehabilitation that involved steady-state running for 12 minutes significantly hindered bridging and bone formation compared to rehabilitation that involved intermittent rest periods between one minute running bouts. Systemic myeloid-derived cell types, previously predicted to impair bone healing, were also downregulated for rehabilitation with short-term rest periods. These results highlight rehabilitation with data-informed levels of intensity, activity, and both short and long term rest as a therapeutic to modulate early mechanical loading and the immune response to enhance bone repair.

This work facilitated a deeper understanding of how specific rehabilitation parameters regulate mechanical cues and bone repair and validated an implantable sensor platform to further investigate mechanobiology. This thesis aids in the development of subject-specific rehabilitation with the novel insight into the importance of rest on bone healing. Our results challenge the fields focus on optimizing the loading magnitude to improve bone repair. In addition, this thesis provides foundational support for the commercialization of implantable sensor technologies to track implant mechanics as a noninvasive feedback of healing status and to inform personalized clinical decisions.

This dissertation includes content from several published articles including Nash* *et al.* (2022) Connective Tissue Research; Nash* *et al.* (2022) Physiology in Health and Disease,

Springer; Williams and Harrer *et al.* (2024) NPJ Regenerative Medicine; and Williams *et al.* (submitted 2024) Science Advances.

*Publication under maiden name: Kylie Nash

CURRICULUM VITAE

NAME OF AUTHOR: Kylie Elizabeth Williams

GRADUATE AND UNDERGRADUATE SCHOOLS ATTENDED:

University of Oregon, Eugene OR
Whitman College, Walla Walla WA

DEGREES AWARDED:

Doctor of Philosophy, Bioengineering, 2024, University of Oregon
Bachelor of Arts, Biochemistry, Biophysics, and Molecular Biology, 2020, Whitman College

AREAS OF SPECIAL INTEREST:

Innovation and Entrepreneurship
Medical Devices

PROFESSIONAL EXPERIENCE:

SBIR Subaward Consultant, Lazarus 3D, performed tensile testing and analyses for biological and synthetic soft tissues for a women's health project

Entrepreneurship Leadership Team, Lunquist Center for Entrepreneurship, advisor to help other technical founders at the University of Oregon and to improve collaborations between Lunquist School of Business and the Knight Campus

GRANTS, AWARDS, AND HONORS:

Chris Lee Fellowship, Knight Campus, 2024

Cameron Fellowship, Lunquist Center for Entrepreneurship, 2024

Knight Campus Innovation Topping Fellowship, Knight Campus, 2024

Women's Leadership Forum Student Scholarship, Orthopedic Research Society, 2023

First Place for Oral Presentation, Wu Tsai Human Performance Alliance Oregon, 2023

Translational Impact Honorable Mention for Oral Presentations, Wu Tsai Human Performance Alliance All-Hands, 2023

Women Innovation Network Fellowship, University of Oregon, 2022

NIH R31 Travel Award, National Institute of Health, 2022

PUBLICATIONS:

Williams K.E. et al. (2024). Patient-Specific Multivariate Modeling for Regenerative Rehabilitation. Science Advances. *Submitted.*

Williams K.E. and Harrer J.A. et al., (2023). Early Resistance Rehabilitation Improves Functional Regeneration Following Segmental Bone Defect Injury. Nature Portfolio Journal Regenerative Medicine. *Accepted 2024.*

Vantucci and Guyer…**Nash, K.E.***, et al., (2022). Systemic Immune Modulation Alter Local Bone Regeneration in a Delayed Treatment Composite Model of Non-Union Extremity Trauma. Frontiers in Surgery. https://doi.org/10.3389/fsurg.2022.934773.

Nash K.E.*, Ong KG, Guldberg R.E. (2022). Implantable biosensors for musculoskeletal health. Connect Tissue Res. https://doi.org/10.1080/03008207.2022.2041002.

Nash, K.E.* et al. (2022). Regenerative Rehabilitation Strategies for Complex Bone Injuries. In: Greising, S.M., Call, J.A. (eds) Regenerative Rehabilitation. Physiology in Health and Disease. Springer, Cham. https://doi.org/10.1007/978-3-030-95884-8_8.

**Publication under maiden name: Kylie Nash*

ACKNOWLEDGMENTS

I am blessed with the opportunity to acknowledge so many supportive and talented people that were integral to my thesis work. Thank you all for the many laughs and lessons throughout the years.

First, I want to express my sincere gratitude to my advisor, Guldberg. You were the reason I took a risk and joined the Knight Campus amongst the first cohort of students. Learning from you has been the greatest takeaways from my time. Thank you for your unwavering mentorship, leadership, comradery, and your willingness to answer my "quick" questions even during networking events. Every time I left your office, I felt understood, encouraged, and renewed with fresh insight. I truly felt like I learned something new every time we spoke ranging from scientific insight, mentorship guidance, or life lessons. Your mentorship ignited my passion for mentoring others. I can only hope I'm half the mentor as you. When conflicts arise, I find myself asking "what would Guldberg do." Although you never got the Knight Campus to chill on the AC, your front row parking spot was quite nice. I always joked that I'd work for you for the rest of my life, just know that's only a partial joke… I'll see you at Penderia.

I also thank each of my committee members for their expert guidance and encouragement along the way. Ghee Ong, thank you for supporting my energy and enthusiasm to always take the sensors one step further. Your optimism wore off on me. I also must thank several members of the Ong lab. Thank you, Walker Rosenthal, Lucas Bambaren, and Salil Karipott for the support with sensor fabrication and troubleshooting. I also thank Nick Willett, Mike Hahn, and Morgan Giers for their constructive engagement and encouragement every step of the way. You have all been integral to the quality of this work and for my personal growth as an independent researcher.

I also must thank all the members from the Guldberg lab. Thank you for putting up with my numerous 7am surgery days. All my studies would not be possible without you all. In particular, I would like to thank Kelly Leguineche for her guidance and training when I first joined the lab. Your time and insight throughout the COVID-interrupted onboarding process truly shaped my thesis. Thank you for all the brainstorming sessions and for talking through all the research challenges. Your guidance helped many problems and saved my sanity prior to bringing bad news to Guldberg. I also want to thank Kait Link for your expertise and guidance. All our animal studies were possible because of your help changing the surgical approach and animal welfare practices. The ladies and I thank you wholeheartedly. I also must thank all my undergraduate students over the years: Alyssa Vongphachanh, Theo Seah, Walker Rosenthal, and Auveen Hajarizadeh. Thank you for all your hard work, enthusiasm, questions, and patience as we navigated many changes to our animal model. Special thanks to Auveen for his independent work that was crucial to my third research aim. I also must thank all my fellow graduate students for navigating this new graduate program with me.

I would also like to thank everyone at the Lundquist Entrepreneurship Center who helped uncover my passion for translating scientific discoveries. Thank you to Andrew Nelson and Robert Guldberg for creating a program that enables non-MBA students to take MBA courses for an Entrepreneurship & Innovation Specialization. Special thank you to Jeff Sorenson and Bob Mighell for embracing my passion and allowing me to forge new ways for the Entrepreneurship Center and the Knight Campus to collaborate. Lastly, thank you to everyone on the Entrepreneurship Leadership Team and to all my MBA professors for elucidating the power of a customer-informed need-based approach to research, product development, and communication.

My career trajectory and personal growth was truly transformed by the intersection of business, research, and clinical care enabled by these people.

I would also like to thank the Penderia team for giving me the opportunity to explore translational research post-graduation. Thank you for being a fellow pioneer at the Knight Campus, paving the way for future Oregon startup companies. Thank you for supporting my passion to always ask the clinically-relevant question. In particular, I'd like to thank Stephen Laffoon for believing in my ability and allowing me to join this team. I'd also like to thank Michael McGeehan, Salil Karipott, and Ghee Ong for supporting my SBIR grant submission. I am truly honored with the opportunity to continue learning from you all.

I also must thank the supporting personnel that made all my thesis work possible. Thank you, Julian McAdams, for tending to all my machine shop needs and for always providing my parts before deadlines. Thank you, Audrey Harris, Kathy Snell, Jillian Phillips, and the entire TeACs staff for always accommodating my surgical and animal study needs and, most importantly, for always ensuring the animals received the best care possible.

Special thanks to Dr. Graham DeKeyser for sharing his clinical expertise and prospective. Conversations with you were integral to the greater context of my research. You always reminded me of the "why" of my work. Thank you for answering my never-ending questions and for your willingness to collaborate. I look forward to our many interactions and your continued mentorship.

I would also like to thank my entire family whose unwavering love, support, and laughs were integral to my persistence through the years. Thank you, Mom and Dad, for teaching me the importance of hard work, proactive planning, and stubborn pursuit of success. Dad, I still repeat "be the ball" before any major presentation. Trevor, Trent, Amanda, and Christina thank

you for always making me laugh around the dinner table or over the phone. Sydney thank you for keeping me sane through the years. Thank you for the many meals I “mooched” off of and for always knowing what I need even before I knew. I also must thank my wonderful dog, Vince or should I say “V diggity, wiggity, woo.” Thank you for the many miles we’ve spent running together and cheers to the many more to come. Thank you for your butt wiggles every time I enter a room and for putting up with my 4am wake up calls. You have exceeded in your role as Guldberg Lab Costume Designer.

Lastly, and most importantly, I’d like to thank my husband, Brett Williams. I am forever grateful for your unconditional love, unwavering faith, and leadership of our family. Thank you for being my rock through this phase and every phase to come.

TABLE OF CONTENTS

LIST OF FIGURES

LIST OF TABLES

Table Page

CHAPTER 1: INTRODUCTION

Skeletal development and fracture healing are potently influenced by mechanical stimuli. In the context of severe bone fractures, mechanical cues are influenced by implanted stabilization hardware and load-bearing rehabilitation. Both the surgical approach and rehabilitation strategies are highly variable and informed by subjective expert opinion and patient feedback. Factors such as fracture pathology, bone quality, and patient comorbidities are also known to significantly influence mechanically-induced bone repair. There remains a clinical need for subject-specific data to inform personalized surgical and rehabilitation decisions to better account for unique patient and fracture needs.

To address this gap, we have developed an implantable sensor through collaborative research that enables real-time, subject-specific strain data to objectively track how fixation plate stiffness and rehabilitation impact the local mechanical environment as a function of time and healing. The overall objective of this thesis was to quantify subject-specific loading and rehabilitation parameters to implement data-informed rehabilitation and improve bone healing after traumatic injuries. The hypothesis was that parameters of rehabilitation (intensity, duration, distance, rest, etc) and mechanical loading (compressive and shear strain) impact bone repair, and that rehabilitation informed by subject-specific data would improve bone healing. Additional background is provided in chapter two and include content adapted from Nash K.E., Ong K.G., Gebreyesus E.A., LaBella S.A., Weiss J.A., Harrer J.A., Willett N.J., Leucht P., and Guldberg R.E., (2022) Springer as well as Nash K.E., Ong K.G., and Guldberg R.E., (2022) Connective Tissue Research.

We tested this hypothesis through the following three specific aims:

1.1 Specific Aim 1: Determine effects of rehabilitation intensity (resistance) on local niche mechanics and functional bone regeneration.

The generally accepted consensus is that moderate mechanical loading can improve bone repair, while excessive loading can hinder mineralization and result in fibrotic nonunion. However, the magnitude of local compressive and shear strains with osteogenic potential are not well quantified and rehabilitation that facilitate these beneficial stimulations are not well understood. The objective of this aim was to investigate the influence of rehabilitation intensity on the temporal progression of mechanical cues and bone healing. We utilized rodent running wheels that were instrumented with or without resistance brakes to create a high versus low rehabilitation intensity. We hypothesized that rehabilitative running with greater intensity (resistance running) would induce greater local strains and result in increased bridging rates, bone volume, and torsional stiffness of regenerated femurs compared to low intensity running and sedentary counterparts. This aim includes content adapted from Williams K.E and Harrer J.A, LaBelle S.A., Leguineche K., Kaiser J., Karipott S., Lin A., Vongphachanh A., Fulton T., Rosenthal J.W., Muhib F., Ong K.G., Weiss J.A., Willett N.J., and Guldberg R.E., (2024, Nature Portfolio Journal Regenerative Medicine) [175].

1.2 Specific Aim 2: Determine effects of rehabilitation regimens on bone healing after different injury sizes.

Studies that investigate the influence of rehabilitation on bone healing often focus on loading magnitude or duration as the driving influencers. Little work is known about the multifactorial effect of rehabilitation on bone healing. More specifically, little work has investigated the simultaneous influence of running distance, duration, and rest time, on bone healing. Most preclinical studies focus on osteotomy or critically-sized bone injury models and typically treat

with biologics, resulting in a limited understanding of bone healing after a near critically-sized bone injury not treated with biologics. The objective of this aim was to investigate different rehabilitation regimens with unique running distance, duration, velocity, number of running bouts/day, and recovery time and their multifactorial influence on bone healing after segmental bone injuries near critically-sized (2 and 3mm injuries) and not treated with biologics. We hypothesized that the effect of rehabilitation regimens on bone healing will depend on injury size, and that larger bone injuries will need longer rest with less exercise to facilitate bone formation compared to smaller bone injuries. This aim includes content adapted from Williams K.E., Muhib F., Dinh E., Leguineche K., Hajarizadeh A., Rosenthal J.W., Guyer T., Seah T., Willett N.J., Weiss J.A., and Guldberg R.E., (submitted 2024, Science Advances) [246].

1.3 Specific Aim 3: Investigate the influence of interval running on bone healing.

Rehabilitation is commonly prescribed post-injury to facilitate musculoskeletal repair. It remains unclear what rehabilitation strategies improve bone repair after traumatic fractures. Mechanobiology research has found that loading protocols with intermittent rest periods improves the osteogenic potential and bone formation of uninjured bones. The translation of this mechanobiology principle within bone repair has not been explored. The objective of this aim was to investigate the influence of rehabilitation with intermittent rest versus without intermittent rest on bone healing. I hypothesized that rehabilitation with intermittent rest would improve bone healing compared to sedentary controls and rehabilitation without rest, due to intermittent rest being crucial to the underlying mechanisms of bone healing

IMPACT

This thesis contributed an enriched fundamental understanding of how rehabilitation parameters influence local mechanical cues and bone healing and developed a data-informed

rehabilitation regimen predicted to improve bone healing with hopes of impacting clinical treatment decisions.

CHAPTER 2: BACKGROUND

Content of this chapter are adapted from *Nash K.E., Ong K.G., Gebreyesus E.A., LaBella S.A., Weiss J.A., Harrer J.A., Willett N.J., Leucht P., and Guldberg R.E., (2022) Springer [1] as well as *Nash K.E., Ong K.G., and Guldberg R.E., (2022) Connective Tissue Research [2].

*Publication under maiden name: Kylie E. Nash

2.1 Pathophysiology of Complex Fractures

Complex bone injuries often leave patients devastated with high complication rates and poor functional restoration due to diminished coordination between the cellular activity within the healing niche and the surrounding tissue (Fig. 1). In fact, 5-10% of the 12 million annual fractures in the United States do not heal in a timely fashion or lack restoration of function entirely [3]. Large or complex bone injuries often stem from accident or combat traumas, tumor resection surgeries, or congenital defects [4]. Open fractures can be classified using the Gustilo-Anderson classification which includes type I, II, or III where type III can be further described as grade A, B, or C [5]. The Gustilo-Anderson classification design ranks injury severity on factors such as wound size, level of contamination, and damage to soft tissue and bone [5]. Injuries are ranked more severe for increasing injury types, so type IIIC is the most severe with a wound size greater than 10 cm in length, high level of contamination, severe loss of soft tissue and bone coverage, plus vascular damage that requires repair [5]. In preclinical research, large bone injuries can also be described as critical-size defects, which do not heal despite surgical stabilization. Bone healing can result in union, delayed union, or nonunion. Following injury, bone union is achieved when the bone is healed and strong enough to resume normal activity, delayed union is when the bone takes longer than usual to heal but function is eventually restored, and nonunion is when the bone does not bridge and mechanical function is not restored following a severe injury.

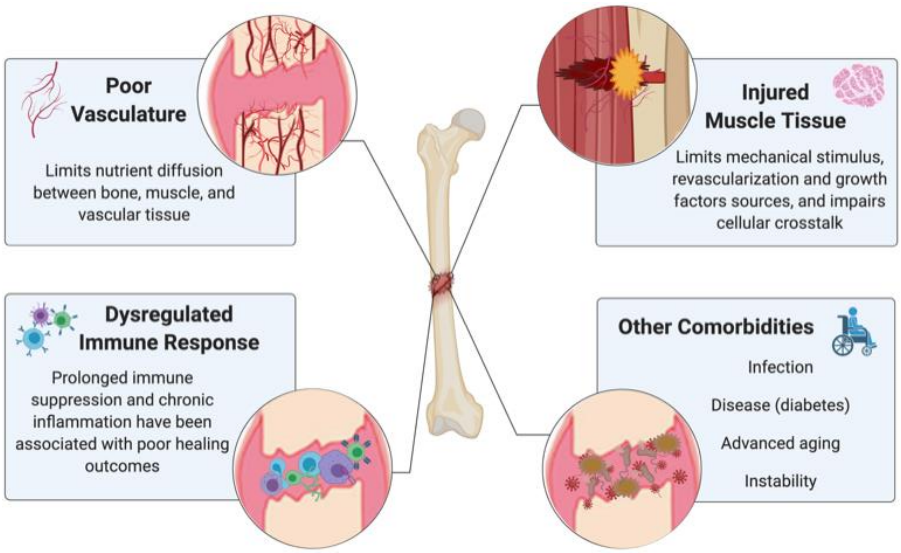

Figure 1. Factors that contribute to bone nonunion healing complications following complex bone injuries. Created with BioRender.com.

In preclinical research, complex bone injuries that result in nonunion can be modeled by inducing a critical-size bone defect in animal subjects [6]. To examine the functional ability of the regenerated bone tissue, defects are made in a weight-bearing bone and *ex vivo* mechanical tests are performed to quantify functional restoration [7]. Radiography and microcomputed tomography may also be performed to longitudinally examine the defect throughout healing. These injury models provide crucial preclinical platforms to evaluate potential regenerative strategies *in vivo* to address clinically observed complications associated with delayed or nonunion bone healing.

2.1.1 Stages of Bone Healing

Following injury, bone healing consists of distinct, yet overlapping stages, including the early inflammatory stage, the repair stage, and the late remodeling stage [8]. Within a few hours of injury, the early inflammatory stage is initiated with hematoma formation to trigger infiltration of inflammatory cells and fibroblasts. The infiltration of these cells results in formation of granulation tissue, ingrowth of vascular tissue, and migration of mesenchymal cells. Nonunion or poor healing

complications can arise during this early stage if the inflammatory response is altered by the use of anti-inflammatory or cytotoxic medications [8].

Next, the repair stage consists of fibroblasts building a stroma to support continual vascular ingrowth and infiltration of osteoprogenitor cells. As vascular ingrowth progresses, mesenchymal stem cells (MSCs) can differentiate directly into osteoblasts to form bone via intramembranous ossification or into chondrocytes to promote the formation of cartilage which serves as a template to be completely replaced by bone via endochondral ossification. The transition from cartilage to bone tissue begins with the differentiation of cartilage-producing chondrocytes into terminally differentiated hypertrophic chondrocytes which is associated with the subsequent invasion of blood vessels. Then MSCs from the periosteum (the enveloping connective tissue for cartilage) or vascular pericytes differentiate into osteoblasts and begin to form woven bone in the mineralized callus that is later remodeled into mature lamellar bone. The newly formed callus and the surrounding blood supply is sensitive to mechanical stimulus and thus requires adequate protection and stability in the form of external fixation via brace, or internal fixation via a plate or nail [9,10]. Stabilizing the defect at this stage is crucial to preserve the newly formed tissue, because instability can prevent ossification of the callus and result in nonunion or poor healing [8,10].

If proper stability is maintained, the callus ossifies to form woven bone across the defect region. At this point the defect will enter the remodeling stage where the shape, structure, and mechanical strength of the bone is restored. Remodeling occurs over a longer period of time (months to years) and is facilitated by mechanical stress, which activates osteogenic cells to promote bone formation in regions where bone is needed and resorption where bone is not needed [8]. Mechanical stimulation is necessary to promote bone modeling and remodeling during later stages of bone healing, but too much too early, can impair healing [3,11].

2.1.2 Role of Skeletal Muscle

Several studies have found skeletal muscle to be a key player in functional bone regeneration following complex bone injury [4,10]. Before injury, muscle and functional weight-bearing, provide the mechanical stimulus necessary to trigger bone modeling and remodeling, as well as proper morphogenesis, maintenance, and repair of other tissue types [12]. Beyond biomechanical stimuli, muscle is also a critical source for vascularization, progenitor cells, and osteogenic myokines to support bone repair after injury [4]. *In vivo* research that utilized a preclinical model of segmental bone and volumetric muscle loss injury further established the relationship between bone and muscle tissue because injury to both tissues resulted in compromised bone healing [13]. They found that a concomitant muscle injury decreased bone healing by approximately 50% compared to segmental bone injury alone for the same treatment [13]. Muscle cells also help bone healing by secreting several osteogenic factors such as insulin-like growth factor (IGF-1), fibroblast growth factor (FGF-2), and transforming growth factor (TGT-β) [14]. Additionally, muscle progenitor cells were shown to differentiate into osteogenic cell lineages when tracked in an open bone fracture and found incorporated into regenerated bone [13]. The relationship between muscle and bone tissue is particularly relevant to regenerative rehabilitation because activation of muscle during rehabilitation can help guide bone regeneration and healing outcomes. Further, regenerative rehabilitation strategies can emulate the relationship between muscle and bone by modulating the mechanobiology via internal and external fixation devices that play a major role in determining the mechanical environment and subsequent pattern of healing [11].

2.1.3 Role of Vasculature

Vasculature is another key aspect to bone healing. In fact, vascular integrity is a key clinical indicator of injury severity, since revascularization is a critical early step for functional bone

healing and is needed to stimulate bone repair [3,6]. However, little is known about the process of revascularization in the context of loading induced bone regeneration. To address this gap in knowledge, a preclinical *in vivo* study done by Boerckel et al. quantified the effects of early and delayed functional loading on new vascular growth using their large bone defect model [6]. The defects were stabilized with compliant internal fixation plates that were unlocked to allow ambulatory load transfer either at the time of implantation or after four weeks of the stiff (locked) internal fixation plate. They found that early mechanical loading inhibited vascular invasion into the defect and reduced bone formation compared to the stiff plate controls. In contrast, the delayed loading significantly enhanced bone formation and stimulated vascular remodeling [6]. Their results demonstrate that neovascular networks are mechanosensitive and biomechanical stimulations have the capacity to modulate postnatal vascular growth and remodeling.

To expand the exploration of mechanobiology for vascular and bone tissue healing, Klosterhoff et al. engineered an implantable strain sensor platform to longitudinally measure strain across the defect stabilized with internal fixation plates in real-time and throughout rehabilitation. This *in vivo* study found an initial increase in deformation magnitude and a subsequent increase in bone formation for the compliant fixator that permitted load-sharing [15]. Further load-shielding from the stiff fixation plate increased the number of relatively small vessels in the defect, while the load-sharing from the compliant fixation plate had similar vessel number and size as the naïve contralateral femur [15]. Therefore, although the increased strain magnitudes from the compliant plates impaired angiogenesis, the loading still supported sufficient tissue revascularization to enhance bone repair. Their work revealed distinct magnitude-dependent mechanobiological thresholds that differentially impair either bone of neovascular growth when exceeded.

To further analyze vasculature in the context of mechanical loading, an *in vitro* study by Ruehle et al. studied the effect of two load initiation times, three strain magnitudes, and two modes of compressive deformation on microvascular network growth within microvascular fragment-containing gels. They found that immediate loading inhibited angiogenesis and expression of vascular-related genes, while delayed loading enhanced microvascular network formation and upstream mechanotransduction signaling pathways. From this, they demonstrated that the magnitude, mode, and initiation time of the extracellular matrix (ECM) loading were all critical regulatory parameters for angiogenesis. Vasculature is a potential target for regenerative rehabilitation strategies because blood supply is crucial for tissue regeneration and preclinical studies found vascular tissue to respond to varying magnitudes of mechanical stimulation [6,15,16]. The knowledge gained from these studies provide potential to enhance revascularization during tissue regeneration to optimize regenerative rehabilitation strategies for complex bone injuries.

2.1.4 Impact of Immune Dysregulation

Healing complications after complex bone injuries can also stem from a dysregulated immune response. Past work has characterized a detrimental dysregulated immune response which consists of chronic immunosuppression and immune paralysis. Trauma-induced immune dysregulation occurs in multiple stages, including an initial systemic inflammatory response syndrome (SIRS) and a compensatory anti-inflammatory response syndrome (CARS), each with unique cytokine profiles [17]. The prolonged exposure to high levels of inflammatory factors and reactive oxygen species generated during SIRS is damaging to the surround tissues, so the CARS compensatory response immediately follows SIRS [18]. In physiological healing, the SIRS and CARS responses resolve themselves within a couple weeks, however, failure to restore homeostasis can lead to a destructive catabolic phase, otherwise known as systemic immune

dysregulation and immune suppression (SIDIS) [19]. Patients with symptoms of SIDIS are prone to complications and greater healthcare cost [17]. A recent study using a preclinical model of orthopedic trauma, demonstrated that distinct systemic immune profiles correlate with this long-term immune dysregulation and impaired bone regeneration [16]. Some of the primary cellular mediators include T regulatory cells (Tregs) and myeloid-derived suppressor cells (MDSCs). These mediators contribute to secretion of inflammatory cytokines and activation of other immune cells. Their work further supports the relationship between early systemic immune responses to trauma and local bone regeneration, with potential to help predict poor functional outcomes and provide novel targets for immunotherapeutic interventions.

2.2 Clinical Treatment Strategies

2.2.1 Masquelet Technique

There is currently no accepted medical standard to treat complex bone injuries, though the most common include debridement of necrotic tissue, prevention of infection, muscle flap coverage, bone grafting, and amputation as the last resort [20–22]. Within the realm of bone grafting, clinicians utilize allografts, autografts, as well as ceramic and polymeric bone graft substitutes. Allografts use bone from a deceased donor, so this practice is challenged with limited graft material as well as lower osteoinductive and osteogenic properties due to the sterilization process. Autografts use bone from the patient, so challenges include limited graft materials and surgical complications such as donor site morbidity. At the same time, ceramic or polymeric grafts have limited bioactivity, so they often rely on osteogenic cells or bone material to accompany the graft. Complications for this strategy include insufficient bioactivity or rejection of synthetic material altogether. The interplay between muscle and bone tissue has also motivated the clinical use of muscle flaps to help revascularize bone and promote healing of large range fractures. However,

muscle flaps exhibit complications such as infection, partial or total flap loss, seroma or hematoma, necrosis, and wound dehiscence [23].

Historically, clinicians have tried using grafts in surgical treatments such as the Masquelet technique (Fig. 2) which uses a temporary cement spacer followed by staged bone grafting to manage posttraumatic bone defects [24]. This strategy involves a two stage surgical technique; the first operation includes debridement of necrotic bone, skeletal stabilization, and the insertion of a polymethylmethacrylate (PMMA) cement spacer to envelope the bone ends [25]. Then after several weeks, the second operation involves the removal of the spacer without disrupting the induced biomembrane and filling the defect with bone graft [23]. For this strategy, the cement spacer is vital for increasing stability, fighting infection, hindering fibrous ingrowth into the defect, and inducing

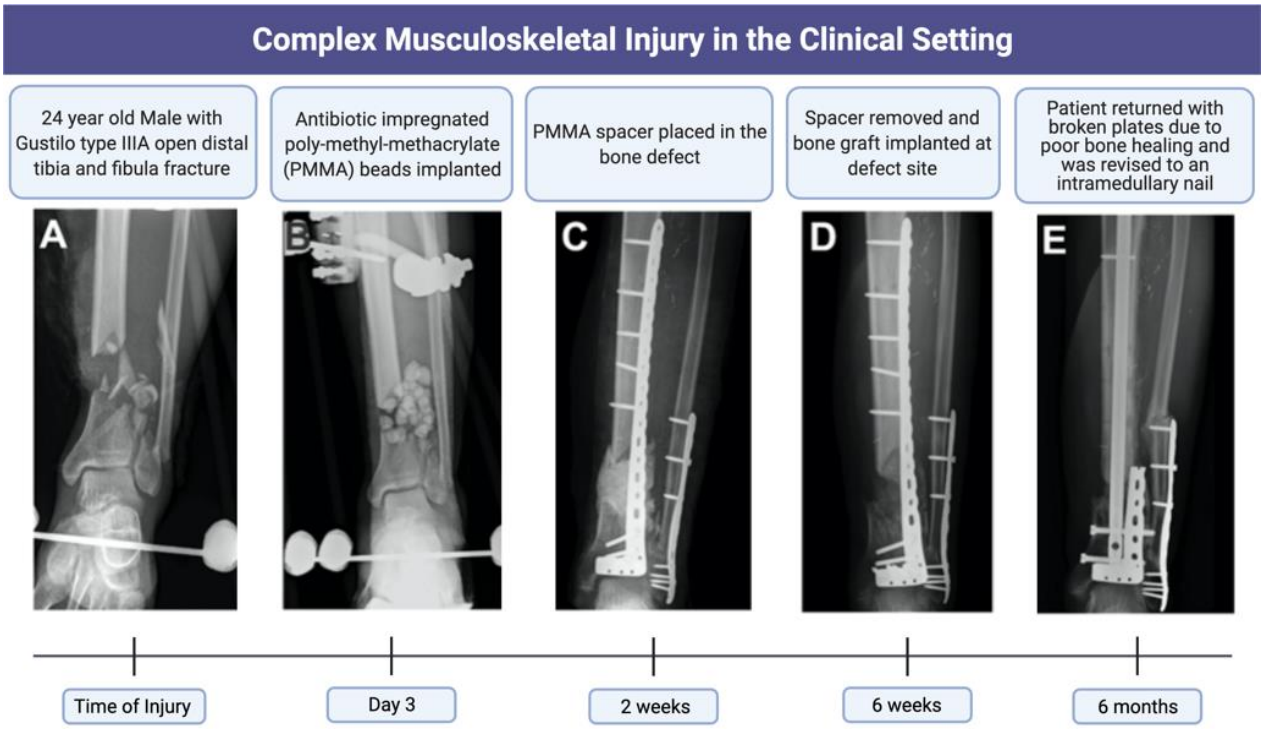

Figure 2. Clinical example of complex musculoskeletal injury that requires revision surgery due to lack in bone healing after initial treatment. Courtesy of Dr. Philipp Leucht from NYU Langone. Created with BioRender.com.

a membrane that harbors and secretes growth factors such as vascular and osteoinductive factors to promote regeneration [19,23]. Patients who underwent the Masquelet technique experienced pain-

free weight-bearing after an average recovery time of 9 months [23]. However, major differences were seen in consolidation time between patients and the correlation between consolidation time and bone defect size [23]. Therefore, the healing timeframe for this technique is unpredictable [23,26].

2.2.2 Distraction Osteogenesis

To avoid surgical intervention, scientists and clinicians have also utilized mechanical loading to promote bone union because interfragmentary movement, determined by the applied load and stability, has a strong impact on bone healing [27]. This was evident in the study by Claes and Heigele that relates tissue formation in a fracture gap to local stress and strain (1999). Claes and Heigele found that varying levels of stress and strain along existing calcified surfaces in the fracture callus controlled whether the callus tissue differentiated into cortical bone, connective tissue, or fibrous cartilage [27]. They knew mechanical loading influenced the healing process, but *in vivo* studies to determine the stress and strain of the cells in a fracture callus were not possible. To overcome this limitation, they employed the finite element method (FEM) to estimate the local stress and strain at the cellular level in callus tissue. This method allowed them to quantify the relationship between the ossification pattern and the loading treatment for the first time. They found the critical values that guided cell differentiation into either an osteoblast or a chondrocyte to further direct either intramembranous differentiation or endochondral ossification. However, the FEM poses limitations because it depends on set parameters that only correlate to simple oblique fractures and their study only described bone healing as three distinct stages [24]. Future work that examines the cellular mechanisms of bone healing may help explain the pathology of delayed or nonunion defects. Longitudinal analysis of fixation techniques is also needed to understand how healing progresses in response to loading. The amount of interfragmentary movement to optimize healing and avoid nonunion complications remains unknown, but work

continues to highlight the potential for mechanical loading to control and promote bone regeneration.

Utilizing mechanical loading, surgeons have tried distraction osteogenesis to address large bone defects. This strategy includes an initial osteotomy followed by gradual distraction to induce the integration of cells, growth factors, and extracellular matrix to form bone [28]. Bone formation using distraction osteogenesis relies on control of mechanical tension by altering the rate and rhythm of distraction to influence cell proliferation, angiogenesis, and genetic expression within the distraction gap [25]. The exact mechanism in which strain stimulates bone formation remains unclear, but research suggests that slow and steady traction can metabolically activate living tissue through mechanotransduction, which stimulates proliferation and biosynthetic cellular function [29]. Similarly, other investigations have found molecular signaling cascades to play an important role in strain induced bone regeneration [25]. After, initial success, this technique was modified to shorten the consolidation time. From this, the rate of distraction was seen as an important clinical consideration because high-speed distraction exhibited painful neuropathy and soft-tissue complications, while slow distraction diminished the osteogenic potential [25]. Although this technique has seen promising results, robust investigations are still underway because of the delicate physiological balance required for all stages of healing. Such investigations involve applying systemic and local factors that may improve healing, as well as other mechanical loading strategies to promote regeneration. Distraction osteogenesis also illuminates the need for personalized medicine because the healthy population may require faster distraction rates than the elderly or ill to maintain osteogenesis.

2.3 Current Clinical Rehabilitation and Limitations

Rehabilitation is a critical component to the healing process—in terms of both tissue repair and functional recovery—and is commonly prescribed to patients after regenerative or reparative intervention for complex bone injuries in the lower extremities. Key factors that influence the rehabilitation regimen include the severity, type, and location of the injury along with the fixation method. Typically, clinicians prescribe relatively conservative regimens that begin with non-weight-bearing for up to twelve weeks before progressing to the next stages of active rehabilitation for severe injuries. Once patients are permitted to use their injured limb, rehabilitation incorporates a variety of loading, strengthening, and pain management strategies.

Clinical rehabilitation can start with non-loading practices for a recommended length of time, and varies based on injury severity, type, and fixation method. The major methods of fixation include internal and external fixation. External fixation methods are commonly used for traumatic injuries that often result in open fractures and severe damage to the surrounding soft tissue [30]. Since external fixation can shield the injured region from excessive axial loading, immediate weight-bearing can be permitted as long as the patient is not experiencing unusual pain [31–34] However, for more severe injuries, patients are often prescribed a six-week non-weight-bearing period following surgery because the open reduction and internal fixation (ORIF) method often used for these more severe fractures, is most effective when the injured region is completely stable [32,33,35–37]. If the internal fixation is coupled with intramedullary fixation, immediate weight-bearing may be permitted, again providing the patient is free of pain [38–40]. Many of these regimens are based on the severity of the bone injury and guidelines often do not account for the severity of soft tissue injury or volumetric muscle loss which can accompany complex injuries. Research implementing rehabilitation for the treatment of volumetric muscle loss has shown significant challenges in restoring function and general guidelines do not currently exist [41].

The most common form of rehabilitation following the non-loading period for complex bone injuries is progressive touchdown weight-bearing [30,42]. This process begins with toe-touch weight-bearing, during which only the toes of the injured limb should touch the ground. This is followed by partial weight-bearing, where the clinician may prescribe 10%, 25%, or 50% weight-bearing following injury. The percentage increases on a patient-by-patient basis until the patient is able to place full weight on the injured limb [43]. Patients may be provided scales or body weight supports to control forces in the lower limb. One of the major issues with restricted weight-bearing is poor patient compliance; even when patients attempt to follow the clinician's recommendations, they frequently exceed the weight permitted. Alternatively, other techniques such as hydrotherapy and lower body positive pressure (LBPP), which allow for better control of the pressure on the injury, may be used [44].

In addition to direct loading on the bone, rehabilitation regimens also focus on muscle strengthening and pain management. Serious leg injuries, especially those which require several weeks of non-loading, lead to significant muscle loss. Studies have found that patients prescribed with muscle strengthening exercises improve strength, balance, mobility, and function [45]. Exercises include standing from a chair, walking up steps, and other functional-based exercises. Pain following injury is typically managed through analgesia and the use of peripheral nerve blocks, which have been shown to aid in functional use of the limb and reduce falls [46,47]. Rehabilitation regimens have been shown to help patients with pain management and as a result reduce the doses of analgesia prescribed [48]. Such rehabilitation strategies often incorporate stretching and strengthening with the goal of restoring basic functions and activities [49].

Preclinical studies have shown that early loading improved healing outcomes in both bone growth and bone strength compared to those with extended periods of non-loading after injury.

However, current rehabilitation strategies still prescribe extended periods of non-loading after injury. Section 8.2.3 will further detail the results of preclinical trials regarding the effects of early loading on tissue regeneration and functional restoration.

2.4 Regenerative Rehabilitation Strategies for Complex Fractures

The notion that bone adapts to mechanical stress during rehabilitation via remodeling processes is often attributed to Julius Wolff in the late 19th century. Wolff observed that trabeculae of fractured bone remodeled over time due to changes in bone shape or mechanical stresses [50,51]. Mechanosensitivity has since been demonstrated in numerous physiological processes in most tissues and throughout the organ to intracellular levels. Near the turn of the century, researchers began formalizing approaches to predict patterns of tissue differentiation, mineralization, osteogenesis, chondrogenesis, and vascular growth based on mechanical loading environments. These approaches are beginning to guide patient and etiology-specific rehabilitation and regenerative strategies. In this section, we review computational methods, wireless strain sensor developments, and preclinical models that have advanced our understanding of tissue adaptation in response to mechanobiological stimuli in fracture healing and remodeling. These approaches may guide regenerative and rehabilitation strategies by encouraging proper tissue differentiation and ultimate union after fracture in long bones.

2.4.1 Computational Models of Tissue Differentiation and Healing

Nearly a century after Wolff's law was established, researchers still disagreed on how stress mechanistically controlled bone morphology. Experimental models have delineated links between strain and patterns of tissue-differentiation during healing, though these pathways are more complex *in vivo*. This section overviews computational approaches to incorporate mechanical and biological regulators of osteogenesis, chondrogenesis, and angiogenesis into

computational models. We first review seminal computational advances in simulating tissue differentiation and healing in response to fracture mechanical environments, and then we demonstrate their capability of probing and designing regenerative rehabilitation protocols.

Computational models of osteogenesis and tissue differentiation first attempted to predict long bone mineral distribution and tissue density in response to mechanical loading. Some of the initial research needed to support these computational aims focused on developing material models to explain bone in the context of fracture healing. A robust theory relating stress to bone orientation and density presented by Fyhrie and Carter proposed that cancellous bone is an anisotropic material that simultaneously maximizes structural integrity and minimizes bone density [52]. In addition to developing material models, they also developed a fundamental approach to simulate the effects of cyclic load histories without explicitly modeling each individual load, a task that may have been computationally cumbersome at the time [53]. Once the material model and approach to simulating cyclic load history were formalized, they were applied in one of the first computational models that predicted a physiological distribution of bone mineral density in response to mechanical loads. Importantly, the authors noted that the degree of tissue stress stimulus determined the degree of bone resorption or apposition [54]. Further studies found that physiological bone density patterns can be predicted in numerous bones as long as the simulated load histories are comprehensive and reflective of multiple activities of daily living [55].

While investigating the effects of a micromotion implant in canine condyles, Prendergast et al., developed a theory of a mechanoregulatory pathway. Their theory stated that biophysical stimuli determine the trajectory of cells during tissue differentiation [56]. The differentiated interface tissue took on either a bony, fibro-cartilaginous, or fibrous phenotype depending on the distortional strain and relative fluid velocity [56]. Subsequent models studied the adaptation of segmental defects

to mechanical loads [52,54]. They created FE models of the callus, medullary tissue, and diaphyseal bone at the defect and applied simplified loading histories of compression or tension to six models with unique initial boundary conditions representing different mechanobiological environments. Notably, a single modeling approach was able to predict experimental tissue differentiation patterns of fracture healing and distraction osteogenesis. This model of tissue differentiation was refined and applied numerous times in different contexts (Fig. 3). Claes et al., found that low magnitude strains encourage intramembranous healing while high magnitude strains and pressures lead to connective and fibrous tissue differentiation [27]. Loboa et al. focused on the continuous change of material properties, allowing their material parameters to continuously adapt to local mechanical stimuli, rather than at fixed time points. Proteoglycan synthesis, collagen fibrillogenesis, crosslinking, and material moduli were regulated by fluid pressure and tensile strain. Further, materials were allowed to adapt into any phenotype unlike prior models which assumed differentiation into one of a few predefined phenotypes [57,58]. Indeed, these modeling approaches were a promising platform to study mechanoregulation of tissue differentiation during fracture healing; however, a few studies demonstrated that mechanoregulation alone was insufficient to account for biological factors and subject variation [54,59]. Thus, models around the turn of the century began to incorporate both mechanical and biological variables to better predict bone adaptation to mechanical stimuli.

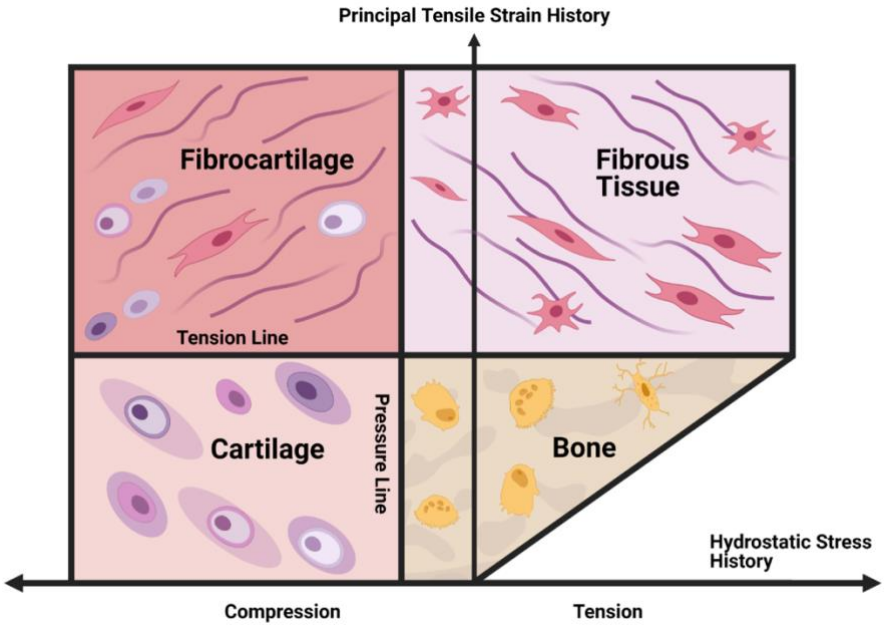

Figure 3. Reproduction of the mechanoregulatory model proposed by Carter et al., 1998 created with BioRender.com. Mechanoregulatory models typically predict differentiation based on state variables such as stress, strain, and fluid velocity. Further, the distribution of tissue types can change over time to reflect the dynamic nature of healing.

In addition to mechanical activity, *in vivo* bone healing outcomes can be influenced by oxygen, growth factor, and metabolite transport and production. Investigators of previous studies began introducing cell-based modeling approaches which simulate differentiation of cell populations rather than only tissue types in response to mechanobiological stimuli. These cells transformed the tissue around them through reactions representing bone apposition and resorption [54,60]. Ament and colleagues adapted the models of Carter et al., 1998 by introducing a fuzzy logic controller to determine tissue differentiation and composition [61]. Previous models had only allowed tissues to differentiate into a single phenotype; fuzzy set theory, however, allowed various degrees of membership to multiple tissue types depending on mechanical and biological stimuli [62]. A subsequent study used fuzzy logic, which included local vascularity as a biological variable to predict trabecular bone fracture healing and remodeling as distinct events [63]. At this time, most models had only represented the influence of biological variables in an abstract manner rather than

evaluating the transport of oxygen, growth factors, or metabolites. Bailón-Plaza and van-der Muelen were perhaps the first to develop a bioregulatory model that simulated the transport, production, and inductive role of growth factors in the context of tissue differentiation during fracture healing [64]. In their model, mesenchyme were allowed to take on chondrocyte, osteoblast, and osteocyte lineages as well as undergo mitosis and produce matrix and other cellular products in response to BMP-2, BMP-4, and TGF-β1. In a follow-up study, a combined mechanobioregulatory modeling approach was used to simulate growth across a fracture while varying the onset and magnitude of loading [65]. In both experimental and computational studies, delayed onset of loading led to low-stiffness tissue properties and nonunion or poor healing. Simulations indicated that by the time of load onset, the concentration of osteoblasts had greatly declined, leading to insufficient endochondral ossification. Early, moderate loads however, were associated with stiff gap tissue and successful bridging. Bailón-Plaza et al.'s approach and observations became common in successive studies that demonstrated the ability of experimentally-based computer simulations to guide regenerative rehabilitation therapies. However, these models still took simplified approaches to representing transport wherein cells, biophysical species, and growth factors were assumed to move only via diffusion.

Geris and colleagues acknowledged that the simplifications of previous models had limited the models' ability to study compromised healing cases. To address this, they extended the bioregulatory models of Bailón-Plaza et al. by simulating endothelial cells that migrated from preexisting vasculature [66]. Endothelial cell movement was guided by both a random component and an angiogenic factor gradient. Osteoblasts and hypertrophic chondrocytes generated the angiogenic factor, attracting endothelial cells to the callus after the formation of the initial fibrous and cartilaginous tissue in the soft callus. The model was sensitive to the production and

consumption of the angiogenic factor - overproduction or saturation of the angiogenic factor did not permit gradient formation, resulting in poor healing. Further, reduced production of angiogenic factor led to slow healing and nonunion. The mechanoregulatory mechanism was reintroduced in a later study where Geris et al. demonstrated that overload-induced nonunion could only be predicted when both angiogenesis and osteogenesis were governed by mechanoregulatory and bioregulatory mechanisms [67]. A similar approach included mechanoregulatory elements to study osteogenesis and angiogenesis in the bone-implant interface [68]. Notably, they predicted dendritic growth of new vasculature similar to angiogenesis, as well as decreased angiogenesis and osteogenesis when high shear loads were introduced between the implant and bone. The basic concepts developed thus far built a basis that at first reproduced experimental results of healing and nonhealing based on mechanical and biological stimuli. More recently, these results have been applied to patient-specific and etiology-specific cases to guide regenerative rehabilitation strategies for the clinic.

With the knowledge that interfragmentary movement strongly relates to bone adaptation and healing outcomes [27], investigators began to study how fracture stabilization protocols in both the operating room and rehabilitation clinic influence interfragmentary movement and long-term fracture healing. Prior simulations of healing relied on idealized fracture site geometry and loading conditions which may smooth over local hotspots of stress and strain introduced by irregular fracture geometries. One of the first patient-specific models of interfragmentary movement was performed while a patient was simultaneously recovering with a stabilized fracture [69]. The patient's fracture geometry and gait-cycle loads during recovery were used as inputs. The patient experienced delayed healing, which based on predicted distributions of strain throughout the callus, the authors believe may stem from insufficient interfragmentary support by the fixation

device during the early course of healing. In addition to patient-specific studies, some began to evaluate fixation procedures themselves. One group found that significant non-axial movement can occur during axial dynamization depending on fixator joint location and the ability for joints to slide [70].

In addition to studying fixator design, recent interest has emerged pertaining to when fixator dynamization or removal can begin. Byrne et al. modeled a fixation device which was automatically removed once the callus had reached a threshold stiffness in an approach that may be useful for patient-specific pre-operative treatment planning [71]. Alierta et al. studied the effects of combined compressive and shear loads during healing across a fixated fracture, which had scarcely been studied experimentally at that time [72]. Further, they studied the effect of fixation on comminuted fractures (in this case an oblique fracture with 3 fragments) and found that comminuted fractures may require stiffer fixation than simple transverse fractures. Wilson et al, modeled inverse dynamization - a recently proposed fixation strategy where some interfragmentary movement is initially allowed in order to promote a large callus to form, at which point, dynamization is restricted [73]. They found that inverse dynamization led to quicker callus formation, but ultimately did not provide significant additional stiffness to the fracture during healing. A similar study by Ganadhiepan et al investigated dynamization with treatment of Ilizarov circular fixators [74]. They found that early dynamic physiological loads may encourage advective transport and improve secondary healing. Simultaneously, their simulations predicted changes in cell population distributions and matrix deposition associated with different fixator material properties. While much attention has been given to external fixators, simulations are also used to study internal stabilization methods. For example, Mehboob and colleagues used simulations to select composite materials for intramedullary rods that best supported callus formation and healing

in transverse or oblique fractures at multiple locations along the length of the femur [75]. Indeed, simulations have enabled a deeper understanding of how fixation techniques and fracture etiology alter the mechanical environment and biological adaptation.

2.4.2 Implantable Sensors for In Vivo Loading Monitoring

The healing outcomes from orthopedic injuries that require the use of temporary or permanent implants depend on the surgical technique, rehabilitation approach, patient's health, and physical activities, as well as the mechanical environments at the implant sites [76]. Today, assessments of the mechanical environment at a musculoskeletal injury site are still typically done using mechanical loading/measurement instruments and/or numerical simulations based on assumed boundary conditions [3]. These methods may be inaccurate in many instances because they are usually performed under ideal and controlled conditions with assumptions that may not capture the actual mechanical loading experienced during the patient's physical activities. Direct measurement of the mechanical loading outside of a laboratory or clinical setting would provide a better assessment of how mechanical forces can promote or impair functional healing of an orthopedic injury [3].

In the 1960s, researchers started to integrate sensors to orthopedic implants through percutaneous wires, so measurements could communicate to external data processing electronics for monitoring *in vivo* mechanical forces in the shoulder, spine, hip, and knee implants [77]. These sensors were mostly used as investigative tools to study the healing process and shed light on the physical environment in the musculoskeletal system [77]. Since then, rapid innovations in electronics, computing, battery, and wireless communications have significantly increased the integration of sensors into orthopedic implants. Modern wireless sensors, which are smaller, safer, and more convenient to use, have been incorporated into various orthopedic implants to further

improve their performance. These sensor-integrated orthopedic implants can allow efficient measurement of clinical data that was not possible before, providing new therapeutic and diagnostic capabilities to enable personalized medicine, which leads to better treatment outcomes for orthopedic injuries [78]. Specifically, sensor-integrated orthopedic implants generate useful information characterizing the environment inside the body, giving an opportunity to tailor treatment regimens, trigger transition in care, and detect adverse events earlier [78]. They also minimize complications, reduce recovery time, and decrease readmission and revision procedures [78]. Moreover, the use of sensors in orthopedic implants gives a greater understanding of the healing processes, tissue-implant interactions, and biomechanics of the injury, hence providing knowledge for the development of improved implants and surgical techniques.

Stress and strain are critical parameters in orthopedic care, providing useful information on the healing conditions after an injury. These parameters can be used to determine the effectiveness of the treatment and predict patient outcomes. While many sensors are available, strain gauges are still the dominant technology for measuring stress and strain [77]. In fact, strain gauges continue to be used in orthopedic implants since the 1960s due to their robustness, sensitivity to applied strain, and convenience to integrate on or within the implants [78].

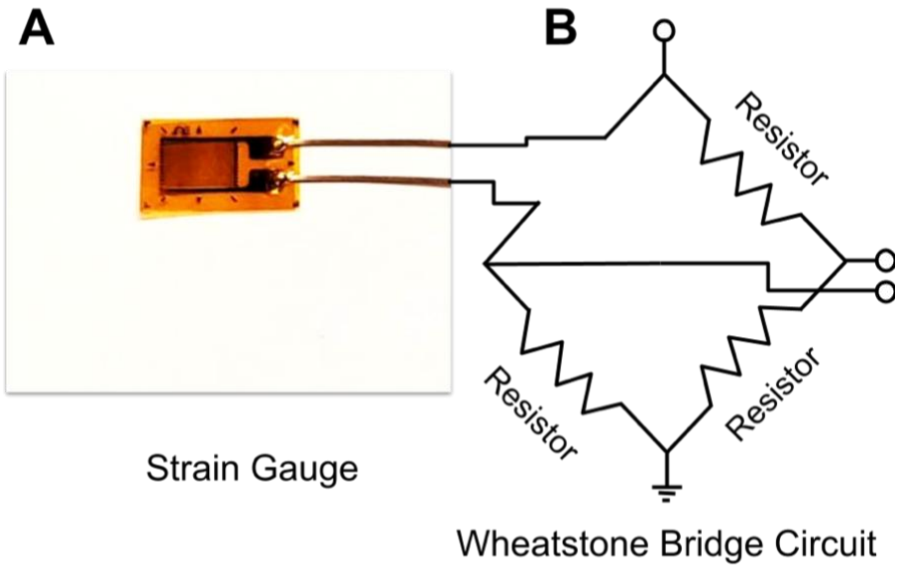

Figure 4. Sensor circuity including **(A)** a resistive foil strain gauge connected to **(B)** a Wheatstone ridge circuit to convert the change in the gauge resistance into a voltage output.

Strain gauges, as shown in Figure 4A, are electronic components that vary their electrical resistance in response to applied mechanical strains. A Wheatstone bridge circuit, illustrated in Figure 4B, is typically implemented to change an input resistance of a strain gauge to a voltage output that can then be processed to a digital output. Typically, strain gauges are a thin layer of electrically conducting pattern deposited onto a polymeric backing substrate [78]. A strain gauge is usually directly attached to the surface of an implant. The deformation of the implant alters the dimension of the strain gauge, creating a proportional change in the gauge resistance. The resistance change is then converted to a digital voltage output as a record of change in strain [78].

Traditional strain gauge sensors require transcutaneous wired connections to supply power and collect *in vivo* data from patients or test subjects. For example, Sato and coworkers developed a piezoresistive strain gauge pressure sensor that was percutaneously wired to external electronics to measure intradiscal pressure [36]. Another group developed a similar strain gauge embedded inside a femoral head prosthesis via percutaneous wires to monitor forces on a hip implant [79]. In addition, Burny and coworkers have also demonstrated the application of strain gauges for

orthopedic monitoring [80] by integrating resistive strain gauges into a modified nail plate implant to perform *in vitro* and *in vivo* evaluations on the effectiveness and safety of the implant system [80].

Wired sensors, while able to provide continuous and high-resolution measurements on orthopedic conditions, are limited to laboratory and/or clinical settings and have an increased risk of infection to the test subjects. Advancements in telemetry systems have allowed for the development of sensors that can wirelessly communicate and transfer data without wires [81], which alleviates these issues. As depicted in Figure 5, a telemetry system commonly consists of two components: a transmitter that is implanted along with the strain gauge (or other types of strain/pressure sensors), and a receiver that is typically connected to a signal processor such as a computer or a handheld electronic recording/displaying device. An example of a wireless orthopedic sensor was developed by Ledet and coworkers for direct *in vivo* measurements of spinal loads on the lumbar spine of baboons [82]. Other strain gauge implants include those developed by Rohlman and coworkers to study loads on vertebral body [83], and the calcium phosphate ceramic-coated strain gauges by Szivek and coworkers [84] that exhibited improved osteointegration.

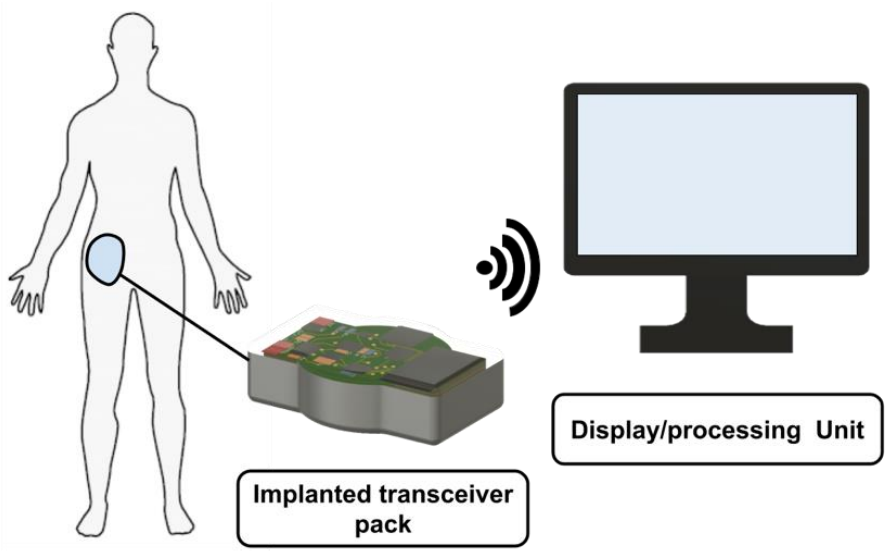

Figure 5. An implantable telemetry system consisting of a transmitter that is implanted along with the sensor(s), and an external receiver that interfaces with a signal processor such as a computer or a handheld electronic recording/displaying device.

Although wireless sensors possess clear advantages to wired sensors in terms of safety and convenience, a limitation of their usage in orthopedic implants is the power requirement at the implanted part of the sensor system. They are also bulky due to the size of the battery. Therefore, wireless sensors typically have a limited operation lifetime, and requires a carefully planned power budget. To extend the performance period of wireless sensors, some sensor-integrated implants employ batteries that can be charged remotely, or using an energy harvesting system that can generate power from mechanical forces (Nelson et al., 2020). For example, Santos and coworkers generated energy needed by a hip implantable sensor by utilizing the motion around it [85]. Another approach to prolong operation time is to reduce the power consumption rate. Integrated circuit technology has enabled the fabrication of implantable sensors (Soares dos Santos et al., 2013) featuring power-saving circuit designs such as the bulk-driven technique, the floating gates, and the subthreshold design [86].

Besides batteries, some sensors are powered by an external device through wireless energy coupling and communicate through electromagnetic fields or acoustic waves. These sensors have been used to measure various parameters in hip prostheses, as well as loads in the knee and spine. The most common wirelessly powered systems are inductively coupled systems, which receive power through electromagnetic energy (Ledet et al., 2018). For example, Graichen and coworkers developed a system that consisted of 6 strain gauges and a telemetry system that utilized radio frequency (RF) to inductively power the electronics and transmit data [87]. It was implemented on three patients with shoulder endoprostheses to monitor *in vivo* load (Graichen et al., 2007).

Another type of battery-free sensors is comprised of only energy-passive elements such as magnetic materials or passive electronic components (capacitors, inductors, and resistors) forming

a combined sensing unit and wireless transceiver. They have no active circuitry and do not require an internal power source, making them small, robust, reliable, and ideal for long-term, *in vivo* monitoring. One example of passive sensors is the magnetoelastic sensor, made of magnetostrictive materials that can convert magnetic energy to mechanical energy and *vice versa*. When under the excitation of a magnetic AC field, the sensor undergoes a mechanical resonance, generating a secondary magnetic flux that can be remotely captured [88]. These sensors, which are wireless, battery-free, and sensitive to stress/strain, are used to measure forces at bone fixation plates or medical sutures [89,90]. They are easily integrated into existing implants because of their simple designs and have demonstrated application to monitor cell adhesion on an implant and bone tissue integration to implant [91]. Another passive sensor is the inductive-capacitive sensor which consists of an electrical resistor, inductor, and capacitor (RLC) that exhibit an electrical resonance when interrogated with an RF wave. By sensitizing the RLC element to stress/strain, these sensors have been used to monitor pulling force and deformation at orthopedic implants [92]. Karipott and coworkers also developed a wireless RLC-based sensor that was inductively powered to detect infection at an orthopedic implant site by analyzing the change in temperature, measured through the shift in resonance frequency due to the temperature-induced variation in the resistor value [92]. Although these battery-free wireless sensors have a much longer operational life compared to their battery-powered counterparts, they need to be passively powered to function, thus preventing them from applications where continuous, uninterrupted monitoring is needed [92]. Moreover, metallic orthopedic implants may limit the ability to use electromagnetic energy, and result in signal distortion, loss of energy, and performance reduction [92].

With these technologies, sensors have been incorporated into orthopedic implants to monitor physical parameters (force, loading, pressure, strain, etc.) in bones at the knees, hips,

shoulders, etc. to study healing outcomes and monitor conditions of implants after surgery. Most of these sensors are based on strain gauges and rely on wireless transmission protocols (with custom communication schemes or standard protocols such as Bluetooth). For example, Klosterhoff and coworkers developed a bone fixation device for rats with an embedded wireless strain gauge sensor to quantify the mechanical environment experienced by healing tissues during physical activities [15]. A digital transceiver based on Bluetooth low energy (BLE) was used for remote-controlled circuit calibration [15]. Although Klosterhoff's sensor was limited as an investigational tool to study changes in mechanobiological cues *in vivo* for an extended period following surgery, other sensors are already in the process or at the early stage of clinical adoption [77,93,94], and a few of them are commercially employed to assist orthopedic surgeries [95].

In conclusion, implantable sensors have become a key component in orthopedic regenerative medicine. These sensors, when integrated within existing orthopedic implants, have allowed new understandings of the mechanics of bone and tissue regeneration, leading to the development of better implants and treatment procedures. While implantable sensors will continue to play an increasing role in orthopedic care, they still face challenges in terms of their efficacy, cost, and biocompatibility for long-term monitoring. Furthermore, the lack of standardization in implantable sensors still causes confusion and miscommunications between sensor developers and physicians [96], slowing down the development process. Section 8.3.2 provides further discussions on the future of implantable sensors for orthopedic regenerative medicine, including new technologies, specific challenges, and innovative solutions to overcome the barrier to successful clinical translation.

2.4.3 Preclinical Regenerative Rehabilitation Studies

Revascularization is a primary limiting factor in tissue regeneration and *in vitro* work has shown that endothelial cells and vascular networks are mechanosensitive, thus supporting mechanical loading as a potential strategy to address vascular limitations and help tissue regeneration [97,98]. To explore this potential, Boerckel et al. analyzed the effects of functional loading on neovascular growth and subsequent tissue regeneration in large bone defects (2011). Their preclinical study utilized the rat segmental bone defect model stabilized with a compliant plate that was either unlocked at the time of implantation (early) or four weeks after surgery (delayed). Microcomputed tomography and histology analysis found robust angiogenesis and collateral vessel formation after the initial vascular response to bone injury. However, early loading significantly inhibited vascular invasion into the defect by 66% and reduced bone formation by 75% compared to the stiff plate controls [6]. In contrast, delayed loading enhanced bone formation by 20% and stimulated vascular remodeling by increasing the number of large vessels while decreasing the number of small vessels [6]. Although early mechanical loading inhibited vascular growth into the defect, it did not change the overall quantified angiogenic response to the injury, which suggests that loading had a localizing effect. Ultimately, delayed loading exhibited an accelerated maturation and remodeling of new vessels which thereby enhanced bone tissue regeneration, while early loading disrupted neovascular ingrowth and impaired bone formation. Their results indicate that neovascular network formation and growth are regulated by mechanical conditions. Further, the timing and magnitude of loading were suggested as key variables and warrant further research to determine the optimal window for therapeutic effect.

Shortly after this study, Boerckel et al. further analyzed the effect of mechanical loading on BMP-2-induced bone regeneration [7]. Following a similar design as their previous work, this

study analyzed 6mm segmental bone defects in rat femurs that were treated with BMP-2 and stabilized by either a stiff or compliant fixation plate, where the compliant plate allowed for compressive ambulatory load transfers four weeks after surgery [7]. Radiography and microcomputed tomography found that loading significantly increased the regenerated bone volume, as well as the amount and distribution of bone formation within the defect. Mechanical testing also found loading to result in bone that was torsional stiffness than that of the unoperated limb [7]. However, new bone distribution was limited to the proximal defect region of the femur, which could stem from the less favorable vascular environment for progenitor differentiation. The lack in progenitor cells means a limited presence of mechanosensitive cells to respond to local stimulus. Histology also found that loading prolonged the presence of woven bone, based on the collagen organization. Overall, the load magnitude resulted in modulated bone maturity, which was previously observed and speculated to result from irregular osteoblast and osteoclast activity [99]. As a whole, this preclinical study demonstrates that altering the fixation plate stiffness to modulate functional load transfers significantly impacted BMP-mediated bone repair. Further, more transfer of axial loads increased bone formation and distribution and modulated the tissue organization and cellular differentiation within the defect. Their work motivates further investigation into mechanical loading as a potential clinical treatment for challenging segmental bone defects. The lack in new bone formation at the distal end also warrants evaluation of the suboptimal vascular environment.

These studies reassured mechanical loading as a bone healing strategy, but work was still needed for clinical translation. Research with more complicated models, such as the composite bone and muscle injury model established by Willett et al., was needed because complex bone injures often impact neighboring tissues [13]. This model combines a critically sized segmental bone

defect with an adjacent volumetric muscle loss injury and was used to quantitatively assess BMP-mediated tissue regeneration and restoration of limb function. Their analysis looked at three groups: muscle injury, bone injury, and composite injury of the femur and quadricep. Treatment included pre-gelled alginate injected into a cylindrical perforated nanofiber mesh. Their assessment included microcomputed tomography to assess bone regeneration, as well as gait analysis and muscle strength measurements to assess limb function. By week 12, the bone injury subjects were consistently bridged, but the composite injury group exhibited bone volume and mechanical strength that were attenuated by 45% and 58%, respectively. The injured muscle strength, normalized to the contralateral intact muscle, was also reduced by 51% in the composite injury group. Gait function was inhibited by all group, but the composite group displayed the greatest functional deficit. The deleterious effects of concomitant muscle injury on bone regeneration may be attributed to a diminished blood supply. Altered blood supply may result in changes to nutrient and waste exchange, inflammation, circulating stem cell recruitment, and thus revascularization of the defect. The loss of muscle volume could diminish bone regeneration because the source of resident muscle stem cells and myokines are limited, especially since these cells have displayed osteogenic capabilities. Overall, the BMP levels which consistently healed large segmental bone defects, failed to promote functional regeneration when challenged with concomitant muscle injury, indicating the need for further intervention. After the effect of mechanical loading on bone, muscle, and vasculature tissue is better understood, future work should implement mechanical loading in concert with BMP treatment to promote healing in multi-tissue injury models.

Motivated to quantitatively assess the effect of mechanical loading on bone repair and revascularization, Klosterhoff et al. deployed a strain sensor platform to examine the evolution of

biomechanical cues within the regenerative niche following injury [15]. The functional loads consisted of two different loading magnitudes similar to previous work with either a stiff or compliant fixation plate [6,7]. Previously the dynamic biomechanical signals were difficult to measure inside the body *in vivo*, so they engineered a wireless implantable sensor that integrates into the internal fixation plates to perturb and remotely quantify the mechanical environment in real-time during ambulation. The data from the strain sensors found an initial two-fold increase in deformation magnitude for the load-sharing compliant fixation plate, subsequent three-fold increase in mineralized bridging, and over 60% increase in bone formation [15]. Additionally, their work formed strong implications that early mechanical cues play a critical role in predicting long term healing response, because the strain magnitude at week 1 had a significant positive correlation with long-term bone healing outcomes. They also found that defects stabilized with the compliant load-sharing plate exhibited vessel size distribution that more closely matched naïve vasculature. Ultimately, the compliant plate allowed for increased strain across the defect during gait relative to the stiff plate, and the increased strain enhanced bone repair. The sensor readings also correlated with the status of healing, suggesting an X-ray-free healing assessment platform. Additionally, the wireless sensor could provide a non-invasive readout of the progression of healing in a personalized, real-time manner, which represents a notable shift in the ability to prescribe and monitor regenerative rehabilitation therapies. This study further motivates inquiry into mechanical loading as a clinical therapeutic, with emphasis on the mechanosensitive thresholds critical to both angiogenesis and osteogenesis to leverage and augment tissue repair.

2.4.4 Current Gaps in Knowledge and Technologies

The field of regenerative rehabilitation works to minimize complications seen with severe injuries that often effects bone, skeletal muscle, nerve, and vascular tissue. However, preclinical

research lacks knowledge and utility of multi-tissue models and thus therapeutics. Well-characterized preclinical models with quantified outcomes for functional restoration are crucial test beds for evaluating emerging technologies and rehabilitation. However, most musculoskeletal trauma models consist of single-tissue defects, which have an undeniable place in the field of regenerative medicine but have limited utility for investigating regenerative strategies for complex, multi-tissue defects. In summary, research laboratories have developed composite bone and vascular injury models, bone and nerve injury models, as well as bone and muscle injury models [4]. However, preclinical research that utilizes these complex models are limited because of their added complexity. In order to advance functional interventions and address multi-tissue injuries, a greater understanding of the biological interactions between damaged tissue is required upon injury and throughout healing. Although certain therapeutics will exhibit promising results in one tissue, unwanted negative consequences could arise in other damaged tissues, as seen with early mechanical loading that affects bone and vascular tissue differently [15]. Selection of the model type is paramount to *in vivo* research, and work with composite models could motivate multistage and multifaceted therapeutic strategies to better address more complicated injuries, with hopes of optimizing therapeutics for clinical use [4].

Another common limitation in the field of regenerative medicine is reestablishing the correct cellular environment for all tissue types involved. In the context of complex bone injuries, this often means an environment to promote adequate osteogenesis and angiogenesis. Further, when utilizing mechanical loading as a rehabilitative strategy, the biological control is extremely important because progenitor cells for bone, muscle, and vascular tissue are highly mechanosensitive [8,27]. Past work found the time of loading to be crucial for bone healing, and strain sensors found that different tissue types may requires specific timing and magnitude of loading to

optimize tissue regeneration [15]. The biological intricacies involved in regenerative medicine is extremely complex and utilizing loading strategies adds to the complexity. Preclinical research needs to continue *in vitro* and *in vivo* work to identify the mechanical thresholds needed to promote functional tissue healing in all tissue types as well as composite models. Further, research should continue to investigate the mechanical boundary conditions that optimize the therapeutic effects of rehabilitation. Additionally, the continued development of wireless strain sensor that ensure loading remains within the boundary conditions can allow for dynamic, patient-specific adjustments to the rehabilitation regimen with hopes of accelerating the functional regeneration of musculoskeletal tissue.

Another emerging aspect of bone healing is the dysregulation of the systemic immune response following some severe bone injuries. This detrimental response involves dysregulation of the systemic inflammatory response and compensatory anti-inflammatory response following injury and is not well understood. The complications that arise from immune dysregulation often result in poor healing outcomes, which are devastating to patients. Novel research is investigating a potential link between systemic immune health and bone healing. This preclinical work is identifying cellular markers and cytokine levels that correlated to compromised bone healing [16]. Future work could use these predictive markers as therapeutic targets. Additionally, research should consider how mechanical loading might modulate the immune response, as well as how the patients' immune profile might impact the therapeutic effect of mechanical loading. The immune system plays a key role in tissue healing and regeneration, so future work should continue assessing immune cells at the time of injury and throughout the healing process.

One of the challenges in orthopedic regenerative medicine is the ability to accurately and continuously track the progression of key physiological parameters. Therefore, technologies that

enable real-time measurement of *in vivo* environmental conditions such as pH, temperature, and oxygen tension in orthopedic wound sites would provide great benefits to patient outcomes, as well as translatable knowledge to improve treatment approaches [100]. Today, preclinical and clinical methods used to quantify *in vivo* parameters in orthopedic regeneration are highly dependent on animal or human injury models [100]. Thus, platforms for longitudinal tracking of physiological cues *in vivo* can increase the resolution and quantity of data acquisition from individual test subjects, which can lower the number of animals and/or human subjects needed for an adequately powered study. Imaging modalities such as ultrasound strain imaging, shear wave elastography, and magnetic resonance imaging are also used in preclinical and clinical studies. However, these methods do not provide continuous measurement, are generally more expensive, and require a larger patient/animal sample size to be effective. On the other hand, FE analysis and computational fluid dynamic analysis are used to gather information such as the surface distribution of stress-strain and oxygen tension, but they are limited by assumed boundary conditions that are difficult to validated without direct measurement with sensors (Klosterhoff et al., 2017b).

The field of regenerative rehabilitation has suffered from a lack of integrated multidisciplinary research support to advance technology and current clinical standards. As a result, there is tremendous variability in treatment approaches and post-injury rehabilitation regimens. To help progress, multidisciplinary projects should focus on evidence-based guidelines to synergize regenerative therapies and rehabilitation protocols to functionally restore musculoskeletal tissue (Fig. 6).

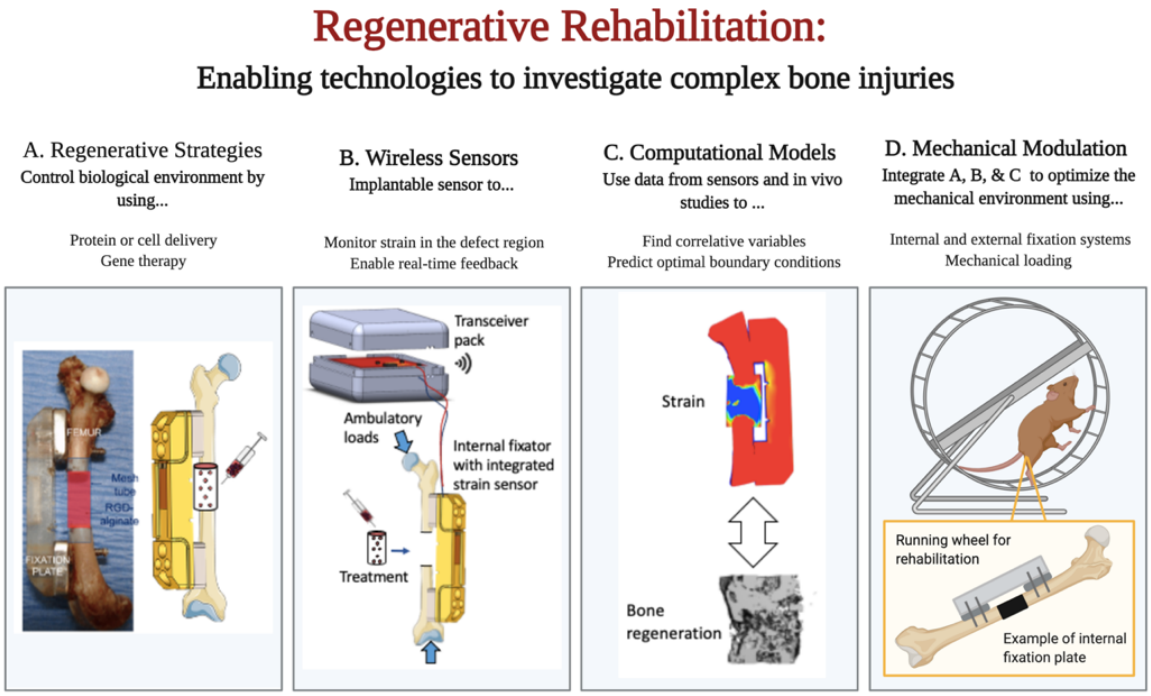

Figure 6. Regenerative rehabilitation enabling technologies to investigate complex bone injuries including **(A)** regenerative strategies such as BMP-2 delivery for bone regeneration [101], **(B)** wireless strain sensors to monitor strains within the defect region of segmental bone injuries [3], **(C)** computational models to build predictive models related to optimal strain boundary conditions, and **(D)** integration of these strategies to optimize rehabilitation regimens for accelerated bone healing of complex bone injuries. Created with BioRender.com.

In the long term, combining both regenerative medicines related to stem cells, orthobiologics, biomaterials, and tissue organoids with rehabilitation protocols related to functional imaging, assistive technologies, biophysical stimuli, and biosensors could optimize functional recovery and performance. Future integrative work should advance technologies and rehabilitative strategies that proactively avoid injury by promoting pre-injury reversal of tissue degeneration; improve post-injury rate and quality of healing; and decrease long-term pain and disability. In preclinical studies, research should focus on rigorous evaluations of regenerative rehabilitation strategies, predictive multivariate models of functional recovery, combined treatment related to regenerative medicine and rehabilitation, as well as evidence-based guidance that allows patient-specific treatment (Fig. 6). Focusing on these emerging aspects of regenerative

rehabilitation will help patient outcomes because the rehabilitative protocol will rely on patient-specific factors to accelerated functional regeneration and overall recovery.

2.5 Implantable Biosensors for Musculoskeletal Health

As technology and analytic capabilities continue to advance, our healthcare system has become increasingly data-driven and less dependent on in-person physician examinations. As a result, biosensors, among other technologies such as mobile devices, are playing an increasing role in healthcare because they can quantitatively track physiological events to aid in clinical outcomes and individual health management [102]. Current biosensors include wearable or implantable devices that can communicate with external devices through USB (wearable devices) or wireless communications (both wearable and implantable devices) such as Bluetooth or Wi-Fi (Fig. 7). Figure 7 includes some examples of implantable technologies for monitoring musculoskeletal health, as well as wearable sweat patches and benchtop biochemical sensors, which may evolve into implantable applications upon future development. Wearable devices have an undeniable place in healthcare because of their potential to minimize pain and discomfort, exhibit fast implementation, bypass biocompatibility considerations, and exhibit easy point-of-care access. However, implantable biosensors are also crucial, as they allow for translatable knowledge of "hard to reach" places and avoid the low signal-to-noise ratio that often hinders wearable devices and stems from poor sensor-skin contact or patient movement. In addition, implantable biosensors can allow for longitudinal analysis of the local environment within preclinical models to help understand and facilitate novel translatable treatments for musculoskeletal injuries or disease. Overall, implantable devices have the potential to aid in clinical understanding of disorders, medical decisions, injury prevention, and post-injury treatment [81,102,103].

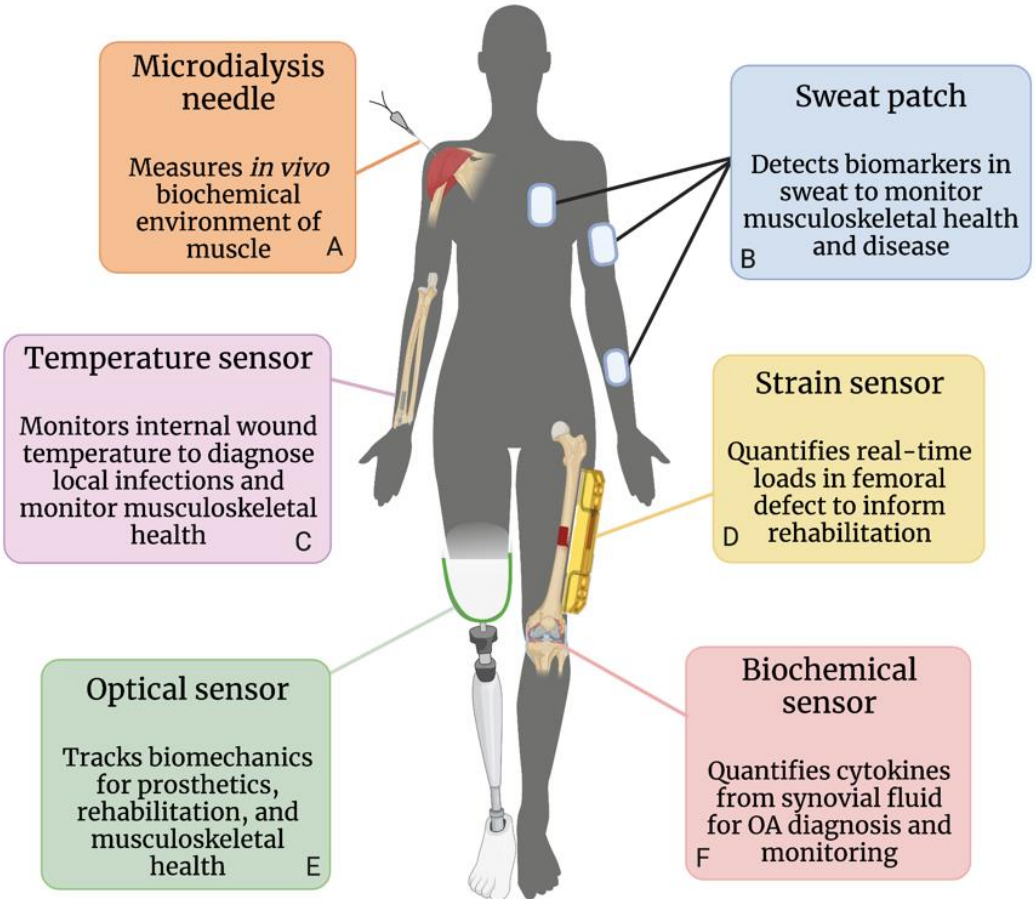

Figure. 7 Schematic of biosensors used to monitor musculoskeletal health. **(A)** microanalytic technique [104,105] **(B)** wearable sweat patches [106–108] **(C)** thermal analysis [92,109] **(D)** *in vivo* strain measurements [3,15,110] **(E)** biomechanics analysis using optics [111–115] **(F)** biochemical monitoring [116–120]. Created with BioRender.com

Part of the data-driven evolution of healthcare includes implantable biosensors, which are predominantly biophysical sensors, but future advancements may elucidate future applications for implantable biochemical sensors. Biosensors can be defined as analytical devices that convert either a physical or biological response into a quantifiable electrical signal [121]. The first implantable biosensor originated in 1960 as a cardiac pacemaker to address arrhythmias. Since then, biosensors have expanded to intricate pacemakers, defibrillators, and implantable devices that stimulate and monitor physiologically relevant processes. The drastic growth in biosensor technologies has affirmed biosensors as crucial in reliable diagnostics and treatment options for millions of patients

[102]. The first implantable devices were all battery powered, controlled by programmable circuits, and reliant on biocompatible electrodes and wires [102]. Since then, biosensors have expanded in their means of power, electrical components, and wireless capabilities. This review dives into the growing application of implantable biosensors for musculoskeletal health by providing an overview of biosensor technologies and how they have helped translatable knowledge of musculoskeletal biomechanics, post-injury recovery, and amputation management.

2.5.1 Overview of Implantable Biosensors

The development of biosensors relies on multidisciplinary knowledge and collaboration because of the breadth in required components and functionality. These complex devices also require proactive organization and understanding of what the biosensor will detect, crucial components for fabrication, and the necessary functionalities throughout all design iterations. The following section will outline relevant parameters to detect for musculoskeletal health, ubiquitous components of biosensors, and key considerations for implantable biosensors.

Biosensors can detect unique parameters related to the biological or physical conditions. For example, biophysical sensors can quantify the biomechanical environment by monitoring physical parameters such as compressive, shear, or tensile strain as well as temperature or pressure *in vivo* [77,122–124]. Conversely, biochemical sensors often monitor the presence or concentration of specific biomarkers including cells, molecules, cytokines, or proteins [125]. Due to the intricacies of biochemical sensors, they are currently limited to wearable or benchtop technologies that often rely on fluid extraction and subsequent analysis. Common bodily fluids used for biochemical sensors include urine, sweat, blood serum, or local fluid around musculoskeletal tissues such as synovial fluid near knee joints susceptible to osteoarthritis, a degenerative disease of joint cartilage and underlying bone. Quantification of these parameters requires in-depth investigation of the

biosensor's reliability, sensitivity, specificity, and selectivity *in vivo*. Biochemical and biophysical parameters are relevant to musculoskeletal health because mechanical conditions influence the biological cascades that control tissue regeneration and remodeling crucial for injury prevention, healing, and degeneration management. Similarly, dysregulated analytes may hinder the physiological state of musculoskeletal tissues. Overall, the mechanobiology of musculoskeletal tissues is highly dynamic, so reliable analysis of local biophysical and biochemical conditions has potential to inform medical decisions and treatment outcomes.

In short, the basic functionality of biosensors relies on five key components: a power source, bioreceptor, transducer, supporting circuitry, and a reliable interface for data transmission as shown in Figure 8 [125]. Once powered, biosensors rely on a sensing mechanism in the form of either a bioreceptor that specifically binds to the analyte of interest or a detection apparatus that reliably gauges physical parameters. Some examples of sensing elements include chemical/biological recognition elements such as enzymes and immobilized antibodies. The functionality of a biosensor also requires a transducing element that converts the sensed parameter into a usable electrical response for quantification as well as supporting circuitry that controls the measurement process of the sensor and modulates the power for the electrical components. A common example of transducers for biophysical parameters is the strain gauge that converts applied forces, pressures, torques, etc. into changes in electrical resistance. Main function of the supporting circuitry includes providing the needed voltage and control for the transducer to operate, digitizing the output data for further processing or transmission. Lastly, data collected by biosensors are transmitted to an external device via custom wireless communication protocol or common protocols such as Bluetooth or WiFi. Advancements in these foundational components

have led to novel biosensors with potential for broad clinical application.

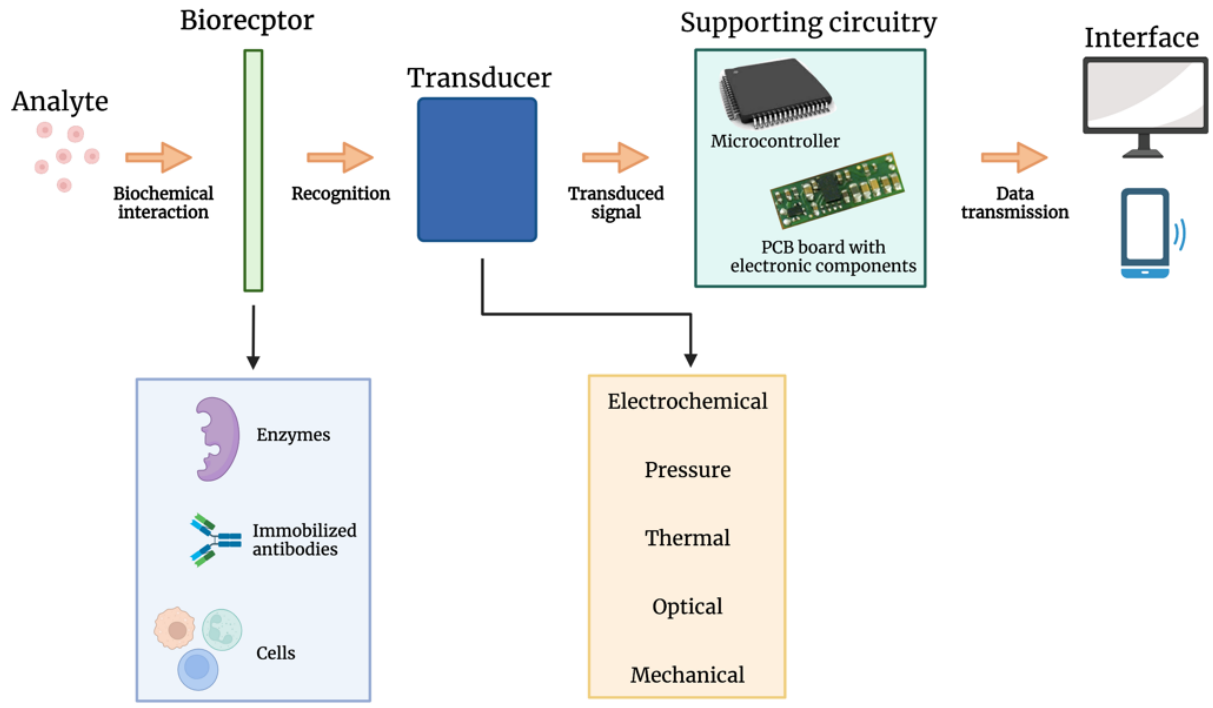

Figure 8. Diagram of functional components of biosensors including reception components to detect an analyte (bioreceptors specific to biochemical sensors), transducers to convert input signal to quantifiable data output, supporting circuitry to allow for specific functionality, and data transmission to capture outputted data. Created with BioRender.com

The general performance of biosensors largely depends on the sensing element that detects either a biochemical or biophysical parameter, often at nanoscale quantities [125]. When developing a biosensor, the design or implementation of various transducers such as strain gauges or temperature gauges, or biological recognition elements such as immobilized bioreceptors are key considerations. For biophysical sensors, the sensitivity, measurement of hysteresis, and signal drift are crucial for reliable and accurate detection. Furthermore, sensor performances are often impacted by electrical noise from the power supply or vibrational noise from the environment [125]. When disruptive acoustic waves are present, many biophysical sensors will detect them as vibrations, which will affect the accuracy of detection. Therefore, to minimize noise, one must consider biosensor placement and external conditions to better discern relevant signals from noise.

Beyond the sensing element, supporting circuitry is also needed for the functionality of

biosensors. Supporting circuitry typically includes an electrical circuits with appropriate power supply. Depending on the circuit function, typical circuitry for biosensing includes common electrical and electronic components such as capacitors, resistors, transistors, or amplifiers. Additionally, many biosensors also rely on microcontrollers to control the functionality of the device, as well as data transmission components needed for USB, WiFi, or Bluetooth communication with external devices. When incorporating a microcontroller, the functionality of the supporting circuitry, such as power management, sensing functions, data transmission, and calibration, can be customized or even optimized on the fly with programming codes or scripts.

Implantable biosensors are particularly fitting for musculoskeletal applications because many conditions or injuries already require a surgical procedure and would benefit from longitudinal monitoring throughout recovery. However, compared to wearable technologies, implantable biosensors come with additional risk to local tissue and systemic complications. Issues such as safety, tissue response, and *in vivo* interference are important practical considerations during the development of implantable biosensors.

When investigating the potential application of implantable biosensors, one must consider potential implications of the invasive approach during delivery and possible later removal of the biosensor. When the body recognizes a foreign implant, a complex response occurs (e.g. fibrotic encapsulation) in both the short and long term, which can adversely affect both the function of the implant and health of the local tissue [126–131]. Proactive measures related to biocompatibility and sterilization can help minimize the response to the implant. In addition, careful selection of biocompatible materials or coatings (e.g. high molecular weight polyermers such as polyethylene glycol/PEG, polydimethylsiloxane/PDMS, or parylene- C [132]) can help minimize the local tissue response. Localized heating caused by power dissipating and unintended stimulation can also

cause harmful damage to local tissue, so biosensors should use a low-frequency carrier wave with frequencies still above physiological thresholds [126]. Biocompatibility is achieved when an implanted biosensors can function *in vivo* without eliciting detrimental local or systemic responses in the body. To promote biocompatibility, biosensors can be coated with certain materials that can minimize the host tissue's reaction around the sensor. For example, biosensors have been coated with porous polylactic acid (PLA) to reduce fibrosis (thickening and/or scarring of connective tissue) [133]. In addition, anti-inflammatory agents (e.g. dexamethasone) have been delivered at the site of implantation in an attempt to suppress inflammation and avoid host tissue rejection of the implanted biosensor [134]. Sterilization of the device can also help avoid a harmful immune response, but certain forms of sterilization may hinder biosensor functionality (temperatures from dry heat or steam can damage components of sensors), so biosensor performance must be tested both before and after sterilization. Some established forms of sterilization include ethylene oxide, radiation, dry heat or steam, hydrogen peroxide (H_2O_2), and ozone, while more novel forms include peracetic acid, ultraviolet light, microwave, sound waves, and pulsed light [135].

To avoid harmful complications and wasted resources, the functionality of the biosensor in an environment comparable to living tissue must be rigorously tested prior to implantation. This environment will entail bodily fluids with a controlled temperature and pH level. To preserve functionality, the core components must be enclosed by a durable, yet biocompatible material to limit biological fluid leakage and vibrational noise. Once the device is ready for implantation, one needs to consider the approach of delivering and removing the biosensor in terms of placement, size, damage to local tissue, and patient comfort. In addition, implantable biosensors are prone to implant migration which can lead to healing complications [122]. Therefore, the biosensor's susceptibility to physical migration during ambulation and mundane activities for both short and

long term care needs to be minimized. Implantations come with several risks related to sensor attrition and physiological complications, so extensively testing in relevant *in vitro* and *in vivo* environments is paramount to clinical success.

2.5.2 Exemplary Biosensors Utilized for Musculoskeletal Health

Beyond biosensors for diagnostic or treatment purposes, implantable biosensors have also provided decades worth of clinical data about the biomechanics of the musculoskeletal system. The use of implantable biophysical sensors for clinically relevant research started as early as 1966 when Rydell analyzed forces acting on implanted femoral components using strain gauges and temporary percutaneous wire that connected the permanent implant [79]. From the well-received significance of *in vivo* data for musculoskeletal behavior, later researchers continued to fabricate and implement biosensors for bone and joint analysis including Lanyon and colleagues who measured bone strain in 1975 using a strain gauge attached to the midshaft of a man's tibia [136]. These two early implantable biosensors continued to motivate additional applications such as measuring strain in fracture fixation, pressure in cartilage, forces in the spine, and forces within the knee, hip, and shoulder joints [137]. In summary, implanted biosensors have yielded *in vivo* quantification of force, torque, strain, displacement, pressure, and temperature [82,138]. Recent advancements in microfabrication, wireless capabilities, and reduction in cost allow these sensors to be incorporated into implants with minimal alterations to the host implant. Orthopedic smart implants are a specific category of biosensors mainly used for research. These implantable devices are incorporated into implants to measure physical parameters inside the body, and their data have led to the refinements of implant design, surgical technique, postoperative care, and rehabilitation. Implantable biophysical sensors embedded in the body or implants benefit the research community the most as the sensors data can immediately aid in testing, validating, and generating relevant

insight into the behaviors of musculoskeletal tissues in response to injury, surgical repair, degeneration, and healing. Further, these biosensors are valuable to companies for medical devices, implants, and prosthetics as they allow for clinically relevant improvements to the design and implementation. Lastly, the future of these biosensors has potential to inform feedback-controlled rehabilitation or therapeutics by integrating the longitudinal data into personalized models that inform clinical decisions. Clinical knowledge starts with research, and implantable biosensors have been the cornerstone for comprehensive knowledge of the *in vivo* biomechanics of musculoskeletal tissue. Now the challenge is translating these research tools into clinical resources to aid in diagnostics, management, and treatment of musculoskeletal injuries and disorders.

Stress and strain are critical parameters for the growth, remodeling, and repair of musculoskeletal tissues. Therefore, *in vivo* knowledge of these forces and any resulting deformities provide critical insight into the tissue's response to injury or disease. Several implantable biophysical sensors have been used to directly measure biomechanics including strain in several musculoskeletal tissues and have seen a promising impact on clinical applications. For example, in the early 1970s Burney and coworkers used percutaneous leads to measure loads during fracture healing by instrumenting external fracture plates with strain gauges [139]. Later, Schneider et al. instrumented a femoral intramedullary nail with a biosensor and telemetry system to monitor femoral forces throughout healing [140]. Their analysis found a 50% decrease in loading over the first 6 months of healing. They reasoned that the decrease in loading and the increase in bone stiffness was a result of tissue healing. This correlation between stiffness and healing supports biophysical sensors that longitudinally measure stiffness and thus monitor healing throughout treatment. In addition, other implantable biophysical sensors for musculoskeletal injury

management have been outlined in D'Lima et al. review article that includes sensors to measure strain in bone, fracture fixation, cartilage, the spine, and major joints like the hip and shoulder [137].

More recently, Klosterhoff et al. deployed an implantable strain biosensor platform to examine the biomechanical cues in a critical-sized segmental bone defect in rat femurs during treadmill rehabilitation. This defect model was treated with BMP-2 and stabilized by either a stiff (made of polysulfone) or compliant (made of ultra-high molecular weight polyethylene) internal fixation plate instrumented with a strain gauge that connects to a transceiver pack via a subcutaneous wire (Fig. 9). This biosensor platform deploys Bluetooth wireless communication to transmit the strain induced within the regenerative niche to nearby monitors in real-time (Fig. 4). The biosensor technology monitors longitudinal strain, providing the opportunity to guide weekly revisions to rehabilitation. These revisions can be informed by biofeedback mechanisms understood through patient-specific data collected in real-time. This model emulates complex bone injuries that face high complication rates and devastating long-term disabilities, which motivates therapeutic strategy that synergistically combines regenerative and rehabilitative treatments. The preclinical work by Klosterhoff et al. found that compliant plates allowed a two-fold increase in deformation magnitude than the stiff fixation plates, which led to a subsequent three-fold increase in mineralized bridging and over 60% increase in bone formation [141]. They further showed that early strains, just one week post-injury, and well

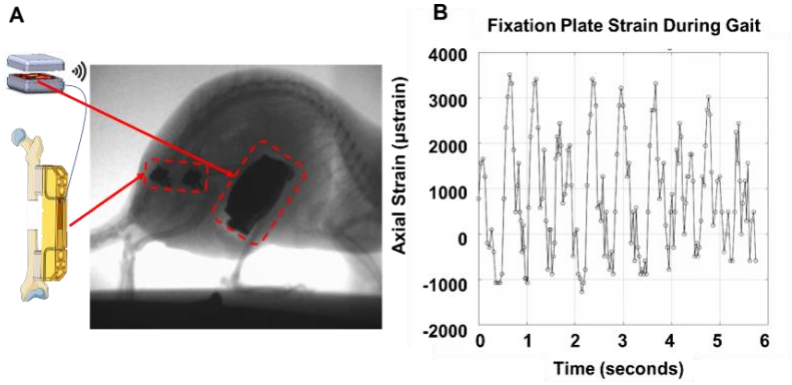

Figure 9. (A) Still image of rat from high-speed x-ray video. Note the fixator plate and transceiver pack both outlined in red **(B)** Biosensor output depicting cyclic strain amplitudes corresponding to discrete steps.

before radiographic evidence of healing, correlate with altered local biological responses and long-term healing outcomes [15,142]. These findings support their implantable strain biosensor platform for non-invasive readouts of healing in a personalized, real-time manner. Further, their findings exemplify the clinical relevance of quantifying mechanical loads in musculoskeletal tissues to monitor healing or disease progression, with potential to accelerate functional recovery of complex musculoskeletal injury via personalized, feedback-controlled rehabilitation. Implantable biosensors for future clinical treatment of complex traumas would benefit from additional advancements in biosensor technologies, including elimination of internal batteries and miniaturization, as well as integration with machine learning algorithms to predict and optimize patient functional recovery.

Since the 1990s, osseointegrated prosthetics have leveraged bone ingrowth into metal implants to improve prosthetics for applicable patients [143]. Although osseointegration has seen promising results, this procedure is still challenged with host bone fractures, infection, and insufficient knowledge of when osseointegrated prosthetics can handle loads. To address this shortcoming, recent developments have focused on implantable biosensors to monitor the *in vivo* bone strain and growth. Recent advances in technology and growing interest in sensor-laden implants that provide clinical data related to the performance of implants, has led to the application of implantable biosensors to monitor and improve osseointegrated prosthetics.

As a noteworthy example, Burton et al. recently developed a biocompatible wireless sensor system to monitor the growth and strain response of bone after implantation [144]. Their thin-film sensor is intended to wrap around the circumference of the host bone during surgical implantation and consists of a two resistor-inductor-capacitor (RLC) circuits. One circuit measures axial strain in bone and the other tracks bone hoop strains in comparison to known target hoop strain to monitor

bone growth [144]. Upon initial characterization of the circuit components, their passive strain sensing system agreed closely with theory [144]. Subsequent simulation and experiments also validated their ability to detect bone strains expected during compressive osseointegration, as well as the proposed hoop strain-sensing system to quantitatively monitor bone growth within the osseointegrated implant. Although these authors were able to develop and validate this sensing system, they have not translated their sensor system to *in vivo* animal models. After testing in animal models their system may encounter complications which will require system revisions. In addition, their sensing mechanism focuses on low levels of strain which may limit the application to humans. The expanding focus on implantable biosensors for osseointegrated prosthetics has deviated from other external sensor systems, such as the external apparatus mounted on the abutment of osseointegrated prosthetics done by Frossard et al, in hopes of detecting bone integration earlier and improving rehabilitation [145,146].

The field of osseointegration continues to evolve and recent advancements in biosensor technology have led to the consideration of implantable biosensors for this application. Wireless biosensors implanted with osseointegrated prosthetics to monitor strain and bone integration has potential to transform clinical understanding and overall outcomes of osseointegrated prosthetics. More specifically, advancements with these biosensors have potential to inform data-driven loading in terms of magnitude and timing for osseointegration patients, as well as minimize current osseointegration complications such as loosening and host bone fractures.

Although increasing research has focused on implantable biosensors for musculoskeletal health, they are often confined to research applications with few products commercially available. One notable biophysical sensor in the market is the open eDisk developed by Theken Disc, LLC for measuring motion and loads within a spinal disc implant. This was the first artificial spinal disc

with an integrated microelectronics module to reduce post-operative complications and accelerate recovery and return to work. The force monitoring capability of this implanted disc allows for real-time and personalized data that assesses whether a patient is able to return to work, while the microelectronic module monitors any dynamic high-load events to immediately alert the patient via a wireless signal to a worn audible alert unit [147]. In addition, the FDA recently granted de novo classification for the Persona IQ smart knee implant, which is the only smart knee implant cleared by the FDA for total knee replacement surgery to date [148]. This technology records and wirelessly transmits a wide range of gait data to a patient's personal base station at home before data are securely delivered to surgeons, via a FDA regulated and HIPPA-compliant cloud-based platform, to assess post-surgery recovery. The smart implant consists of a cemented tibial plate and tibial extension, and the biosensing is enabled through the stem that is instrumented with internal motion sensors (3D accelerometer and gyroscope). Proprietary algorithms convert the raw data into clinically relevant gait metrics that allows easy post-operative monitoring by both the patient and healthcare providers. One of the most striking aspects of this clinically available smart implant is the ability to monitor patient's gait daily through one year of recovery, with potential for 20 years of longitudinal data collection if data collection is less frequency after the first year [148]. Biosensors for treatment of musculoskeletal tissues are not clinically available, but further validation of implantable technologies in preclinical and clinical models may encourage future translation. Some of the challenges associated with implementing biosensors include safety regulations, cost issues, lack of long-term research, biocompatibility as well as privacy and security concerns due to wireless signal transmission [77]. Besides these challenges, the future is promising for implantable biosensors due to the rapid developments in associated technologies to help address some of the current limitations with preclinical biosensors.

2.5.3 Future Directions with Biosensor Technology

Osteoarthritis (OA) is a progressive joint degenerative disease that involves gradual molecular, cellular, and tissue modifications that no physical therapy or drug has effectively treated [117,149]. The current method of diagnosing this degenerative disease is through clinical examinations and imaging only during late stages. Similarly, the current method to assess biomarkers related to OA often involves Enzyme-Linked Immunosorbent Assays (ELISA), which are generally costly as they require highly skilled workers, expensive laboratory equipment, and long analysis time [150]. However, biochemical sensors that measure biomarkers released by joint metabolism may provide an advantageous way to diagnose and monitor the disease progression since reliable detection of biomarkers is critical for understanding patients' condition. The current biosensors used for OA applications include several wearable biosensors to characterize gait for OA patients [151–153] as well as microfluidic biosensors to analyze immune cells of interest [154]. The biophysical gait sensors study the impact of physical therapy on the management of OA, while the biochemical microfluidic sensors monitor immune biomarkers with potential to target and analyze markers relevant to OA pathogenesis [155]. Biochemical sensors have potential for broad clinical impact, because of their potential to monitor a plethora of biomarkers that are relevant to various disease or injury conditions. These biosensors involve wearable technologies which help avoid common biochemical laboratory analysis that requires expensive laboratory equipment, time intensive analysis, and trained personnel. However, these wearable biochemical sensors are limited to systemic biomarkers analysis and require painful fluid extraction and dilution steps for local analysis. Implantable biochemical sensors could provide longitudinal data with just one procedure, as opposed to the multiple painful synovial fluid extractions. Longitudinal data could be useful for injury or disease management, especially for musculoskeletal cases that already require surgical

intervention. Advancement into implantable biochemical technologies could also avoid fluid dilution steps and allow for local analysis of relevant biomarkers. Overall, advancements to the current wearable technology and potential future implantable applications may allow for proactive diagnosis, patient-specific data to inform clinical decisions, and translatable knowledge for future therapeutics.

Although implantable biosensors continue to play an increasing role in healthcare, they still face challenges in terms of power efficacy, size, and biocompatibility for long-term monitoring. Furthermore, the lack of standardization in clinical implantable biosensors result in confusion and miscommunication between the biosensor developers and physicians, ultimately slowing down the translation process [96].

The power supply is usually a limiting factor for implantable biosensors and they are traditionally battery operated, so maximizing the battery or power budget is particularly important for implantable applications [126]. The method of powering implantable devices depends on the circuit energy consumption rate, operational period, size constraints, and implantable safety considerations [81]. Battery power avoids external wires that connect the implant with external circuitry, which can help avoid surgical complications including wire breakage, infection, and electrical noise, but they are larger in size and have limited operation lifetime [126]. Therefore, batteries require a carefully planned power budget. Progress in several low-power or power-saving circuits have helped prolong battery life in fabricated biosensors [86,126]. Alternatively, wireless power strategies that generate and harvest energy from mechanical, thermal, or kinetic forces surrounding implants have been investigated [81,103]. For example, energy in the form of heat or movement can generate electricity using thermoelectric generators [103]. In addition, novel technologies are utilizing bio-fuel cells such as glucose or amylum to generate electric power from

renewable biodegradable materials [156,157]. Other battery-free methods to power implantable biosensors include energy coupling through electromagnetic fields or acoustic waves, or energy-passive elements such as magnetic materials or passive electronic components. For example, magnetoelastic sensors convert magnetic energy to mechanical energy and vice versa, have no active circuitry, and do not require an internal power source like a battery or energy harvesting system [158]. Implantable biosensors rely on permanent and sufficient power supply to ensure proper operation, so investigating reliable, sustainable, and continuous methods to power biosensors will be in constant demand.

Wireless biosensors can be powered through passive or active means, where passive devices are often powered though wireless energy coupling with external sources (e.g. interrogator), while active devices rely on an internal power source (e.g. battery or energy harvesting system) [81]. Passive biosensors often have a simpler design and smaller size, but are limited to brief snippets, depend on remote power to operate, and often require a reader device to remain in close proximity which restricts the potential for continuous data acquisition throughout daily activity [159]. One advantage of passive power is an operation lifetime that is not limited by batteries. On the other hand, active biosensors often contain electrical components such as microcontrollers and battery powered transducers that allow for remote monitoring and continuous data recording, but the operation lifetime and footprint of the biosensors are hindered by the battery [81]. The decision on the powering method for particular biosensors depend on the required size, functionality, and placement. Passive biosensors are particularly useful for prototyping new technologies because of their simple design, robustness, and long operational lifetime without loss of power, making them ideal for long-term implantable applications where retrieval of sensors are not needed [81]. In contrast, active biosensors are useful for their complex functionality, and ability

for remote and continuous data acquisition. Overall, both passive and active powering methods are important for biosensors to monitor musculoskeletal health as they both provide custom and multiplexed measurements, which is of increasing importance in our evolving healthcare.

To avoid patient discomfort and large costs, size is also a crucial consideration for implantable devices. Devices that are battery operated have limited miniaturization potential since batteries are often bulky and account for most of the sensor volume. Other battery-free power sources include energy harvesting technologies, wireless power transfers such as near, mid, and far field effect, inductive coupling, capacitive coupling, and ultrasound [160]. Careful design of printed circuit boards (PCB) can also aid in miniaturization. Flexible and rigid-flex PCBs are particularly interesting for miniaturization as they reduce the number of connectors and allow folding to complex shapes instead of the previous titanium or ceramic bulky housing units to seal electronic components. Flexible electronics were initially developed for wearable applications but have expanded to implantable applications as small, flexible components for easier and more sustainable implantation [161]. Further, soft, stretchable, and flexible electronics are now utilized for implantable biosensors since they reduce the number of connectors to promote miniaturization and they can conform to soft, curvilinear, and elastic tissues while supporting multimodal functions [162]. Three-dimensional printing technology has also allowed these flexible PCBs and electronics to be stored in geometrically unique housing units to further ease implantation of biosensors.

Multiplexed biosensors could drastically advance clinical management of diseased or injured musculoskeletal tissue. The complex mechanobiology of musculoskeletal health warrants the simultaneous monitoring of multiple parameters allowed by multiplexed biosensors. Multiplexed biochemical sensors could simultaneously detect several proteins, cytokines, hormones, etc. to better elucidate the cellular mechanism driving physiological changes to

musculoskeletal tissue. On the other hand, multiplexed biophysical sensors could detect several biomechanical properties to better understand the mechanobiology of musculoskeletal tissue. Implantable multiplexed biosensors have yet to be utilized for musculoskeletal applications, but these devices still exhibit increased clinical relevance as they would provide knowledge that better simulates physiological events. The delayed development into implantable applications is largely due to the complex functionality as well as the increased cost, risk, and efforts required to sense multiple parameters and bring this technology to market.

In hopes of minimizing biocompatibility limitations (e.g. fibrous encapsulation and inflammation) as well as avoid secondary removal surgeries, increasing interest has evaluated biodegradable sensors for either short or long term *in vivo* monitoring [163,164]. These devices rely on biodegradable metals (Mg, Fe) or polymers (PLLA, PCL, and PPy) that break down into non-toxic components after a predetermined functional lifetime [122]. In addition to the improved biocompatibility, biodegradable sensors are advantageous because they avoid removal surgeries altogether [165]. One example of a recent biodegradable biosensor is the passive pressure sensor developed by Luo and coworkers [166]. The structural and dielectric material for these wireless biosensors was made of PLLA and PCL, while the conductive portion was made of Zinc and Iron bilayers. Although implanted biodegradable sensors help minimize post-surgery complications, they are all passively powered due to the lack of biodegradable batteries. However, novel advancements in biodegradable batteries have increased the potential of actively powered biodegradable sensors. For example, Tsang et al. developed a magnesium/iron battery in PCL that exhibited adequate energy density and reduced size [167]. Additionally, biodegradable electronics such as iron microparticle and PCL interconnected system developed by Zhang et al. [168], and silk fibroin substrate fabricated by Kim et al. [169], have advanced the possibility of a fully biodegradable

implantable biosensor. These biodegradable technologies are still in their preliminary stages and will require rigorous bench top testing and *in vivo* monitoring before they are clinically deployed.

The lack in clinical standards and slow translation of emerging technologies have resulted in tremendous variability in musculoskeletal treatment approaches. However, technology for personalized health has been rapidly evolving as each generation exhibits better sensitivity and selectivity while being more resource conscious. Deploying implantable biosensors to examine the variability of musculoskeletal tissue response to disease, injury, and subsequent treatments can help inform personalized clinical treatment [170–173]. For example, the patient-specific data collected by implantable biosensors can provide the inputs for predictive computational models that can aid in clinical treatment decisions. Utilizing implantable biosensors can revolutionize healthcare, since treatment can rely on biofeedback mechanisms enabled by these implantable biosensors and predictive models. Further, personalized health can account for confounding factors such as genetic predisposition which may influence a patient's condition, prescribed treatment protocol, and response to medical intervention [174]. To help advance the ability to monitor musculoskeletal health, multidisciplinary projects should utilize implantable biosensors to allow for evidence-based guidelines that allow patient-specific treatment.

CHAPTER 3: EARLY RESISTANCE REHABILITATION IMPROVES FUNCTIONAL REGENERATION FOLLOWING SEGMENTAL BONE DEFECT INJURY

Contents of this chapter were adapted from Williams K.E and Harrer J.A, LaBelle S.A., Leguineche K., Kaiser J., Karipott S., Lin A., Vongphachanh A., Fulton T., Rosenthal J.W., Muhib F., Ong K.G., Weiss J.A., Willett N.J., and Guldberg R.E., (2024). Nature Portfolio Journal Regenerative Medicine [175].

Author contributions

Conceptualization: KEW, JAH, SAL, KL, JK, TF, JAW, NJW, REG

Data Collection and Analysis: KEW, JAH, SAL, JK, AL, TF, JWR, FM

Interpretation: KEW, JAH, JK, NJW, REG

Writing and Editing: KEW, JAH, SAL, KL, JK, SK, FM, KGO, JAW, NJW, REG

3.1 Introduction

Non-union fractures present a significant clinical challenge, requiring surgical intervention and often result in post-operative complications. While most bone fractures heal spontaneously without surgical or therapeutic intervention, up to 5-10% of fractures fail to heal and result in non-union [176]. These fractures are often treated with surgical reconstruction and stabilization with fixation hardware in combination with bone grafts or other regenerative treatments as needed [177]. The complex nature of severe bone injuries often results in post-operative complications, which can lead to costly subsequent surgical and therapeutic intervention [178]. In addition to surgical repair, patients are often prescribed rehabilitation to promote functional recovery. However, rehabilitation regimens are often conservative and begin with extended periods of non-loading for up to 12 weeks, before progressing through partial weight bearing, range of motion and muscle

strengthening exercises, and full weight bearing [179,180]. Success of these rehabilitation regimens also relies on patients' discipline, communication, and judgment of pain and swelling [30]. After this extended process consisting of multiple surgeries and years of painful recovery, patients are often left with long-term disability due to extensive atrophy and fibrosis of the surrounding muscle and soft tissue, even in cases that are considered successful surgical management and bone repair [181–183]. [177,184]. These factors underscore the need for improved rehabilitation strategies that strive for consistent functional recovery of bone and surrounding tissue.

The emerging field of regenerative rehabilitation focuses on early integration of rehabilitation to enhance the body's capacity to restore function to the injured limb. It is well established that musculoskeletal cells and tissues (including bone) respond and adapt to mechanical stimuli, and that the relationship between fixation, tissue-level strains, and interfragmentary movement plays a pivotal role dictating the fracture healing process [50,185,186]. Fixation strategies that load the fracture site result in increased cartilage and chondrocytes in the bone regenerative niche, supporting the hypothesis that increased interfragmentary movement promotes endochondral ossification, whereas stable fixation promotes intramembranous ossification by shielding the fracture from strains [6,142,187]. However, fixation strategies resulting in excessive strain are detrimental to healing and result in non-union [188,189]. In the clinic, physical stimuli can modulate biochemical signaling pathways to stimulate the regenerative response of the target tissues [190]. Using this concept, researchers are leveraging mechanical stimuli for functional healing of weight-bearing musculoskeletal tissue.

Rehabilitation strategies for bone healing require a careful balance between the stability of the bone fixation system and the initiation of mechanical stimulation. Pre-clinical research has begun interrogating this balance through the modulation of fixation plate designs and subject

activity. However, lack of standardization between studies and models have led to conflicting results. Several studies have documented that low fixation stiffness is detrimental to healing, as it allows for excessive strain and interfragmentary motion [187,191,192]. Meanwhile, other studies have observed that increased fixation stiffness suppressed callus formation and subsequent bone healing compared to compliant fixation systems [15,142,193–195]. Researchers have also investigated how the onset of increased mechanical stimuli affects bone healing. Studies have demonstrated that reducing plate stiffness (i.e., dynamization) at 1 week post injury did not improve bone healing and impeded vascularization into the defect region [6,196]. Conversely, another study showed that dynamization at 1 or 2 weeks post injury led to improved regenerated bone volume and mechanical properties overall, but the course of healing occurred at a slower rate [197]. Similar trends were seen when dynamization began at 3-4 weeks post injury [6,7,192,198]. More recently, it was found that increasing plate stiffness after the initial callus formation (i.e., reverse dynamization) accelerated bone healing and mechanical strength [187,195,199,200]. Specifically, these studies found that increased mechanical stimulation promoted soft callus formation during the early phases of healing, while rigid fixation promoted mineralization in the later stages of bone healing [199]. This lack of consensus regarding the timing and magnitude of mechanical stimulation is largely due to the lack of standardization between studies regarding the methods and magnitude of mechanical stimulation, fixator stiffness, bone defect size, and animal model [201–203]. Regardless, the principles of mechanobiology suggest that healing responses depend on tissue-level strains. Thus, discrepancies in the literature may be resolved by investigating how individual rehabilitation strategies alter the transfer of ambulatory strains from fixation plates to the regenerative niche. Furthermore, this approach could identify optimal rehabilitation parameters to enhance healing and functional recovery.

Recently, implantable mechanical load sensors were developed to measure the mechanical stimuli experienced in implants and regenerating tissue. Windolf *et al.* developed an implantable load sensor that continuously monitored implant loading over several months of fracture healing [204]. The implantable sensor enabled the evaluation of bone healing in a sheep mid-shaft tibial osteotomy model and could eventually be utilized to evaluate patient healing and develop patient-specific treatment strategies [205]. Barcik *et al.* also employed a force sensor in sheep to measure the stiffness of the regenerated tissue. The fixator enabled this study to implement loading protocols that were modified based on healing progression [206]. These technologies have the potential to provide real time, continuous insight into the relationship between loading parameters and bone healing. However, target load parameters and load histories to stimulate bone formation have not yet been established.

Previously, our labs developed implantable, wireless strain sensors and coupled them with finite element models to longitudinally calculate the tissue-level strains following injury and rehabilitation [15]. In a study comparing stiff versus compliant fixation plates, we found that the compliant fixation group demonstrated improved mineralized bridging, 60% greater bone formation, and a two-fold increase in strain magnitude compared to the stiff fixation group [15]. However, torsional stiffness of regenerated femurs from either group did not reach that of intact, contralateral limbs, indicating the potential for further modulation to the local mechanical environment to improve functional healing [15]. Furthermore, defects were supplemented with bone morphogenetic protein 2 (BMP-2), which is rarely used for extremity trauma management in the clinic, limiting the generalizability of these results [207]. Beyond modulating fixation plate materials and design, the mechanical loads and tissue strains can be altered through rehabilitation intensity.

Other musculoskeletal injury models have found beneficial effects of increasing exercise intensity, however full characterization of rehabilitation parameters is still lacking in the field [12].

In this study, we aimed to elucidate the effects of strain within the regenerative niche on segmental bone healing in a rat model. To do so, we surgically created subcritical (2 mm) defects, allowed animals to recovery in sedentary conditions for 1 week, and then animals were either kept in sedentary conditions for the remainder of the study or randomly allocated to rehabilitation with a running wheel with (resistance rehab) or without (no resistance rehab) resistance that was applied by a programmable brake. The impact of rehabilitation on the local mechanical environment and subsequent bone healing was longitudinally monitored through a series of studies by using custom implantable strain sensors, radiographs, and microCT scans. Mechanical testing and histology of explant femurs were performed to investigate how the rehabilitation intensity impacted bone healing. Finally, subject-specific finite element simulations were performed to measure the strains within the regenerative niche based on longitudinal strain data from fixation plate sensors. We hypothesized that mechanical loads induced by resistance rehabilitation would result in increased local strains within the regenerative niche that would then accelerate bone formation and improve functional recovery. This approach may ultimately advance the field of regenerative rehabilitation by enabling data-informed rehabilitation decisions to improve functional recovery following complex bone injuries.

3.2 Methods

3.2.1 Strain Sensor Fabrication

A digital transceiver unit was developed as previously described [3]. This device relies on wireless Bluetooth Low-Energy (BLE) microcontroller (MCU) to receive commands and transmit data via a custom PC software (Visual Studio) and is powered by a 620 mAh lithium coin-cell

(CR2450, Panasonic). The transceiver unit was encased in a 3D printed housing unit with two multistranded stainless steel wires (A-M systems) connected to a strain sensor (EA-06-125BZ-350/E, Micro-measurements) integrated into a custom internal fixation plate used to stabilize the femoral defect. The internal fixation plate is radiolucent and fabricated with ultra-high-molecular-weight polyethylene (UHMWPE, Quadrant) to promote load sharing across the defect. Before implantation, each device was calibrated using a three-point bending flexural test on a tensile testing machine (TA Electroforce 3220) to physiologically relevant strain magnitudes [3].

3.2.2 Surgical Procedure

As previously described [3,15,101,142,207,208], unilateral 2 mm segmental defects were created in the left femur of 17-wk old female SASCO rats that weighed between 200-275 grams (Sprague Dawley, Charles River Labs). Rats were anesthetized by isoflurane (Vet One Fluriso) for the entire surgical procedure with rodent toe pinch and respiratory checks every 15 minutes. Rats were subcutaneously given a dose of 1 mg/kg of Slow-Release Buprenorphine based on their preoperative weight at 1mg/mL concentration immediately prior to surgery. During surgery, femurs were stabilized with load-sharing internal fixation plates prior to creating the defects [15]. Due to the novel technology involved in this study, we first performed a pilot study followed by a larger, follow up study (Fig. 10A**)**. A subset of animals within each group in the larger, follow up study were provided fixation plates integrated with strain sensors. For these animals, transceiver packs were mounted in the abdominal cavity and the wire connecting these pieces were subcutaneously fed through a keyhole incision in the abdominal wall superior to the left inguinal ligament. Defects were left empty to better discern the impact of exercise without biologic treatment as a confounding factor. Animals were randomly allocated to experimental groups: sedentary control, no resistance rehabilitation, or resistance rehabilitation. Postoperative

complications such as tissue necrosis, hardware failure, or signs of persistent mobility deficiency were considered exclusion criteria and resulted in early euthanasia (sedentary n = 2, no resistance n = 2, resistance n = 1). Animals without postoperative complications were euthanized by CO_2 asphyxiation after 8 weeks of recovery. All procedures were approved by the University of Oregon IACUC (20-32) or Atlanta Veteran's Affairs Medical Center IACUC (V019-19).

3.2.3 Voluntary Wheel Running and Housing Conditions

Prior to surgery, all rats were acclimated to running wheels where they had voluntary access to in-cage running wheels with no resistance applied (Scurry Rat Running Wheel, Lafayette Instruments®). After surgery, rats were singly housed in standard sedentary cages (Tecniplast rodent housing cage) and allowed 7 days to recover. All rats received nesting, enrichment materials including a PVC tube, crinkle paper, Nylabones, and nestlets before and after surgery. Non-sedentary animals were then granted voluntary access to a running wheel with either no resistance or pre-programmed 25%-40% body weight resistance applied via programmable brakes (rat brake, Lafayette Instruments®). Running wheels with resistance created higher intensity rehabilitation due to the friction between the resistance brake pad requiring greater force to move the wheel (Fig. 1b). Animals were weighed on a weekly basis and the resistance levels were changed to ensure resistance levels were maintained throughout the 7 weeks of rehabilitation. Running activity (m/day) was longitudinally monitored using onboard rotation monitoring sensors (Scurry Rat Activity Sensor, Lafayette Instruments®). Animals in the sedentary group were singly housed in standard cages with no wheel for the full 8-week recovery duration.

3.2.3 Wireless Strain Data Acquisition and Analysis

Strain measurements were transmitted in real-time via Bluetooth connection to a nearby laptop and plotted on a custom Microsoft Visual Studio C# graphical user interface (GUI) during

10-minute wheel running sessions performed twice weekly. These measurements started after the 7-day post injury recovery period and continued until the week 8 endpoint. Strain measurements were collected for animals with implanted sensors and given access to a wheel (no resistance and resistance animals). A custom MATLAB (Mathworks) script identified local maxima and minima pairs to track individual step cycles and compute the average 90^{th} percentile of strain amplitudes per animal across each week of post injury rehabilitation.

3.2.4 In Vivo MicroCT and Radiography

Animals were anesthetized with isoflurane (Vet One Fluriso) for in vivo radiography and microCT scans acquired at 2, 4, and 8 weeks post-injury. Digital radiographs were captured at 40 kV with a 7 s exposure time (Faxitron MX-20). MicroCT scans were performed using 48 µm voxel, 55 kVp, 145 µA, and 750 ms integration time (VivaCT 80, Scanco Medical). Radiographs were accessed for bridging by blinded scorers. Representative longitudinal 3D reconstructions were exported using Scanco software to track healing across weeks 2, 4, and 8.

3.2.5 Ex Vivo MicroCT and Biomechanical Testing

Animals were euthanized by CO_2 asphyxiation, left and right femurs were dissected and cleaned of soft tissue, fixation plates were carefully removed from the left femurs, and femurs were wrapped in PBS-soaked gauze and placed in 15mL conical tubes at 8 weeks post injury. Ex vivo microCT scans were performed by centering the conical tubes on the appropriate tube holder (VivaCT 80, Scanco Medical) and using 36 µm voxel, 70 kVp, 114 µA, and 200 ms integration time for the initial pilot study or 24 µm voxel, 55 kVp, 145 µA, and 750 ms integration time for the follow-up studies. A standard 1.5 mm long cylindrical volume of interest (VOI) was used to evaluate trabecular bone formation between intact bone ends of 2 mm segmental defects. Results were reported as bone volume (BV). After scans, all femurs were stored at –20 °C in phosphate

buffered saline (PBS) soaked gauze until biomechanical testing was performed 3 days later. As described in Klosterhoff *et al.*, explanted left (defect) and right (intact) femurs were biomechanically tested to determine the failure strength and torsional stiffness [15]. Ex vivo femurs were tested to failure in torsion at 3°/sec using a load frame (TA Electroforce 3220). Functional analysis involved inter-animal comparisons between defect (left) and intact (right) femurs as well as comparisons between the sedentary and resistance rehabilitation groups.

3.2.6 Finite Element Analysis

The mechanical environment (compressive and shear strain) in the rehabilitative niche was quantified by finite element simulations of one no resistance- and one resistance-running animal at 2- and 4-weeks post injury. First, an idealized geometric assembly of a left femur and fixation plate assembly was created from our previously published study [15]. Week two post-injury geometries were created by sectioning the intact idealized femur to create a 2.0 mm defect. The top and bottom of the defect were treated as fibrous ectopic tissue. The middle region of the defect comprising the granulation tissue was modeled by generating a cylinder between the proximal and distal ends of the femur. Week four post-injury geometries were similarly derived from the idealized initial geometry. Subject-specific defect geometries were extracted from microCT images and then the idealized femur was aligned with the visible portions of intact bone in the defect microCT images. Ectopic bone surfaces were approximated from radiographic measurements in the current study. All geometries were meshed with 10-node quadratic tetrahedral elements of a similar size as used in our previous models, which were validated by mesh convergence studies [15]. Nodes between model components were welded into a single compatible mesh such that contact did not need to be explicitly modeled. Geometries, volume meshes, and material property assignments were performed in Mimics and 3-Matic (Materialise). Simulations

were performed in FEBio (www.febio.org, version 3.7, Salt Lake City, UT) and results were visualized with FEBioStudio (version 2.0) [209].

All materials were modeled as isotropic elastic solids. The material coefficients for the sensor plate, riser, and intact femur were assigned from our previously published study [15]. The same homogenous material properties were assigned regardless of rehabilitation intervention since minimal healing and tissue differentiation were expected at 2-week post injury. Granulation tissue and fibrous tissues were assigned material coefficients from the literature (Supplemental Table 1,[210]). Material coefficients for the defects at 4-weeks post injury were derived from microCT image data. The Young's modulus was assigned to each finite element from the relationship $E = s_E\rho^{1.49}$ where s_E is a scalar (MPa) and ρ is the local image intensity (arbitrary units in the range [-1000, 12631]). The Poisson's ratio was assigned to each finite element from the relationship $\nu = s_\nu\rho^{0.64} + 0.166$ where s_ν is a scale factor (no units). These coefficients were selected so that the values agreed with prior literature (Supplemental Table 1, [15,210]). Ectopic growth was not entirely detected by the microCT images; thus, ectopic tissues were assumed to be homogenous with material coefficients derived from the literature [211].

Model loading and boundary conditions were prescribed similar to previous simulations (Supplemental Methods 1,[15,212]). The distal end of the femur was fixed in all directions. A spatially-varying pressure was assigned to facets on the surface of the femoral proximal surface from the Euler-Bernoulli beam-bending relationship seen in equation (1):

$$\sigma = \sigma_c + \sigma_{ml} + \sigma_{ap} = A\left(\frac{1+0.1202y-0.2404x}{total\ cortical\ area}\right). \quad (1)$$

The total normal stress σ was the sum of the axial compressive stress (σ_c), the bending stress about the medial-lateral axis (σ_{ml}), and the bending stress about the anterior-posterior axis (σ_{ap}). Here, x was the medial position of the element surface and y was the anterior position of the element

surface. The parameter *A* was iteratively varied until the average compressive (3rd principal Lagrange) strain across the fixation plate matched experimental measurements of compressive strain from the implantable strain sensors for each model (Supplemental Methods 2 and Supplemental Table 2). Compressive (3rd principal) and shear strain values were then extracted from the elements in the defect to generate descriptive statistics and comparative analyses between models. Elements from mineralized tissues were excluded to restrict the analysis to the granulation tissue.

3.2.7 Statistical Analysis

All statistical analyses were performed with Prism 9 (GraphPad) unless otherwise noted. Power calculation was performed with G*Power software using historical and pilot data to determine a sufficient group size of 7. Ordinary One-Way ANOVA with Tukey's multiple comparisons was used to compare endpoint bone volume across experimental groups. Mixed effect analyses were used to investigate which variables (time, rehabilitation condition, or the interaction) may contribute to difference in hindlimb functional outcomes differences between sedentary and no resistance animals. Average weekly distance (m/day) across time and between rehabilitation groups were assessed by multiple unpaired t-tests. Mixed effect analyses with Tukey's multiple comparisons were also utilized to investigate the mechanical properties of explanted femurs from animals in sedentary conditions versus resistance rehabilitation. Data are displayed as mean ± SEM since experimental groups had unequal sample sizes due to postoperative complications and the inclusion of multiple studies. Mann-Whitney U-tests were performed for measurements derived from FE simulations using Origin 2020b (OriginLab, Northampton, MA). Statistical significance is shown with asterisks and exact p-values are listed in figure headings.

3.3 Results

3.3.1 Resistance rehabilitation starting week one post-injury improved bone healing

The effect of rehabilitation intensity on bone healing was assessed using a femoral segmental 2 mm bone defect model, which is on the cusp of a critically-sized bone defect. Bone regeneration was assessed longitudinally by radiographs and microCT. After 8 weeks of recovery, 50% of sedentary animal femurs (n = 8) experienced bridging compared to 90% of rehabilitated animal femurs (no resistance rehabilitation, n = 4, resistance rehabilitation, n = 9), suggesting that a 2 mm segmental bone defect in female Sprague Dawley rats is not consistently critically-sized

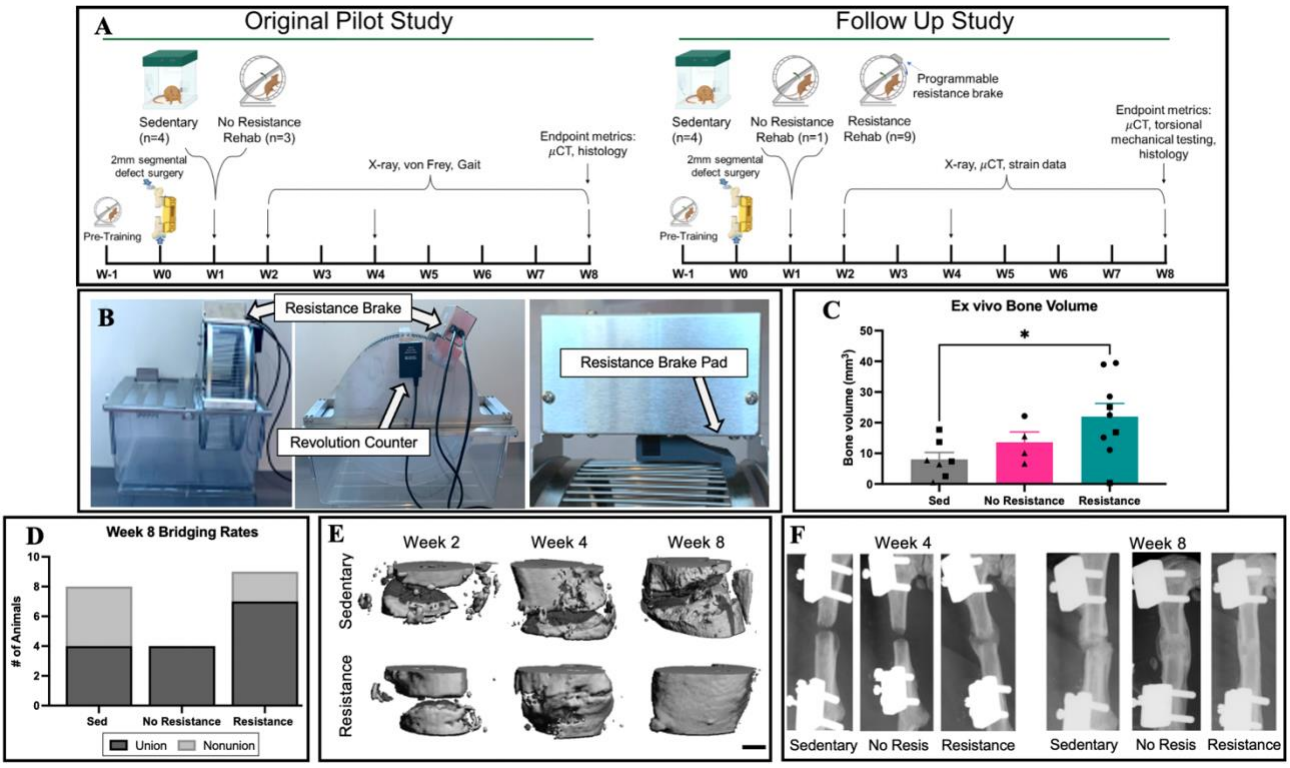

Figure 10. Resistance rehabilitation starting one-week post-injury improved bone healing. **(A)** Schematic overview of pilot and follow up studies. **(B)** Rehabilitation implemented commercial running wheels (Scurry Rat Running Wheel, Lafayette Instruments®) equipped with counters and programmable breaks that can apply resistance and track individual subject's running activity (number of rotations or distance). Resistance brake pads were modified in-house to apply more consistent friction along the lateral edge of the running wheel. **(C)** Bone volume within centered 1.5 mm of 2 mm defects after 8 weeks of recovery. * p = 0.0306, ordinary one-way Anova with Tukey's multiple comparisons test. Mean ± standard error. **(D)** Contingency graph of week 8 bridging rates. p = 0.17, Chi-Square test. **(E-F)** *In vivo* representative radiographs and microCT reconstructions reveal early callus formation and consolidation for resistance rehabilitation group only. Scale bar = 1 mm. Triangles = pilot study, squares = follow up study, and circles = animals with sensors implantation from the follow up study. No statistical difference is seen across studies for bone volume results.

(Fig. 10D). Resistance rehabilitation was associated with significantly greater bone volume within the defect region of microCT scans when compared to sedentary counterparts (Fig. 10C). In addition, early (4 week) callus formation and mature callus consolidation (week 8) were only observed in radiographs of resistance rehabilitation animals (Fig. 10F). Although the majority of femurs from sedentary and no resistance animals were bridged by week 8, representative radiographs and microCT reconstructions revealed distinguishably less dense tissue compared to intact bone throughout the defect region, suggesting less mature healing (Fig. 10E-F). Taken together, resistance rehabilitation starting one-week post-injury was shown to improve bone formation which may be explained by higher intensity exercise leading to early callus formation and more mature healing within our 8-week timeframe.

Histological analysis for representative sedentary and resistance rehabilitation animals at week 8 suggests different mechanisms of bone formation across groups (n = 1) (Fig. 11). In

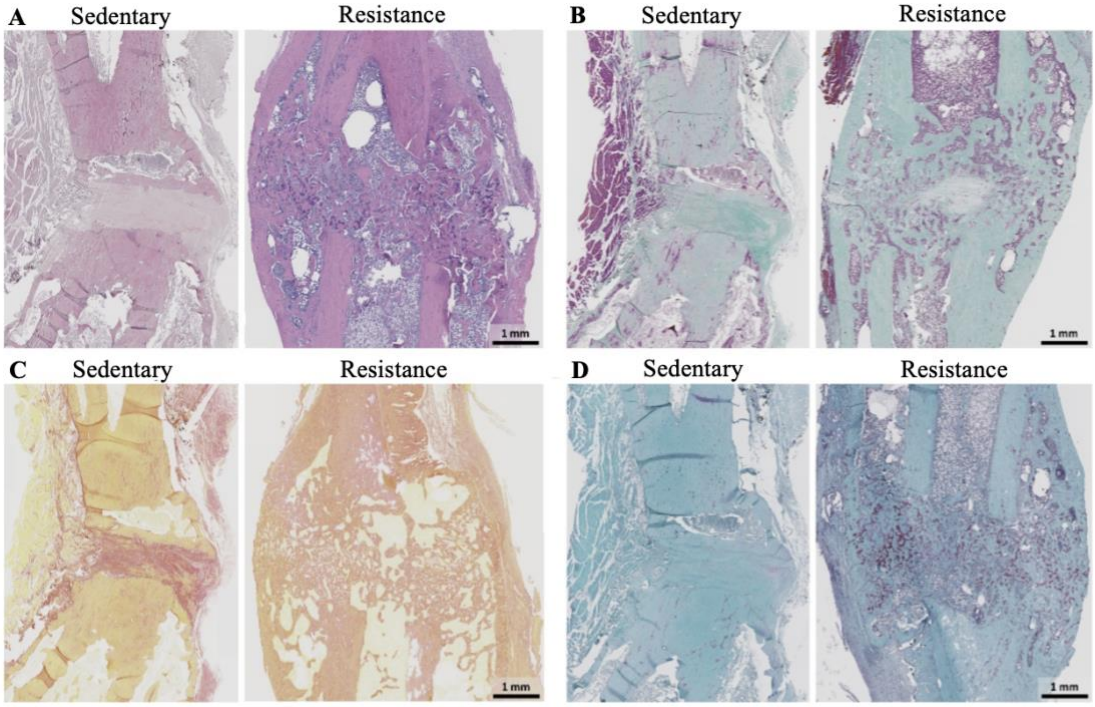

Figure 11. Representative histological analysis of regenerated bone at week 8 with the following stains: **(A)** H&E, **(B)** Goldner's Trichrome, **(C)** Picrosirius Red, and **(D)** Safranin O. Scale bar = 1 mm.

sedentary animals, appositional bone formation extends from both ends of the bone with fibrous tissue in the center, while the resistance animals displayed a robust callus bridging the defect site (Fig. 11A-B). Fibrous tissue was visible in the center of the defect in the sedentary rats, while both cartilage and woven bone were visible in the callus of the resistance group (Fig. 11C-D). This suggested that this bone regenerated through endochondral ossification (Fig. 11C-D). This is corroborated by data from the literature demonstrating that lower strains correspond to appositional bone formation, while greater strains promote endochondral ossification [213–215].

To investigate the impact of resistance rehabilitation on the mechanical properties of the regenerated tissue compared to sedentary counterparts, we performed torsion testing to failure of

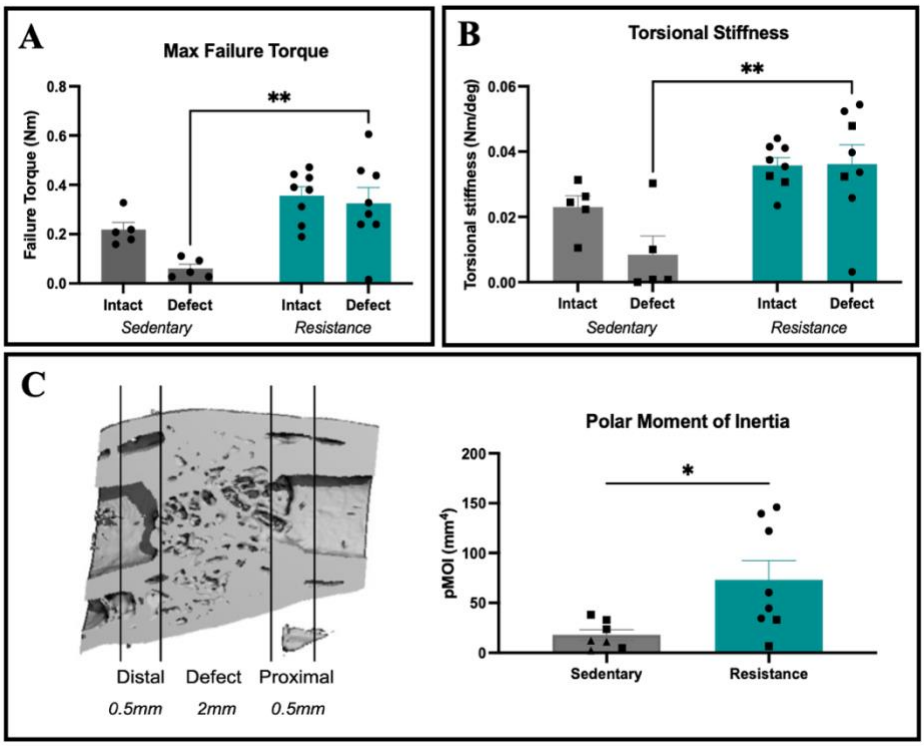

Figure 12. Resistance rehabilitation led to improved mechanical strength of regenerated femurs that matched intact femurs. **(A)** Failure torque of ex vivo femurs under 3°/sec ramp, ** p = 0.0023 for sedentary defect versus resistance defect, mixed-effects analysis with Tukey's multiple comparisons. Mean ± standard error. **(B)** Torsional stiffness was assessed as the slope of the linear region of the torque-rotation curve. ** p= 0.0013 for sedentary defect versus resistance defect, mixed-effects analysis with Tukey's multiple comparisons. Mean ± standard error. **(C-D)** *Ex vivo* polar moment of inertia calculated over 3 mm mid-diaphysis region depicted in microCT reconstructions cross-section. * p = 0.0213, two-tailed unpaired t-test. Mean ± standard error. Squares = follow up study, and circles = animals with sensors implantation from the follow up study. No statistical difference was seen between

the defect and intact femurs. Torsional mechanical testing revealed that resistance rehabilitation (n = 9) increased failure torque and torsional stiffness of defect limbs compared to those from sedentary animals (n = 5) (Fig. 12A-B). Furthermore, resistance rehabilitation led to tissue healing with mechanical properties that matched intact femurs (Fig. 12A-B). Data were fitted to a linear mixed effects model with Tukey's multiple comparisons which revealed a significant effect of rehabilitation condition on the endpoint failure torque (p-value = 0.0041) and torsional stiffness (p-value = 0.0050). Polar moment of inertia of the defect region and bone ends was also significantly increased for rats that underwent resistance rehabilitation compared to sedentary counterparts **(**Fig. 12C**)**. These results were consistent with the greater callus formation observed in our histology and radiography. Taken together, resistance rehabilitation led to improved healing and mechanical strength of femurs compared to sedentary animals.

3.3.2 FEA revealed resistance rehabilitation increased compressive and shear strain within the regenerative niche

Physical rehabilitation is a promising approach to mechanically stimulate the regenerative niche and encourage the body's endogenous capacity to heal. Variability in rehabilitation regimens as well as the dependence of tissue differentiation on load onset and magnitude makes it difficult to establish a consensus from the existing literature. Therefore, we assessed the temporal progression of mechanical cues by measuring internal bone plate strain during running wheel activity starting one week after surgery in a subset of the the no resistance and resistance rehabilitation groups (n = 1-3). Furthermore, *in vivo* ambulatory strain measurements were monitored in a subject-specific, real-time manner by our previously developed and validated strain sensor integrated that we integrated into the internal fixation plates [3]. Dynamic strain cycle amplitudes corresponding to individual steps were computed from strain sensor measurements and

the 90th percentile strain magnitudes were recorded for 7 weeks of post injury rehabilitative running (Fig. 13C). Ambulatory strains across the fixation plate gradually declined until bridging

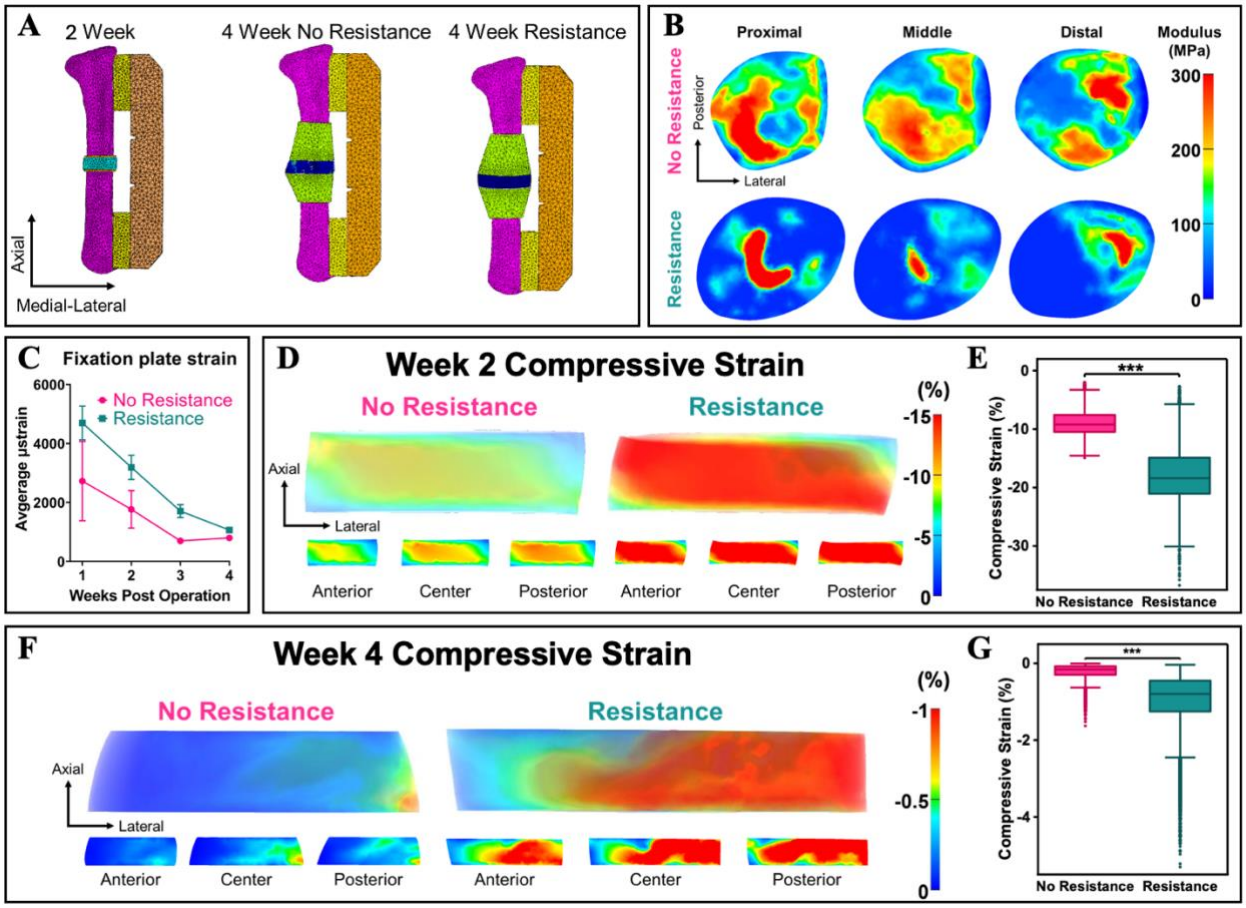

Figure 13. Rehabilitation intensity modulates defect-level strain distributions. **(A)** Finite element meshes used to evaluate transfer of loads during ambulation between the fixation plates and defects for individual animals. **(B)** Transverse plane slices show the spatial distribution of the Young's modulus for the week 4 models. The no resistance defect displayed intermediate tissue differentiation throughout while the resistance defect only displayed tissue maturation near the intact femur. **(C)** Longitudinal graph of the fixation plate strain as a function of rehabilitation time. The strain decreased as healing progressed, but resistance was associated with higher strains across all weeks. Mean ± standard error. **(D-E)** 2 week post injury results. **(D)** Finite element predictions of 3rd principal (compressive) strain for defect regions are presented in the transverse plane with transparent renderings and slice plots. Strains at 2 week post injury formed a diagonal band between the proximal-medial and distal-lateral regions of the defect. Resistance led to an increase by a factor of 2.0 in the average compressive strain. **(E)** Resistance rehabilitation resulted in significantly higher predictions of mean compressive strain within the defect at week 2. ***: $p < 0.001$, Mann-Whitney U test. Error bars represent 1.5 x inter-quartile range (IQR). **(F-G)** 4 week post injury results. **(F)** Finite element predictions of 3rd principal strain at 4 weeks post injury. Strain is concentrated on the lateral and central regions of the defects. Resistance led to a greater than 4-fold increase in the average strain. **(G)** Resistance rehabilitation resulted in significantly higher predictions of mean compressive strain within the defect at week 4. ***: $p < 0.001$, Mann-Whitney U test. Error bars represent 1.5 x IQR.

was observed in radiographs and microCT scans **(**Fig. 13C**)**, which is consistent with previous literature [15]. FE models were then developed using ambulatory strains and microCT images to predict the defect level strains for each physical rehabilitation regimen at weeks 2 or 4 post-injury **(**Fig. 13A**)**. On average, resistance rehabilitation was associated with a 2.2-fold increase in plate compression throughout week 2 post-injury (Table 1). FE simulations for one representative animal in each group indicated a significant, 2.0-fold increase in 3rd principal strain within the defect region due to resistance ($n = 1$) ($p < 0.001$; Fig. 13D-E**)**. For these simulations, compressive strain was greatest in the region spanning the proximal-medial and distal-lateral ends of the defect. Similar trends were observed for shear strain ($p < 0.001$: Fig. 14). Throughout week 4 post-injury, resistance was associated with an 3.3-fold increase in plate compressive strain and a significant, 4.45-fold in defect compressive strain due to resistance ($p < 0.001$; Fig. 13F-G). Here, compressive strain was greatest on the lateral ends of the bones near the interfaces between intact femurs and defect tissues. Again, similar trends were observed for shear strain in response to resistance rehabilitation (p-value < 0.001; Fig. 14). To approximate the changes in strain transfer between the fixation

Time	Rehab Protocol	Modulus (MPa)	Poisson's Ratio	Plate Compression (μstrain)	Defect Compressive Strain (%)	Defect Shear Strain (%)	Defect/Plate Strain Ratio
2 wk	No-Resistance	1.0	0.17	1,088 ± 54	-8.9 ± 2.2	5.4 ± 1.3	81.8
2 wk	Resistance	1.0	0.17	2,422 ± 345	-17.8 ± 4.9	11.0 ± 2.9	73.5
4 wk	No-Resistance	134.0 ± 83.7	0.22 ± 0.03	228 ± 25	-0.22 ± 0.19	0.15 ± 0.11	9.7

Table 1. Summary of material properties used in the model and defect mechanics throughout healing from strain sensors and FE simulations.

plates and the healing defects, we measured the ratio of the average compressive strain in the defect to measured compressive strain on the plate surface. There was a drastic reduction in this metric

between weeks 2 and 4 for both animals (over 8-fold for the no-resistance subject, over 6-fold for the resistance running subject) due to bone formation in defects. Notably, defect/plate strain ratio was greater in the no resistance running animal at week 2, but the defect/plate strain ratio was greater in the resistance running animal at week 4.

3.4 Discussion

The benefits of mechanical stimulation for musculoskeletal repair have been investigated using strategies such as axial loading via flexible fracture fixation [7,15,216] and controlled mechanical loaders [217], low-frequency vibration treatment [218], and ultrasonic stimulation [219,220]. However, there remains a clinical need for data-informed rehabilitation regimens, and a better understanding of how principles of mechanobiology are translated into clinical decisions that improve functional outcomes. To address this need, we investigated the impact of running intensity during rehabilitation on healing outcomes and tissue biomechanics throughout the course of bone healing. Femurs with segmental defects were stabilized with compliant fixation plates integrated with sensors that measured local axial strain during low (no resistance) versus high (resistance) intensity running. Bone healing was monitored via longitudinal radiographs, microCT scans, as well as endpoint mechanical testing and histology. Our findings provides critical insight into the effects of rehabilitation intensity on bone healing after a segmental bone defect.

This study sought to assess bone healing after implementing a more rigorous rehabilitation protocol compared with our previous work that found improved bone formation with treadmill walking in combination with a low dose of local BMP-2 growth factor therapy [15]. In the present study, we utilized a smaller defect so the bone healing results was independent of exogenous growth factor dosing. Animals were provided voluntary access to running wheels, facilitating daily running activity (m/day) that were at least 10x greater than treadmill running regimens [15].

Furthermore, we utilized resistance brakes to modulate rehabilitation intensity. Resistance rehabilitation that started one-week post-injury not only induced significant improvement in bone formation and recovery of mechanical properties compared to sedentary counterparts, but preliminary results suggested early rehabilitation improved tactile pain response. It is widely known that mechanical stimuli are sensed by tissues and cells, which respond by releasing signaling molecules; however the underlying mechanisms are poorly understood [221,222]. One of the many responses impacted by mechanical stimuli is the inflammatory response, which is known to decrease in response to long-term exercise, potentially resulting in reduced pain [222,223]. Resistance rehabilitation with compliant fixation significantly increased the failure torque and torsional stiffness of the defect femurs as compared to femurs from sedentary counterparts. Although not significant, the failure torque ($p = 0.1337$) and torsional stiffness ($p = 0.1719$) of intact femurs had an increasing trend for animals that underwent resistance training compared to femurs from sedentary counterparts. These data suggest that early resistance rehabilitation results in bone adaptation in the non-injured limb to withstand greater loads induced by resistance running, which is consistent with previous literature [186,224–227]. After segmental defect surgery, early resistance rehabilitation led to increased bone healing and strength and promoted full restoration of mechanical properties, which had not been previously achieved in our compliant fixation model. Unsurprisingly, implantable strain sensors measured an increase in fixation plate strain for resistance running animals compared to no resistance animals. Subject-specific finite element models revealed that resistance running induced a beneficial increase in compressive and shear strains within the regenerative niche as compared to no resistance running throughout weeks two and four post-injury (Fig. 13 and 14). Overall, our data support resistance rehabilitation, starting one-week post-injury, as a promising therapeutic to increase bone formation, bone healing

strength, and promote full restoration of mechanical properties to intact levels for defects on the margin of critically sized without the use of biologics.

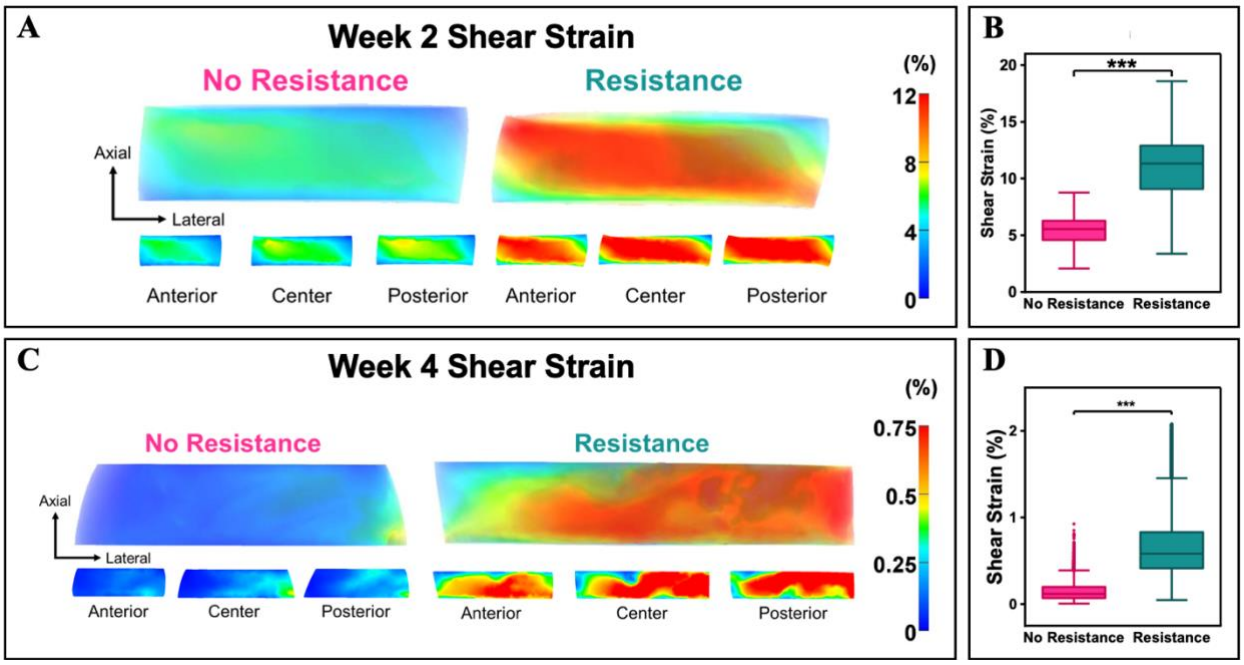

Figure 14. Lagrange shear strain maps through 2- and 4-weeks post-injury. **(A)** Finite element results for defect regions are presented in the transverse plane with transparent renderings and slice plots. Strains at 2 week formed a diagonal band between the proximal-medial and distal-lateral regions of the defect. **(B)** Shear strain distributions differed with rehabilitation regimen. ***: $p < 0.001$, Mann-Whitney U test. **(C)** Finite element results for animals through week four post injury. Strain at 4 weeks post injury is more concentrated on the lateral, central regions of the defects. **(D)** Compressive strain distributions differed with rehabilitation regimen. ***: $p < 0.001$, Mann-Whitney U test.

The increased compressive and shear strains associated with resistance rehabilitation had a beneficial effect on healing of near critically-sized bone injuries; however, excessive strain can be deleterious. Boerckel *et al.* quantified the effect of early and delayed loading on neovascular growth in a rat model of 8 mm bone defect regeneration using compliant fixation plates [6]. In their study, fixation plates were unlocked to allow transfer of ambulatory loads to the defect either at the time of implantation or after 4 weeks of stiff fixation [6]. Early mechanical loading significantly reduced bone formation by 75% compared to stiff plate controls, which suggested that early loading of high magnitudes in a large defect is deleterious to healing [6]. Previous work by Ruehle *et al.* also found that immediate loading inhibited neovessel sprout tip cell selection and

angiogenesis while delayed loading (five days) enhanced vascularization, suggesting the need for a brief, critical period of recovery prior to loading [16]. In acknowledgement of this necessary period of delay, we initiated resistance rehabilitation one-week post operation, resulting in enhanced bone healing of 2 mm segmental defects. However, the variable bone healing results across the literature highlight the significant need for personalized platforms to assess the impact of ambulatory loads on the local mechanical environment throughout healing.

Several studies have investigated how ambulatory load transfers allowed via compliant fixation plates impact healing of critically-sized bone defects treated with BMP-2 [6,7,15,195,228]. Boerckel *et al.* compared healing of 6mm defects stabilized with either a stiff fixation plate or a compliant plate and treated with 5 micrograms BMP-2. They found that delaying ambulatory loading until week 4 increased bone formation but did not result in mechanical restoration to intact levels. Similarly, Klosterhoff *et al.* compared healing of 6mm defects treated with 2 micrograms BMP-2 and stabilized by either a stiff or compliant fixation plate [15]. Animals were also granted 20 minutes of treadmill walking per week starting after one week of recovery. Compliant fixation and treadmill walking resulted in increased compressive strain magnitudes, bridging rates, and bone formation, however, similarly did not achieve mechanical restoration [15]. Glatt *et al.*, also compared healing of 5mm defects treated with 11 micrograms of BMP-2 and stabilized with external fixation plates at different stiffnesses [228]. Radiographs and histology revealed that low stiffness fixation produced the best healing after eight weeks [228]. A follow-up study then assessed healing due to constant fixation stiffness or reverse dynamization (fixation stiffness was increased after 2 weeks). MicroCT, histology, and radiographs revealed that reverse dynamization resulted in greater bone formation and mechanical properties that matched intact levels. All these studies found promising bone healing results with different loading regimens and timing, suggesting that bone healing

response is more complex than merely a single strain value threshold. In addition, these studies did not result in complete functional restoration. It is also worth noting that these studies all supplemented rehabilitation with BMP-2, which has been established as a robust bone forming growth factor, [101,207,208,229,230] and is likely a confounding factor in these healing results. In comparison, we found that resistance running significantly increase bone formation as compared to sedentary counterparts and restored femurs to intact strength without the use of biologics.

Although mechanical loading has been a longstanding therapeutic for musculoskeletal injuries, the magnitude of loading through all stages of fracture healing is not well understood [225,231,232], largely because of the technological challenges of acquiring accurate, local measurements. We addressed this hurdle by utilizing implantable strain sensors to track longitudinal, real-time measurements of bone plate strain throughout rehabilitative activities to assess healing and predict bone healing well before radiographic evidence. In fact, the relationship between early strain amplitudes and healing outcomes previously revealed a significant positive relationship between strain amplitude one week after injury and regenerated bone volume after 8 weeks of healing [15]. For the present study, these same sensors revealed that resistance running increased local strains across the fixation plate and within the regenerative niche, which led to improved bone healing of 2 mm bone defects. A limitation of the sensor platform used for these rodent studies is that it requires a transceiver pack and has a restricted battery life. Further development of battery-free sensors that do not require a transceiver could facilitate clinical translation and potentially enable data-informed revisions to rehabilitation parameters that improve functional healing.

The goal of this study was to explore how rehabilitation intensity can be utilized to produce mechanical loading advantageous to bone healing of defects on the margin of critically-sized. We

previously used finite element simulation to predict the difference in defect-level mechanics facilitated by stiff or compliant fixation plates supporting 6mm defects during two weekly, 10-minute treadmill walking at 3 weeks post injury [15]. Defects supported by compliant fixation plates experienced a 60% increase in bone formation when compared to defects supported by stiff fixation plates. Compliant plates facilitated defect compression between ~1-6% while stiff plates facilitated compression below 1%. In the present study, only a compliant plate was used, and animals were provided unrestricted access to running wheels with or without resistance. Both the prior and present studies began rehabilitation at 1- week post injury. We found that resistance rehabilitation facilitated defect compression in the ~1-6% range at 4 weeks post injury while rehabilitation without resistance facilitated defect compression in the ~0-2% range. Thus, compression in the range of ~1-5% strain at 3-4 weeks in the course of healing was associated with greater bone formation in both the previous and current studies. Notably, increased rehabilitation intensity was necessary to achieve a similar range of compression in this study. This was likely due to differences in defect geometry and severity of trauma. Researchers have also previously proposed that maintaining a 2-10% strain between fracture ends enables relatively stable secondary fracture healing, while excessive or insufficient strain may affect secondary healing and lead to non-union or delayed union [225,233–237]. However, these observations were made without implantable sensors to track local biomechanics longitudinally, and they relied on various animal models, defect sizes, and fixation strategies. Nevertheless, we found that defect compressive strains for both no resistance and resistance animals were on the higher end of this range after 1 week of rehabilitation. These data demonstrate the importance and potential of patient-specific pre-surgical planning and rehabilitation protocols based on the condition of each injury [238,239].

Literature has established that cage enrichment improves the mental and physical fitness of laboratory rodents including rats [240]. Recent work has also found that psychosocial stress can negatively impact fracture healing, while free-running wheel access is highly rewarding to rodents [241–243]. The healing improvements in the rehabilitation groups could be partially explained by the improved fitness state of these animals, with resistance potentially intensifying the impact of exercise on the whole fitness of the animal. However, sedentary rats received enrichment throughout recovery to support their mental and physical fitness as well. All groups were housed in conditions that minimized stress and provided rewarding enrichment.

In this study, several limitations are worth noting including (1) only female animals were included (2) resistance varied with each revolution during wheel running (3) not all groups were included in each study, and (4) simplification were made for computational models of tissue material behavior. First, female rats were selected to avoid confounding complications due to the rapid skeletal growth and weight gain observed in male rodents. Future work is warranted to investigate the effect of sex on rehabilitation-induced bone regeneration. Second, the resistance brakes exhibited variable resistance throughout each revolution due to brake pad pressure on a spinning wheel that was not perfectly true. The inconsistent resistance level was not fully quantified, but the increased strain on the defect was measured. Third, due to the novel technology that this work involved, we performed a pilot study followed by a larger study to mitigate the chances of unwarranted pain or suffering of rodents. Study conditions did not significantly impact bone volume and mechanical testing data, thus allowing us to combine results to investigate statistical differences between experimental groups. In addition, all rodents were the same strain, sex, and age, and they all underwent similar orthopedic procedures. A final limitation of the study is the choice of linear isotropic elastic solids for computational modeling of tissue material

behavior. This simplification neglects the viscoelastic and fluid properties of healing bone. Nonetheless, this assumption is appropriate for the purpose of quantifying the average ambulatory load transfer to the regenerative niche. Bone growth and remodeling occur on a much larger time scale than ambulatory loads (weeks-months versus seconds). Previous computational models of tissue differentiation have found that tissue growth kinetics are primarily affected by the transient (i.e., steady state, time-averaged) stress rather than the dynamic stress [244,245]. Thus, we chose not to model viscoelasticity or fluid motion for this study.

Overall, our findings support early resistance running as a post injury treatment for near critically-sized segmental bone defects because it facilitated advantageous loading conditions, which resulted in improved bone healing. Previous literature is contradictory on whether early ambulatory loads are advantageous or deleterious to healing, highlighting the need for personalized measurements to inform rehabilitation decisions that accommodates for fracture type, geometry, and severity [6,7,15,228]. We combined implantable strain sensors and FEA to highlight a promising platform for tracking patient-specific, real-time defect strains throughout rehabilitation and healing. Future efforts will take advantage of this platform to identify rehabilitation revisions in real-time during rehabilitation in hopes of improving and accelerating functional recovery after traumatic bone injury.

CHAPTER 4: PATIENT-SPECIFIC MULTIVARIATE MODELING FOR REGENERATIVE REHABILITATION OF BONE HEALING

Contents of this chapter have been adapted from Williams K.E., Muhib F., Dinh E., Leguineche K., Hajarizadeh A., Rosenthal J.W., Guyer T., Seah T., Willett N.J., Weiss J.A., and Guldberg R.E., (submitted 2024). Science Advances [246].

Author contributions

Conceptualization: KEW, FM, NJW, JAW, REG

Data Collection and Analysis: KEW, FM, ED, AH, JWR, TG, TS

Interpretation: KEW, FM, JAW, REG

Writing and Editing: KEW, FM, KL, AH, JAW, REG

4.1 Introduction

Complex bone injuries continue to exhibit high complication rates and poor functional recovery, partially due to the insufficient understanding of how rehabilitative loading impacts bone healing. Severe bone defects require surgery to place stabilization hardware followed by postoperative rehabilitation [177]. Prescribed rehabilitation heavily relies on patient-based subjective feedback on pain levels, hard-to-interpret radiographs, and the intuition and experience of physicians [179,180]. The lack of quantitative metrics to inform rehabilitation decisions has led to conservative recommendations that often involve weeks of non-loading [247]. Although animal segmental bone defect models have shown that loading starting one week after injury improved bone healing, these insights have had limited impact on clinical rehabilitation approaches [15,65,142]. Therefore, a better understanding of how early rehabilitation conditions impact bones' endogenous potential to regenerate is crucial to aid in the clinical approach to post-injury rehabilitation. Further, technology that enables quantitative subject-specific

monitoring to inform clinical rehabilitation decisions is critical to advance rehabilitation strategies.

Decades of literature has established that bone is a mechanoresponsive tissue [6,7,15,142,216,227,228,231,232,237]. The idea that mechanical stimuli result in bone adaptation was advanced by Wolff *et al.,* whose early theories promoted the idea that intact bones remodel in response to functional loading patterns [248]. Since then, extensive research has found that loading can also aid in bone repair by improving callus formation, consolidation, and remodeling [15,225,249,250]. However, research has also found that excessive loading can severely disrupt important regeneration programs like revascularization and callous consolidation, resulting in nonunion [6,65]. Most loading strategies designed to facilitate bone healing have focused on structured loading regimens that are controlled by fixation plate stiffness or loading apparatuses, which have limited clinical applicability [6,7,15,142,191,192,195,200,228,251–256]. Perren, Claes, and several others have identified interfragmentary strain as a critical factor in fracture healing, which motivated a large focus on the local mechanical environment after bone injury [235,257–260]. Several animal and human studies found impaired bone healing when stabilized with fixation that is either too flexible or too rigid [6,261–264]. For instance, high magnitude strains at a fracture site, due to inadequate stability or excessive loading, can result in fibrous tissue, inhibiting initial callus formation and often resulting in fibrous non-union [261,262]. Paradoxically, some studies have also demonstrated that excessively rigid fixation may impair fracture healing as well [15,225,265,266]. These studies often investigate one or two variables at a time (e.g. loading magnitude, loading rate, fixation plate stiffness, etc). However, clinical rehabilitation following musculoskeletal injuries inevitably involves multiple rehabilitation parameters that simultaneously influence healing. In this study, we used a segmental bone defect, ad lib wheel running, and revolution

counters to track subject-specific activity and calculate six exercise parameters (running duration, running distance, number of running bouts, running bout duration, running velocity, and daily rest time) to ultimately investigate their multifactorial influence on bone healing.

Previous preclinical research on rehabilitative loading has largely focused on the effects of load magnitude and timing on bone formation. These studies utilized a rodent segmental defect model with similar femur fixation hardware and surgical approaches as our current study. Bone healing outcomes throughout these studies depended on the magnitude of loading (determined by fixation hardware stiffness), the post-injury onset of loading, and the concentration of local biologics. In a rat femoral defect model, Boerckel *et al.* sought to investigate how the timing of load onset impacted bone healing. They used a stabilization plate with a locking mechanism that changed plate stiffness when deployed. Immediately unlocking the plate postoperatively resulted in high magnitude strains that significantly inhibited bone formation after 8 mm defects that were treated with low dose Bone Morphogenetic Protein-2 (BMP-2), primarily by disrupting revascularization. In contrast, unlocking the plate after callus formation (week 4) was beneficial [6]. Klosterhoff *et al.* also investigated how fixation plate stiffness impacted bone healing without dynamic changes in plate stiffness. They found that fixation with lower stiffness facilitated an increase in compressive strains within the regenerative niche during treadmill walking, which ultimately led to improved bridging rates and bone formation in a 6 mm defect treated with low dose BMP-2 [15]. In this study, the lower stiffness hardware was relatively more rigid than the unlocked fixation strategy from Boerckel *et al.* that inhibited healing, underscoring the need to more thoroughly characterize local strains [6,15]. Importantly, these studies delivered local BMP-2, a well-established biologic that robustly induces ossification [13,207,267]. The use of BMP-2 confounds an understanding of the inherent

mechanosensitive response by directing earlier, more significant cartilage and mineral deposition [268–270].

To eliminate the use of biologics, Williams and Harrer *et al.* explored how rehabilitation intensity can be utilized to produce loading magnitudes advantageous to bone healing after segmental bone injuries that were not treated with BMP-2 [175]. A segmental 2 mm bone defect in rat femurs exhibit variable spontaneous bridging rates, making it ideal for assessing the potential of mechanical loading regimens to direct bone healing without the need for biologics. This also addresses a significant blind spot in the literature, which generally focuses on very large supercritical defects or small osteotomies that heal via intramembranous ossification. Animals exercised on a running wheel with or without friction applied, producing high (resistance) versus low (no resistance) intensity rehabilitation conditions. Resistance rehabilitation that began one week after injury resulted in increased compressive strain within the regenerative niche, increased bone formation compared to sedentary counterparts, and restored femora mechanical properties to intact strength [175]. These previous studies have revealed the importance of loading onset and magnitude on both critically (6 – 8 mm) and near-critically sized bone defects (2 mm). Despite these crucial insights into the mechanobiology principles of bone healing, there remains a need for more studies to track and analyze multiple rehabilitation paramters to understand their combined influence on bone healing.

In this study, we sought to examine the combined effect of several rehabilitation parameters on bone injuries of two different sizes, motivated by the goal of subject-specific rehabilitation. We surgically created 2 and 3 mm bilateral segmental bone defects in rodent femurs that were stabilized with internal fixation plates. After surgery, we allowed animals to recover in sedentary conditions for one week, and then randomly assigned them to either

sedentary conditions or one of three rehabilitation conditions. Experimental groups included sedentary controls, low distance rehabilitation controls (2 hrs/day of wheel access with restricted distance), restricted rehabilitation (2 hrs/day of wheel access), and unrestricted rehabilitation (24/7 of wheel access). Rehabilitation parameters (running duration, running distance, number of running bouts, running bout duration, running velocity, and daily rest time) and subsequent bone healing were longitudinally monitored via revolution counters on the running wheels and radiographs and microCT scans, respectively. Explanted femora underwent histology to investigate how rehabilitation conditions impacted tissue-level adaptations for representative subjects. Subject-specific finite element (FE) analyses were also performed to track strains within the regenerative niche in response to rehabilitation conditions, mineralization status, and injury size. AI-based, genetic programming algorithms were also used to evaluate the multifactorial effect of rehabilitation on bone healing outcomes. Building on the working theory that bone healing requires a balanced loading regimen, we hypothesized that restricted rehabilitation would increase the bridging rates and endpoint bone volume compared to unrestricted rehabilitation and sedentary controls. We also hypothesized that the impact of rehabilitation would depend on injury severity due to different biological needs and mechanosensitivity.

4.2 Methods

4.2.1 Surgical Procedure

As previously described, 17-week old female Wistar (Envigo) rats that weighed between 275-325 grams received bilateral femoral 2 and 3 mm segmental bone defects (10). This study utilized 28 animals, totaling to 56 segmental bone defects. After defects were made, femora were stabilized with compliant (Ultra-High Molecular Weight Polyethylene) internal fixation plates

with a flexural stiffness of 145.2 $\pm$ 10.6 N/mm based on previous characterization [3,15]. Defects were left empty, and animals were randomly allocated to rehabilitation groups (sedentary control, restricted rehabilitation and unrestricted rehabilitation). Due to unexpected similarities in running distance between the restricted and unrestricted rehabilitation groups, we later added a low distance control group that underwent identical surgical conditions. Immediately prior to surgery rodents were given a subcutaneous dose of 1 mg/kg of Sustained-Release Buprenorphine based on their pre-operative weight and 3 mL of Lactated-Ringer solution (VetOne). An additional 2 mL of Lactated-Ringer solution was given subcutaneously every 24 hours throughout the first 3 days of recovery. 48 hours after surgery, rodents were given standard Buprenorphine subcutaneously at a dose of 0.03 mg/kg. Postoperative complications such as hardware failure were considered exclusion criteria and resulted in early euthanasia (low distance control: n = 1 and unrestricted rehabilitation: n = 2) bringing the total number of animals to 25 animals and 50 segmental bone defects (n = 5-7 defects per group). Animals that did not experience complications were euthanized by CO2 asphyxiation at 8 weeks and representative femora were harvested for histology. All procedures were approved by the University of Oregon IACUC (Protocol 20-32).

4.2.2 Voluntary Treadmill Running

Prior to surgery, rats were pre-trained for a 14-day period where they had voluntary access to in-cage running wheels (Exotic Nutrition, 14”). Running wheels were modified in-house to allow continual activity data collection via revolution counters (Lafayette Instruments®). Both the wheels and revolution counters were mounted in standard cage bottoms via 3D printed parts. After surgery, rats were individually housed in standard cages (Tecniplast) and given 7 days to recover with no wheel access. After recovery, sedentary animals remained in standard cages with no wheel access and non-sedentary animals followed specific rehabilitation regimens. The restricted

rehabilitation group was singly housed in a standard cage and manually transferred to their wheel cages from 8-10 pm daily for their 2 hrs/day of ad lib wheel running. The added low distance control group was singly housed in cages that had a wheel with a brake applied to prevent running until the brake was released from 8-10 pm daily. Lastly, the unrestricted rehabilitation group was individually housed in wheel cages with a wheel that had no brake, allowing 24/7 voluntary running. Cumulative running activity, in the form of distance (meters), was longitudinally monitored using revolution sensors (Scurry Rat Activity Sensor, Lafayette Instruments®). A python script was then used to calculate daily average running distance (m/day), running duration (mins/day), number of running bouts per day (bouts/day), velocity (m/s), running bout duration (s), and rest time (hrs). Running duration was defined as the total daily time (mins/day) the rat was considered running on the wheel due to increasing cumulative distance within a 6 second time period; a running bout started once the revolution counter detects a change in cumulative distance and then ends when 6 consecutive seconds elapsed with no change in cumulative distance; running bout duration was defined as the average time animals spent on the wheel once they started a running bout; and rest time was the maximum daily number of hours that the cumulative distance did not change.

4.2.3 In Vivo Radiographs and microCT scans

To monitor bone formation, in vivo radiographs and microCT scans were acquired at 2, 4, and 8 weeks post-injury while rats were under anesthesia. Digital radiographs were captured at 40 kV with a 7 s exposure (Faxitron MX-20). MicroCT scans were performed using 48 □m voxels, 55 kVp, 145 mA, and 750 ms integration time (VivaCT 80, Scanco Medical). Trabecular bone formation was evaluated inside standard 1.5 mm and 2.5 mm long cylindrical volumes of interest

(VOI) that were centered between the intact bone ends of 2 mm and 3 mm defects, respectively. The results were reported as longitudinal bone volume (BV).

4.2.4 Histology

After animals were euthanized, representative femora from all rehabilitation conditions and across both defect sizes were harvested for representative histology (n = 1 across 8 groups). Representative animals were selected based on week 8 in vivo radiographs. These femora were fixed in 10% Neutral Buffered Formalin (NBF) for 72 hours and then transferred into Ethylenediaminetetraacetic acid (EDTA) until the bone tissue was completely decalcified. At this point, samples were shipped to Inotiv Inc. (Boulder, CO) to undergo sample processing and staining. Femora were longitudinally sectioned at 5 micrometers and stained with Hematoxylin Eosin and Safranin O/fast Green. Histology slides were then imaged on the Leica THUNDER Imager Brightfield at 5X magnification.

4.2.5 Partial Least Squares-Discriminant Analysis (PSLDA)

Activity data averaged across weeks 1 to 3 of post-injury rehabilitation and endpoint bridging scores were compiled. Bridging scores included a score of 1 for union and 0 for nonunion. PLSDA was conducted in MATLAB (MathWorks, R2021b version 9.11) using the Statistics and Machine Learning Toolbox (version 12.2). Data were normalized and scaled prior to running the analysis to eliminate skewed analysis that would be biased towards rehabilitation variables with higher values. For the analysis, the "plsregress" MATLAB function was used to perform the partial least squares regression and then fit a classifier using the latent variables. A scatter plot was then created to visualize latent variables one and two according to their scores. Bar plots were then created to explain each latent variable according to the input rehabilitation parameters and their contributions of these variables to the partial least squares components. The accuracy was

calculated using cross-validation with the “kfoldloss” function. The confidence intervals across variables within LV1 and LV2 were calculated using the “bootci” function and variance of each latent variable was calculated using the “PCTVAR” output from the “plsregression” function. R-squared was also calculated using the predicted and actual response values.

4.2.6 DataModeler

Nonlinear multivariate regressions were performed using the DataModeler software (Evolved Analytics) to investigate potential relationships between rehabilitation parameters and endpoint bone volume. DataModeler uses an evolutionary algorithm for multivariate modeling applications to characterize the nonlinear relationship between inputs and outcomes. DataModeler uses genetic programming to build hundreds of algebraic models and breed “fit” models over successive generations. The fittest models are based on high accuracy and low complexity and aggregate into a predictive model ensemble. This modeling approach provides several advantages over standard regression methods, including (1) use of nonlinear regression, (2) giving a range for each prediction regime encompassed by the divergence of several models that preserves real statistical uncertainty, (3) stochastically choosing subsets of the records (n’s) for each generation, minimizing model bias, and (4) allowing user input where prior knowledge exists (augmented intelligence), such as manual filtering of variable combinations included. Activity parameters were averaged across weeks 1 to 3 of postoperative rehabilitation and regressed against endpoint bone volume for 3 mm defects. We did not average activity data after the callus formation stage (week 3 of rehabilitation) because of the potential relationship between healing status and activity parameters (e.g. the group with increased bone formation might have greater running distance due to better recovery) making it harder to delineate whether rehabilitation is influencing bone healing or vice versa. Focusing on early weeks of post-injury rehabilitation also helps addresses a

significant blind spot in the literature, which generally focuses on rehabilitation onset after bridging occurs. When we regressed activity parameters against endpoint bone volume for 2 mm defects no relationships were revealed likely because the 2 mm bone volume lacked variability across rehabilitation groups. Nonlinear algebraic models from 10 independent evolutions were generated using DataModeler's Model Creation function. Model creation was constrained to a 10-minute simulation to avoid overfitting, and only robust models were considered for analysis using the "Robust On" function. Each model received unique accuracy (1 - R2) and complexity scores and was plotted as a function of these two terms. 108 models with complexity <100 and a 1 - R2 value <0.2 were selected as the "fittest" models observed at the knee of the Pareto front. The complexity score is based on the mathematical equation of the model. Low complexity models have mathematical equations that describe a system with relatively simple terms (e.g. small number of parameters, basic mathematical operations, and minimal interactions between variables). We wanted to minimize complexity while maximizing accuracy to elucidate relationships relevant to biological systems. Although the exact value of the accepted complexity and accuracy scores are arbitrary, we selected these inclusion criteria to examine over 100 diverse models. These models were then analyzed using the "VariablePresence" and "VariableCombinations" functions to identify the influential rehabilitation parameters and parameter combinations. Next, the top parameter combinations were selected and used as a filter setting for the next round of model generation. Another round of nonlinear algebraic models from 10 independent evolutions were generated using only the top three rehabilitation parameters as input variables (running distance, running duration, and rest time). These models were further evaluated using the "ResponsePlotExplorer" and "SurfacePlotExplorer" functions to visualize the 2D and 3D response of bone volume as a function of running distance as well as the combination

of running distance and rest time. The algorithm leaves the top of the 3D response plot open to indicate areas of uncertainty due to poor representation from experimental animal data. This region of uncertainty is also present in the white region of the contour plot. A Mathematica Notebook script was used to overlay red dots representing datapoints from each animal on the 3D surface plot and the corresponding 2D contour plot to reveal areas where the model is well represented.

4.2.7 Finite Element Analysis

Segmentation and Mesh Generation. At weeks 2 and 4 post-injury, local mechanical parameters were assessed via longitudinal FE simulations conducted on representative segmental defect models. Within this study, one 2 mm defect and one 3 mm defect model were selected from each of the four rehabilitation groups to encapsulate the average healing trajectory. These eight subjects were explicitly selected to represent the overall healing pattern within each group, as they were neither the best nor the worst healer of their respective groups. Initially, idealized configurations of the stainless-steel risers and fixation plate used for fracture stabilization were constructed alongside left or right femur models (Fig. 15A) [15]. The femur model was divided into cortical and trabecular bone, with a hollow region representing bone marrow (Fig. 15D). Given that all subjects had a 2 mm defect on their left femur and a 3 mm defect on their right femur, the final assembly was tailored accordingly. Defect geometries, including ectopic regions and portions of the intact femur, were delineated via semi-automated segmentation of the microCT scan images acquired at weeks 2 and 4 post-injury (Fig. 15B) utilizing the MIMCS software (version 24.0, Materialize, Leuven, Belgium). For subjects with partial or no bridging, the outer border of the healing region was difficult to discern in the microCT image data, so we manually generated a region boundary that ensured the inclusion of volume between the femurs and enabled subject-specific material assignment within the healing region. Subsequently, FE meshes consisting of 10

node tetrahedral elements were generated for all parts using the 3-matic software (version 16.0, Materialise, Leuven, Belgium), with the target element size for each part chosen based on previous mesh convergence studies [15].

Material Properties and Boundary Conditions. The resulting FE model was imported to FEBio Studio (Version 4.6, Salt Lake City, UT)[271]. Parts with incompatible meshes were tied together using the "tied elastic" feature [272]. All materials were represented using an isotropic neo-Hookean hyperelastic constitutive model. Our preceding study empirically determined the material coefficients (elastic modulus, E, and Poisson's ratio, υ) for the stainless-steel riser and the fixation plate (E = 200,000 MPa, υ = 0.3 for risers; E = 525 MPa, υ = 0.4 for fixation plate) [15]. The elastic moduli for cortical and trabecular regions of the femur were derived from a prior study on rats of comparable age to our subjects (E = 8803 MPa, υ = 0.33 for cortical bone; E = 2169 MPa, υ = 0.33 for trabecular bone) [15,273]. We established a correlation between the intensity of the microCT images of hydroxyapatite phantoms and their density, and combined it with another equation that relates hydroxyapatite density to the elastic modulus [273]. This allowed us to assign a position-dependent elastic modulus, E, within the healing defect region using the "image map" tool in FEBio Studio [274] and the equation:

$$E = 4.49\text{e-}4 \times (I - 19.5)^{1.87}, \qquad \text{(Eqn. 1)}$$

where I is the microCT image intensity (Fig. 15C).

The proximal end of the femur was subjected to a spatially varying pressure load, while the distal femur was fully constrained, consistent with our prior research [15,212]. Subjects in the current study did not have instrumented strain sensors on the fixation plates [3]. We utilized strain values measured from a prior pilot study to determine the loading needed to mimic the activity of sedentary and rehabilitation subjects at weeks 2 and 4. In that study, *in vivo* tensile strain on the

fixation plate was recorded for animals in sedentary and unrestricted rehabilitation conditions who lacked bridging after week 8 of recovery. We designated two subjects without bridging as reference subjects - the sedentary subject with a 3 mm defect and the unrestricted subject with a 3 mm defect - since their healing conditions matched the subjects from the pilot study performed to collect fixation plate strain data. Through an iterative process, we determined the scale factor for the distributed pressure load that resulted in tensile (1st Principal Lagrange) strain on the simulated fixation plate that matched the experimentally measured strain values. We applied equal force on two sedentary subject models, mimicking the conditions of the sedentary subject with a 3 mm defect. For the six non-sedentary subjects, the loading resembled the conditions of the unrestricted subject with a 3 mm defect. Applying similar loads across subjects allowed us to understand the impact of mineralization on the local mechanical environment. We measured the compressive (3rd Principal Lagrange) and shear (Maximum Shear Lagrange) strain for elements in the segmental

defects. The FEBio solver was used for all FE analyses [209]. A nonlinear, incremental-iterative solution procedure was used based on the BFGS quasi-Newton method.

4.2.8 Statistical Analysis

All data were reported as Mean ± standard deviation (SD). Significance was determined at $p < 0.05$. Mixed Effect ANOVA with Tukey's multiple comparisons test was used to analyze the impact of rehabilitation conditions and time on weekly activity parameters. Two-way ANOVA with Tukey's multiple comparisons test was used to analyze bone formation as a function of rehabilitation conditions and time. All activity and bone healing statistical calculations were

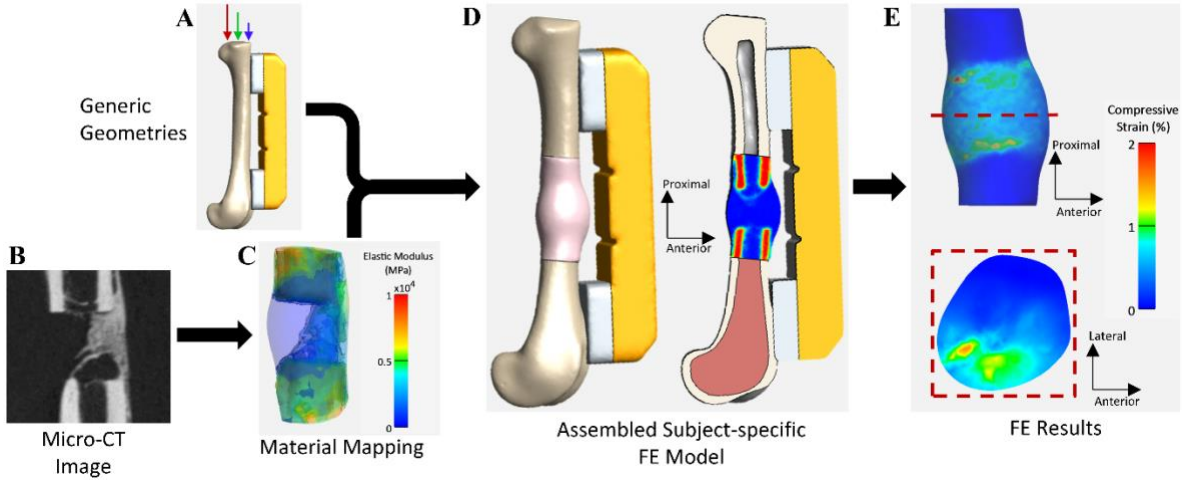

Figure 15. Illustration of an FE workflow employing subject-specific data to approximate local mechanics in surgically created healing bone defects. **(A)** Depiction of generic geometry of the femur, risers, and fixation plate utilized in all FE models to simulate loading during rehabilitation activity. Arrows at the proximal end of the femur represent the application of spatially varying loads during rehabilitation. **(B)** MicroCT scans of the defect with newly mineralized tissue and parts of intact bone were captured at week 4 post-injury. **(C)** Position-dependent elastic modulus was assigned in the defect region on a subject-specific basis based on local microCT intensity. **(D)** Each assembled FE model was constructed by integrating the generic geometric models with subject-specific defect geometry. The cross-sectional view illustrates the trabecular bone and the spatial variation of elastic modulus within the defect region. **(E)** Representative FE results demonstrate the spatial variation of compressive strain within the defect and the influence of mineralization and bridging on strain values. Top view of strain distribution at a cross-section (red dashed line) is shown inside the dashed box.

performed using GraphPad Prism 10 software. Data from FE analysis is represented as volume-weighted mean ± standard deviation (SD), and all statistical analyses were conducted using Origin 2024 (OriginLab, Northampton, MA).

4.3 Results

Within this study, our experimental groups consisted of (1) sedentary controls (2) low distance controls where rodents were housed with running wheels that were only unlocked, allowing rodents to run on the wheel, from 8-10pm each day; (3) restricted rehabilitation where rodents were housed in standard conditions and brought to the wheel cage for ad lib exercise from 8-10pm each day; and (4) unrestricted rehabilitation where rodents were housed with running wheels that remained unlocked allowing ad lib 24/7 running access. Across the rehabilitation groups, we examined rodents' wheel running duration, running distance, number of running bouts, running bout duration, running velocity, and daily rest time (Fig. 16). Longitudinal activity data revealed that hours of wheel access and housing conditions resulted in three distinct rehabilitation profiles (Fig. 16). Unexpectedly, both the restricted rehabilitation and unrestricted rehabilitation groups ran roughly the same daily distance although they were given 2 and 24 hours of daily wheel access, respectively (Fig. 16). The low distance control group ran significantly less daily running distance, duration, and bouts per day than the other two rehabilitation groups (Fig. 16). The only rehabilitation parameter that was not significantly different across rehabilitation conditions was running velocity, largely due to high individual variance (Fig. 16). Both the low distance and restricted rehabilitation groups rested for significantly more hours per day than the unrestricted rehabilitation group throughout all weeks of rehabilitation (Fig. 16).

Longitudinal bone volume quantifications by in vivo microCT scans revealed that rehabilitation condition did not significantly influence average group bone healing of 2 mm segmental bone defects (Fig. 17A). In contrast, bone healing after 3 mm defects was significantly impacted by rehabilitation conditions (Fig. 17B). Unrestricted rehab, which resulted in animals training more often and resting for fewer hours each day, significantly reduced bone formation compared to restricted rehabilitation ($p = 0.0053$) and sedentary counterparts ($p = 0.0203$). Bridging rates depended on injury severity, as the unrestricted rehabilitation group exhibited an 80% bridging rate for 2 mm defects but a 0% bridging rate for 3 mm defects (Fig. 17C). Representative microCT 3D reconstructions of 3 mm defects revealed nonunion with clear absence of bone formation across all animals in the unrestricted rehabilitation group, while the restricted rehabilitation group exhibited complete union across 57% of animals (Fig. 17C-D).

	Low Distance Control	Restricted Rehab	Unrestricted Rehab
Distance:	65.08 ± 13 m/day	197.3 ± 33 m/day	180.8 ± 16 m/day
Duration:	3.722 ± 0.5 mins/day	11.40 ± 1.6 mins/day	24.78 ± 2.1 mins/day
Bouts/day:	23 ± 3 bouts/day	66.65 ± 9 bouts/day	158.6 ± 14 bouts/day
Bout Duration:	9.616 ± 0.12 s/bout	10.2 ± 0.05 s/bout	9.326 ± 0.02 s/bout
Velocity:	0.22 ± 0.002 m/s	0.25 ± 0.003 m/s	0.11 ± 0.0001 m/s
Rest time:	23.51 ± 5.6 hrs	22.65 ± 0.5 hrs	10.22 ± 2.9 hrs

Figure 16. Rehabilitation conditions impacted several exercise parameters. n = 6 for low distance control; n = 7 for restricted rehabilitation, and n = 5 for unrestricted rehabilitation. Graphic created with biorender.com. Mean ± SD.

To help distinguish between unions and nonunions based on rehabilitation parameters, we performed partial least squares discriminant analysis using activity data (running distance, running duration, running velocity, running bouts/day, running bout duration, and rest time) and endpoint bridging status (1 = union, 0 = nonunion) determined by microCT scans. This linear regression analysis demonstrated poor separation across latent variable 1 (LV1) and latent variable 2 (LV2) and a moderate R-squared (Fig. 18). The latent variables are combinations of the measured

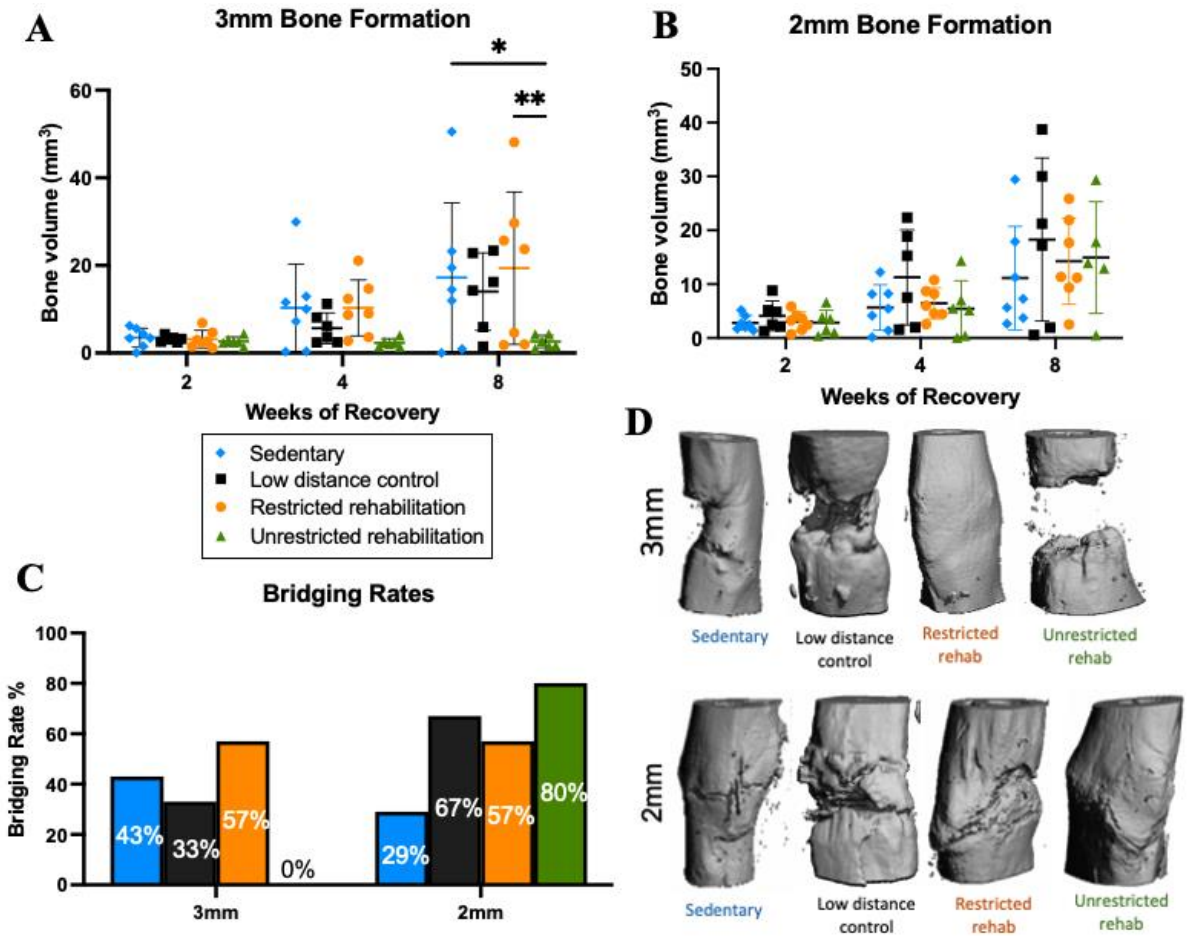

Figure 17. The influence of rehabilitation on bone healing depends on defect size. **(A)** Bone volume within centered 2.5 mm of 3 mm defects after 8 weeks of recovery. * p = 0.0203 for sedentary versus unrestricted rehabilitation at week 8, Two-Way Anova with Sidak's multiple comparisons test. ** p = 0.0053 for restricted rehabilitation, housed out of cage versus unrestricted rehabilitation at week 8, Two-Way Anova with Sidak's multiple comparisons test. **(B)** Bone volume within centered 1.5 mm of 2 mm defects after 8 weeks of recovery. **(C)** Endpoint bridging rates based on radiograph and microCT scans. **(D)** *In vivo* representative radiographs revealed nonunion with minimal bone formation within the defect region only for the unrestricted rehabilitation group. Data are Mean ± SD for all graphs.

rehabilitation variables with loadings that correspond to variable importance on endpoint bone volume. The confidence intervals for LV1 and LV2 also revealed overlap. For example, the 95% confidence interval for running distance was -4.2 to 4.4 for LV1 and -3.06 to 3.82 for LV2, indicating a lack in separation across latent variables (Fig 3b-c).

AI based genetic programming algorithms performed multivariate regression analyses and

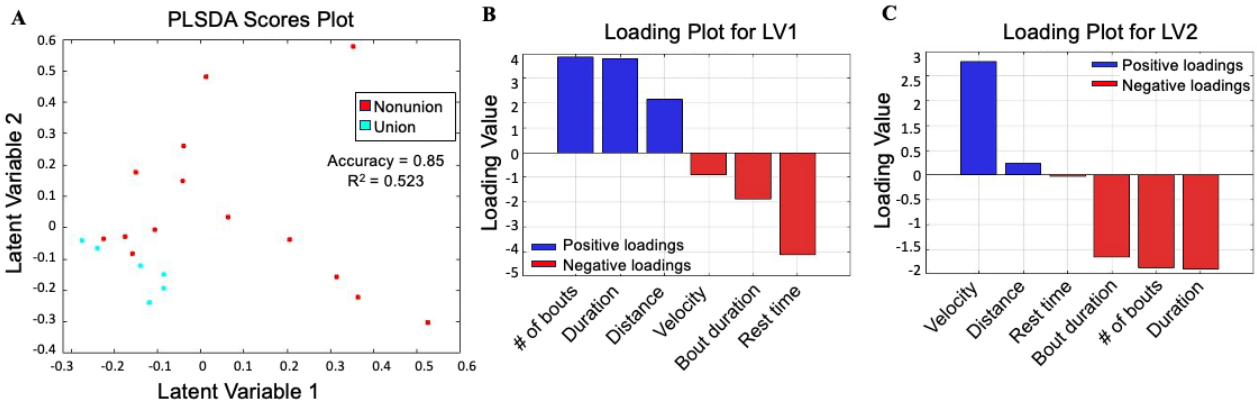

D Rehabilitation Parameters	95% Confidence Interval for Latent Variable 1	95% Confidence Interval for Latent Variable 2
Running Distance (m/day)	-4.22 to 4.40	-3.06 to 3.82
Running Duration (mins/day)	0.97 to 6.36	-3.98 to -0.20
# of Running Bouts (#/day)	1.14 to 6.43	-3.92 to -0.34
Running Bout Duration (s/bout)	-6.63 to 0.54	5.06 to 1.38
Velocity (m/s)	-2.81 to 4.35	-2.32 to 5.68
Rest Time (hrs)	-5.09 to -2.05	-3.26 to 1.81

Figure 18. PLSDA of activity data across weeks 1 to 3 of rehabilitation on bone healing outcomes exhibited poor model fit. (**A**) PLSDA analysis established latent variable 1 (LV1) and latent variable 2 (LV2) to explain healing outcomes via rehabilitation parameters. (**B-C**) Latent variable loading plots visualized the contributions of each rehabilitation parameter to bone healing outcomes. Blue bars represent positive correlation. Red bars represent negative correlations. (**D**) Table of the 95% confidence interval across each rehabilitation variables within LV1 and LV2 using bootstrapping.

generated 1,315 unique models to relate rehabilitation parameters with endpoint bone healing (Evolved Analytics, DataModeler software). Similar to our previous study, 108 models from the "knee" of the Pareto front were selected to investigate models with less complex mathematical equations (i.e. small number of parameters, basic mathematical operations, and fewer interactions between variables) and high accuracy scores (Fig. 19A) [275]. Rehabilitation distance, duration, and

rest time were present in nearly all the 108 “fittest” models, suggesting that these parameters are likely influential to bone formation (Fig. 19B). Our multivariate regression analyses included variables that were dependent on each other (e.g. running duration is directly related to running bout duration and the number of running bouts per day). Therefore, feature selection was performed to only include independent variables that were present in models with high accuracy and low complexity (distance, duration, and rest time) for the nonlinear evaluation of rehabilitation parameters and bone healing (Fig. 19A-B). After feature selection to only include running distance, duration, and rest time, we were able to visualize the relationship between these parameters and bone healing. Response plots, which visualize predicted bone volume in response to rehabilitation inputs, revealed a distinct nonlinear relationship between average daily running distance and endpoint bone volume (Fig. 19C). Three-dimensional surface plots also revealed a distinct nonlinear relationship between the effect of average daily running distance and rest time on endpoint bone volume (Fig. 19D). Data from all animals with the same bone volume are connected to produce contour lines to visualize the influence of running distance and rest time on bone volume (Fig. 19E). Overlay of individual datapoints (in red) on the 3D surface plot and 2D contour plot illustrated that our dataset lacked animals that ran a moderate amount of daily distance and rested for a moderate number of hours (Fig. 19E). The 2D response plot further illustrates this region of uncertainty with a greater yellow envelope, which corresponds to model variance, around the curve peak (Fig. 19C). However, the model predicts improved bone healing within this region since the regions surrounding it are well represented with increasing amount of bone volume (Fig. 19C-E).

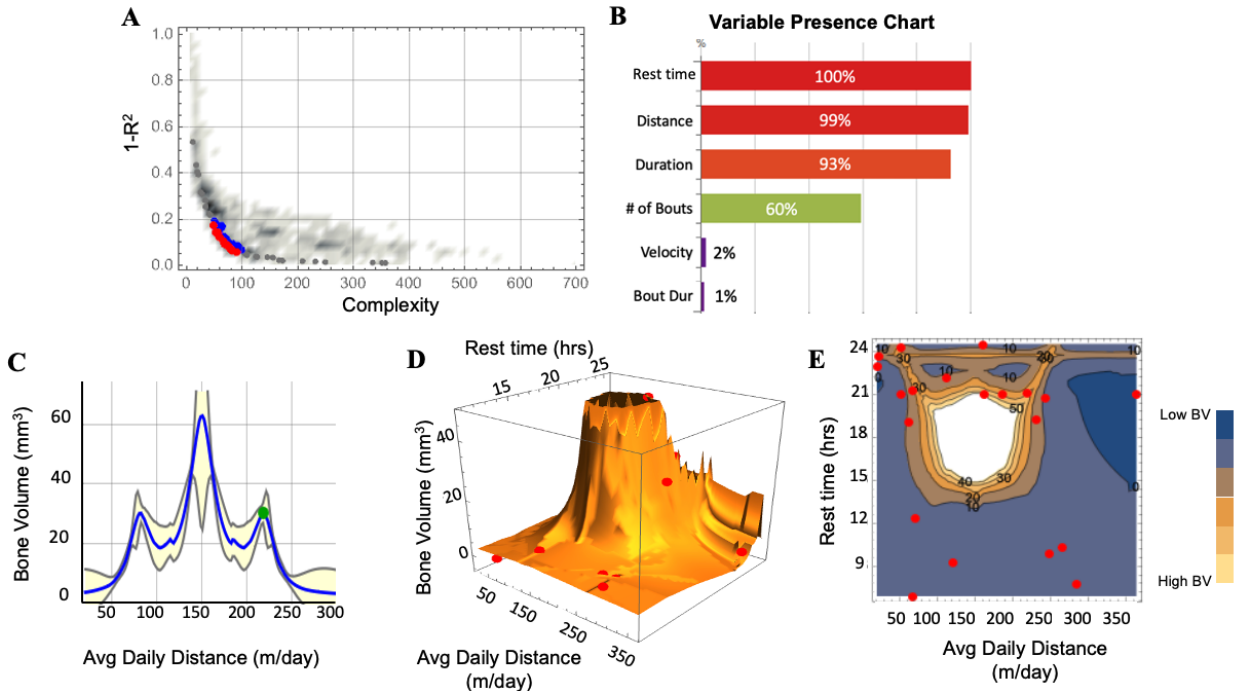

Figure 19. Nonlinear multivariate models support early restricted rehabilitation paired with longer rest times to improve bone formation. **(A)** The top models were selected at the "knee" of the Pareto front, representing the most accurate models with the lowest degree of complexity. **(B)** Variable presence chart reveals the percentage of models that contained each rehabilitation parameters. **(C)** 2D response profile plots revealing the relationship between daily average distance and bone volume across models that only include max rest, running distance, and running duration variable combinations. The blue line represents the predictive model ensemble, and the yellow envelope demonstrates the variance in the ensemble as a function of each variable. **(D-E)** 3D response surface plot and 2D contour plot, respectively, illustrate bone volume as a function of rest time and average daily distance. Red datapoints indicate individual animals.

We examined local compressive and shear strain distribution within the regenerative niche in individual subjects at weeks 2 and 4 following injury using FE analysis. A marked disparity was evident in the local strain environment for subjects exhibiting bone bridging compared to those without bridging at the defect site (Fig. 20A). Compared to the values measured at week 2 post-injury, there was a decrease by a factor of 1.2 to 2.3 in average compressive strain for the six subjects with bone bridging at 4 weeks of recovery. In contrast, the mean compressive strain at the defect of the unrestricted subject with 3 mm defect increased from 1.72% at week 2 to 2.17% at week 4, indicating that a lack of early callus formation results in sustained high-magnitude local strains (Fig. 20C). Although not as drastic, the low distance control subject with a 3 mm defect

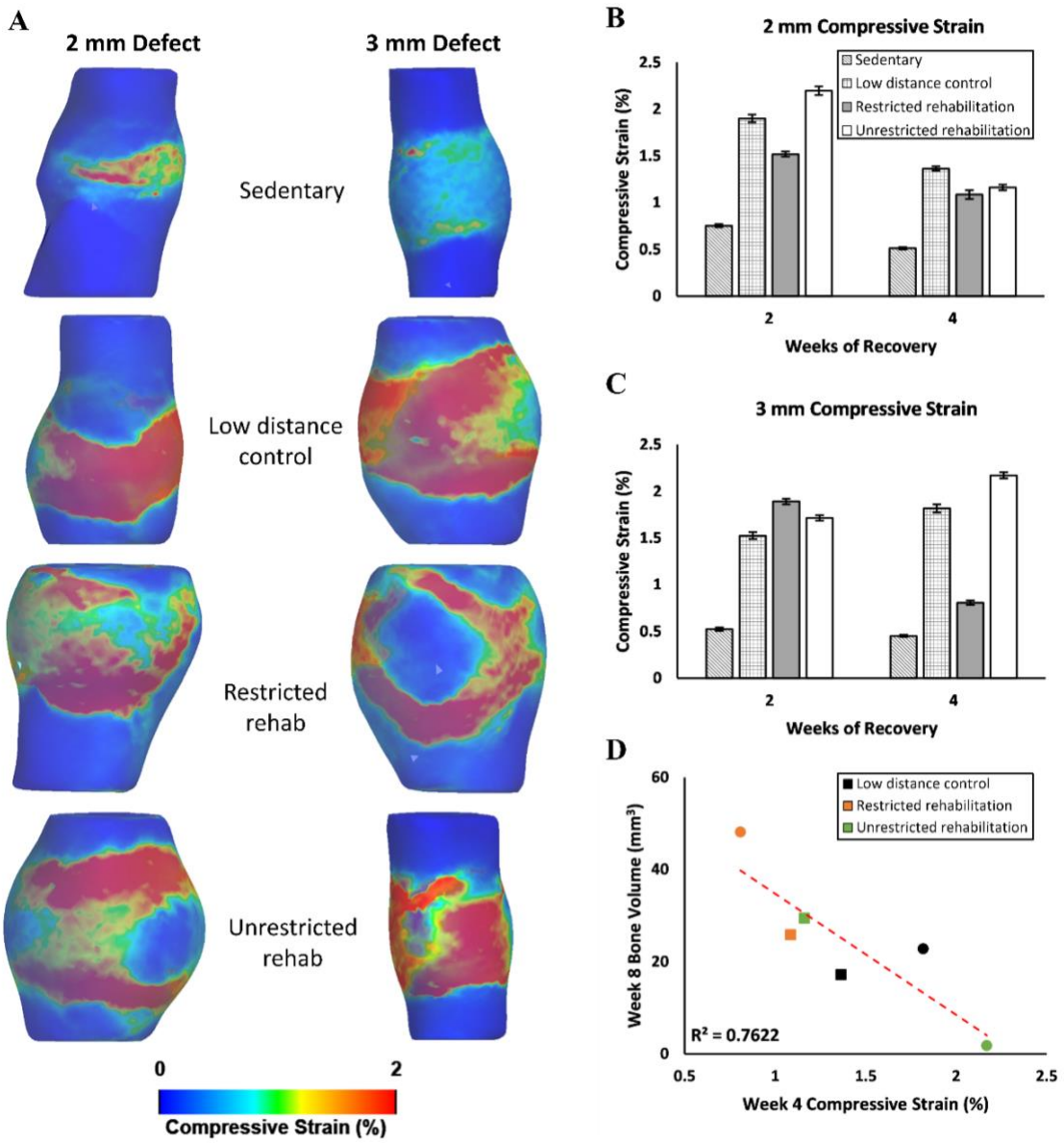

Figure 20. Rehabilitation condition and defect size influence local compressive strain distribution and endpoint bone volume. **(A)** Local compressive strain distribution at the defect site for eight representative subjects was assessed at week 4 post-injury. **(B)** The impact of rehabilitation condition on local strain distribution appears negligible, with similar average compressive strain observed across all subjects at week 2 post-injury. **(C)** Subjects with 3 mm defects demonstrate greater sensitivity to rehabilitation, indicated by variations in mean compressive strain observed after four weeks of injury. **(D)** Week 8 post-injury bone volume of non-sedentary subjects negatively correlates with compressive strain in both 2 mm (square) and 3 mm (circle) defect models measured at week 4 post-injury.

also experienced an increase from 1.52% at week 2 to 1.82% at week 4. Overall, the compressive strain values of subjects that underwent post-injury rehabilitation exhibited a moderate dependence on bone volume (R2 = 0.6624), where higher bone volume corresponded to lower compressive

strain values at week 4 post-injury (Fig. 21. The changes in shear strain followed the same trend as the compressive strain for all subjects (Fig. 22). In addition, the extent of change varied depending on the rehabilitation condition and defect size (Table 2). Sedentary subjects with a 2

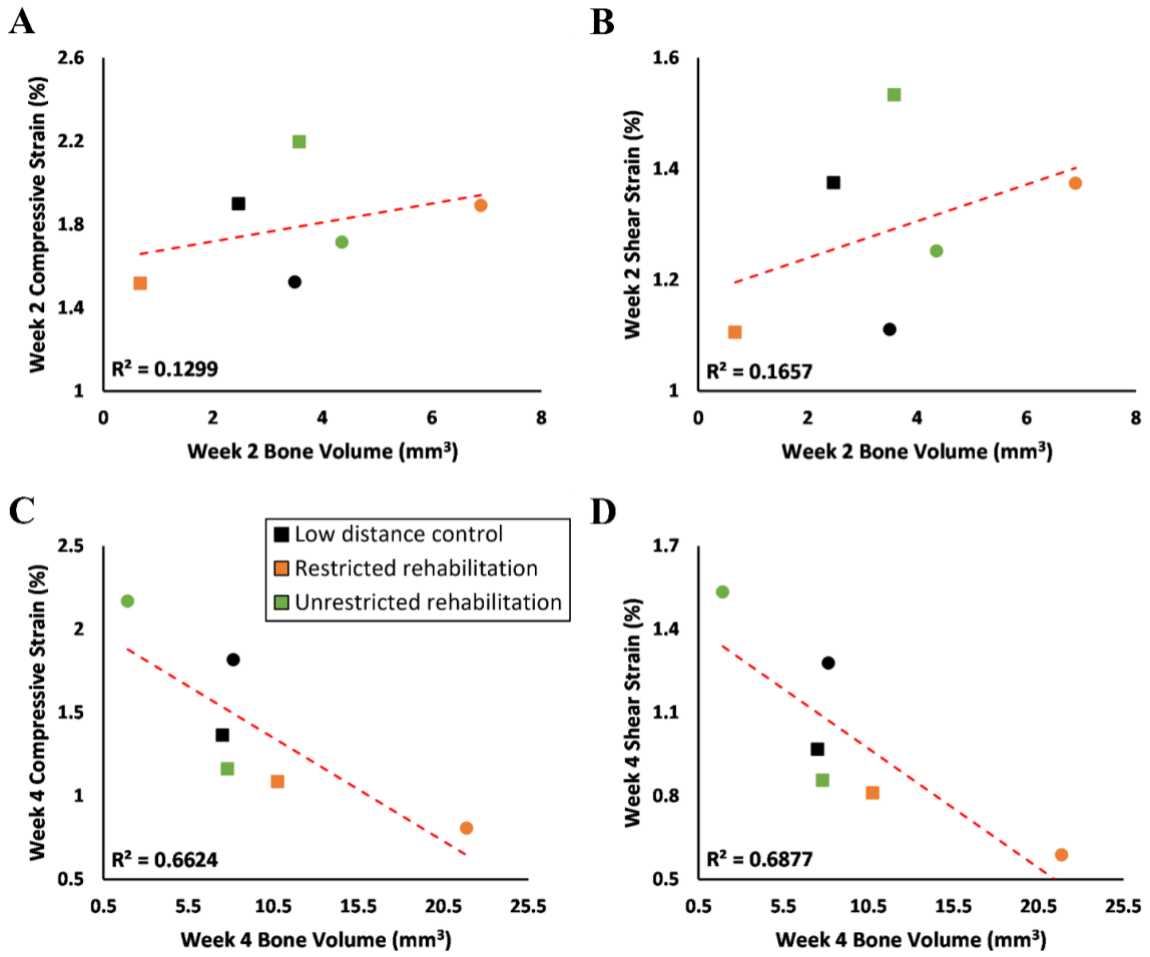

Figure 21. Correlation between bone volume and average strain within the defect region. **(A, B)** At week 2 post-injury, compressive and shear strains positively correlate with bone volume at that timepoint. Due to very low mineralization in week 2, the correlation is weaker than the correlations for week 4 data. **(C, D)** At week 4 post-injury, the compressive and shear strains have a stronger correlation with the bone volume at that time point. Unlike in week 2, we observed a negative correlation for the strain parameters in week 4.

mm defect experienced a reduction in compressive strain by a factor of 1.46, while those with a 3 mm defect showed a decrease by a factor of 1.16. (Fig. 20B-C, Table 2). Conversely, subjects undergoing restricted rehabilitation demonstrated even larger reductions in strain, particularly those with a 3 mm defect, which experienced a reduction in compressive strain by a factor of 2.3

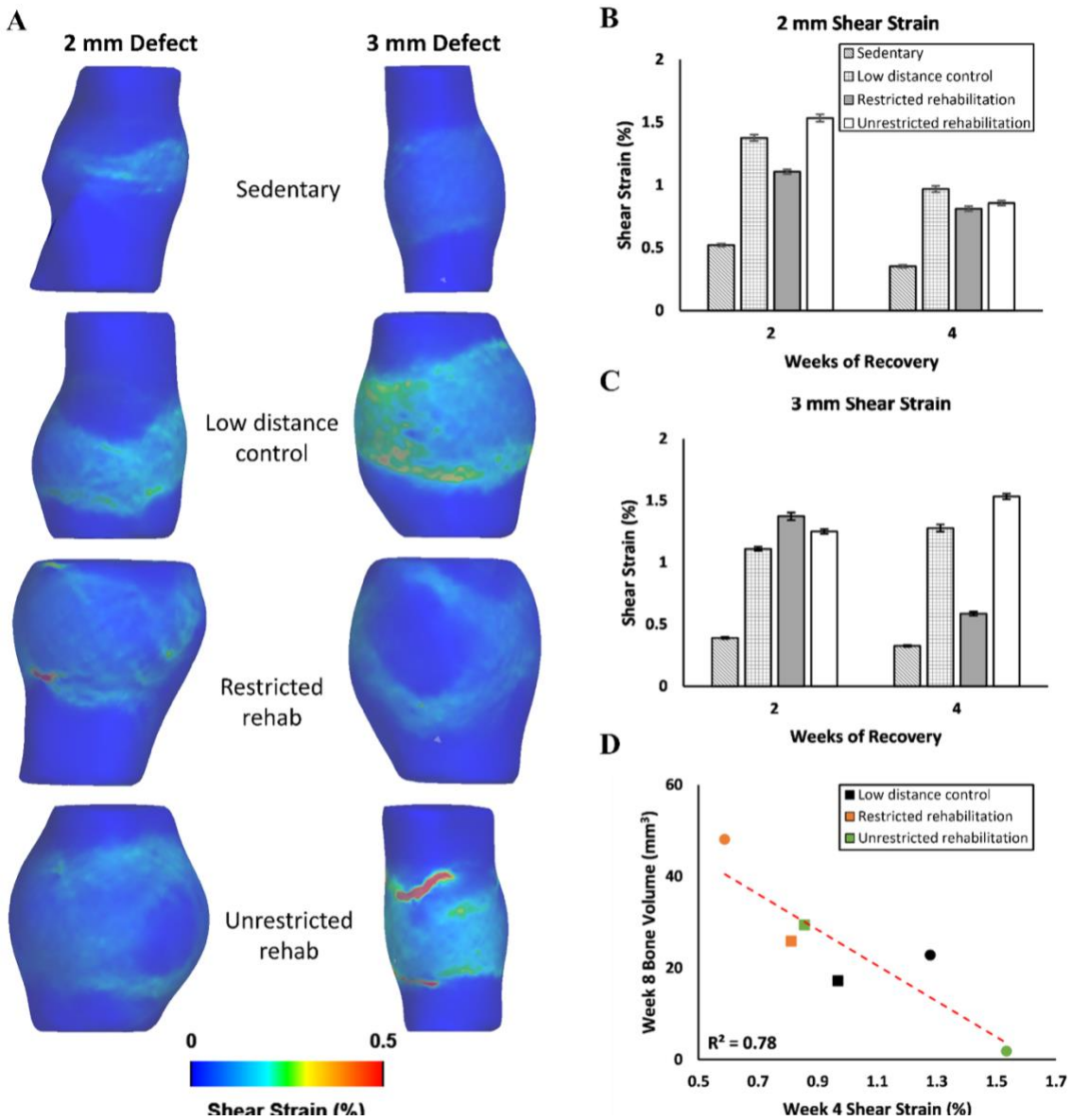

Figure 22. The size of the defect and post-injury rehabilitation affect the magnitude of shear strain within the defect region. (**A**) Spatial shear strain distribution at the defect of eight representative subjects measured at week 4 post-injury. (**B**) Implementing post-injury rehabilitation increased local strain compared to strains from sedentary conditions. Local shear strains were not impacted by the different rehabilitation profiles as the average shear strains at week 2 post-injury for all rehabilitation subjects are similar. (**C**) Subjects with 3 mm defects were more sensitive to rehabilitation, as evidenced by the variation in mean shear strain at week 4 post-injury. (**D**) Bone volume at week 8 post-injury for the non-sedentary subjects was negatively correlated to the shear strain of 2 mm (square) and 3 mm (circle) defect models measured at week 4 post-injury.

within two weeks and a decrease by a factor of 1.4 was observed for those with a 2 mm defect.

Although we modeled only a single representative subject from each group and thus could not

perform statistical analysis, the results clearly suggest that the impact of the rehabilitation activity was more pronounced in subjects with a 3 mm defect than those with 2 mm defects (Fig. 20C).

We also investigated how strain at an earlier time point may impact bone healing volume in the defect at later time points (Fig. 20D). Under the same loading condition, subjects that underwent post-injury rehabilitation and experienced higher compressive strain in the defect site by week 4 exhibited lower bone volume by week 8 (with $R2 = 0.7622$). Conversely, we observed the opposite relationship in the sedentary subject group; the subject with a 2 mm defect with higher-than-average strain at week 4 had 42% greater bone volume by week 8 than the subject with a 3 mm defect. These data suggest that smaller bone injuries benefit from higher-magnitude local strains when subjects are kept sedentary.

Since we collected subject-specific injury geometry, activity, and strain data, we wanted to examine subject-specific longitudinal data to better understand the effects of rehabilitation on local mechanics and bone healing. Our study enabled the tracking of subject-specific longitudinal healing status via 3D microCT reconstructions, regenerative niche mechanics via FE models, and endpoint tissue phenotype via histology (Fig. 23). Subject-specific data revealed that a subject that ran less than the predicted optimal running distance resulted in nonunion with high levels of compressive strain throughout weeks 2 and 4 and fibrotic tissue within the defect region by week 8 (Fig. 23A). A subject that ran more than the predicted optimal running distance also resulted in nonunion with high levels of compressive strain throughout weeks 2 and 4 post-injury and a thick cartilaginous band spanning across the defect region by week 8 (Fig. 23C). Lastly, a subject that ran a near-optimal amount of daily running distance had local strains that decreased in magnitude overtime and uniform bridging with signs of remodeling throughout the defect region by week 8 (Fig. 23B).

Table 2:					
Timepoint	Defect Size	Rehab Group	Elastic Modulus (MPa)	Compressive Strain (%)	Shear Strain (%)
Week 2	2mm	Sedentary	274.70 ± 15.42	0.75 ± 0.017	0.52 ± 0.011
		Low distance control	106.04 ± 6.09	1.9 ± 0.041	1.38 ± 0.026
		Restricted rehab	100.02 ± 6.61	1.52 ± 0.028	1.11 ± 0.018
		Unrestricted rehab	139.33 ± 10.99	2.19 ± 0.046	1.53 ± 0.029
	3mm	Sedentary	294.27 ± 16.87	0.53 ± 0.012	0.39 ± 0.008
		Low distance control	143.14 ± 5.78	1.52 ± 0.024	1.11 ± 0.016
		Restricted rehab	225.81 ± 13.93	1.89 ± 0.046	1.37 ± 0.031
		Unrestricted rehab	86.79 ± 2.05	1.72 ± 0.029	1.25 ± 0.019
Week 4	2 mm	Sedentary	611.29 ± 27.65	0.51 ± 0.018	0.35 ± 0.012
		Low distance Control	489.89 ± 34.37	1.36 ± 0.038	0.97 ± 0.025
		Restricted rehab	607.59 ± 32.22	1.09 ± 0.03	0.81 ± 0.02
		Unrestricted rehab	376.24 ± 19.98	1.16 ± 0.029	0.86 ± 0.019
	3 mm	Sedentary	1106.27 ± 52.72	0.45 ± 0.011	0.33 ± 0.0.75
		Low distance control	437.05 ± 25.48	1.82 ± 0.043	1.28 ± 0.029
		Restricted rehab	771.42 ± 28.68	0.81 ± 0.024	0.59 ± 0.017
		Unrestricted rehab	156.51 ± 4.51	2.17 ± 0.033	1.53 ± 0.022

Table 2. Summary of the defect mechanical parameters measured at the surgically created segmental defect region.

4.4 Discussion

Mechanical loading strategies to improve bone healing have largely investigated loading magnitude as the dominant parameter dictating the regenerative response by modifying fixation plate stiffness [6,7,15,142,191,192,195,228] or applying controlled external loads [200,251–256]. These studies often involved the controlled investigate of one or two variables at a time even though clinical rehabilitation is inevitably multifactorial. The present study examined six distinct rehabilitation parameters (running distance, running duration, running velocity, number of running bouts, running bout duration, and rest) and their combined influence on segmental bone repair. Our injury model involved bilateral 2 and 3 mm segmental bone defects in rodent femora that were stabilized with compliant fixation plates and not treated with biologics (n = 5-7). Bilateral defects were utilized to reduce the number of animals for this study and reduce the potential for animals to shield their injured limb, minimizing the variability of the load experienced by the bone injuries within an experimental group. To create distinct post-injury rehabilitation conditions, animals were either left in sedentary conditions or given wheel access that was unrestricted (24/7) or restricted (2 hrs/day). Bone healing, running wheel activity data, and subject-specific FE models of the regenerative niche were longitudinally monitored and the relationship between rehabilitation parameters and bone healing was assessed via multivariate linear and nonlinear regression analyses. This experimental setup allowed us to investigate the combined influence of six different rehabilitation variables to understand (1) which variables were important to bone healing and (2) how to tune these variables for improve bone healing.

Within this study, we examined three rehabilitation conditions to examine the combined effect of rodents' wheel running duration, running distance, number of running bouts, running bout duration, running velocity, and daily rest time on bone healing (Fig. 16). We found that rodent wheel access (2 versus 24 hours per day) and housing conditions (with or without running

wheel in home cage) resulted in three distinct rehabilitation profiles that can be summarized as a (1) low activity profile, (2) frequent activity with little rest, and (3) moderate activity paired with longer daily rest, which respectively corresponded to the low distance control, unrestricted rehabilitation, and restricted rehabilitation groups (Fig. 16). The impact of these unique rehabilitation profiles on segmental bone defect healing depended on injury size. More specifically, unrestricted rehabilitation resulted in 20% nonunion for smaller 2 mm defects and 100% nonunion for larger 3 mm defects (Fig. 17). Our results ultimately suggest that for more severe injuries, restricting exercise and ensuring adequate rest is critical to avoid negative effects on bone healing such as disruption of the vasculature or excessive interfragmentary movement. However, it's worth nothing that these results are in the context of one defect stabilization method. Previous work in our 6 mm rodent segmental defect model investigated the influence of fixation plate stiffness on bone healing. They found that fixation plates with higher flexural stiffness resulted in decreased local strains and significantly impaired bone healing [15]. In the context of our current study, changing the fixation plate stiffness would likely impact the necessary levels of activity and rest needed for improved bone healing. For example, a more compliant fixation plate may require less daily distance and longer daily rest periods since the fixation plate would share more of the ambulatory load with the healing callus. Previous work has shown that fixation plates that are too compliant (axial stiffness = 8.4 ± 0.4 N/mm) can significantly impair healing [6]. On the other hand, fixation plates that are too stiff might also mitigate the influence of rehabilitation on bone healing by shielding too much of the ambulatory loads.

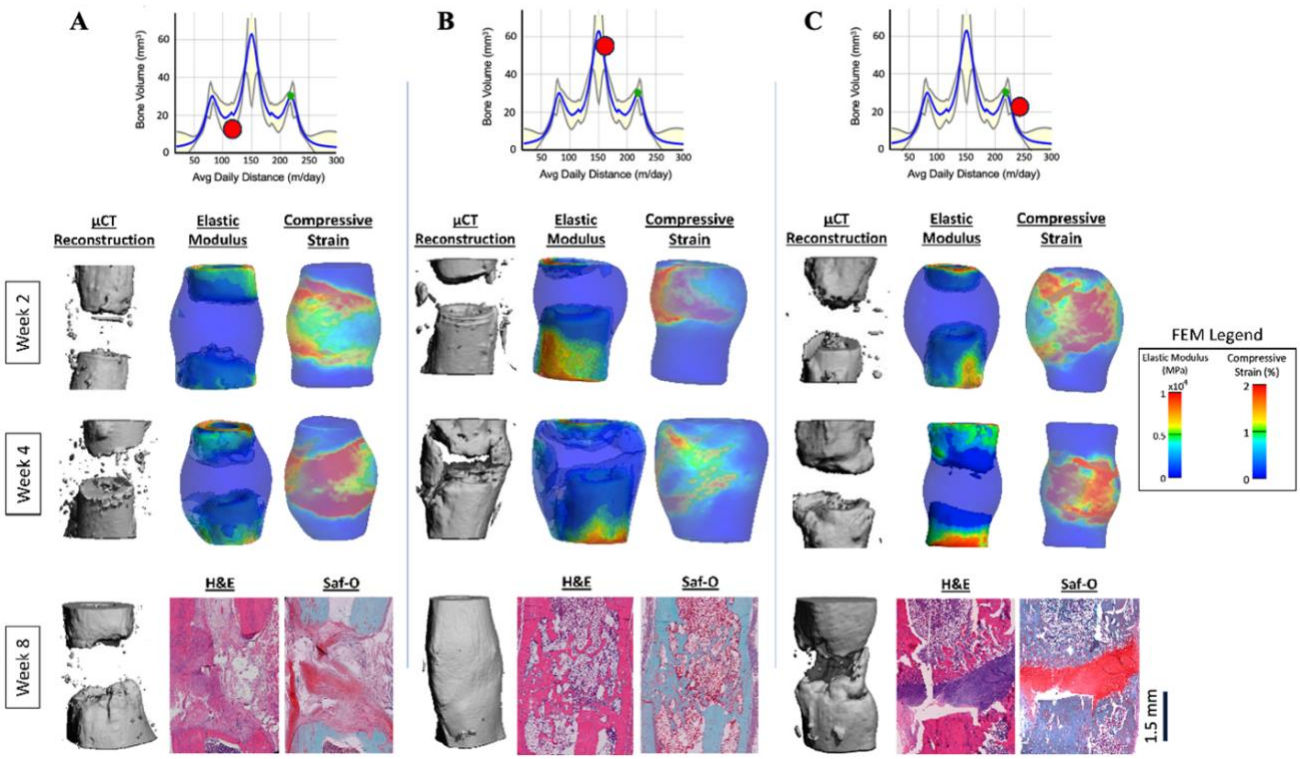

Figure 23. Subject-specific holistic understanding of rehabilitation distance and longitudinal 3 mm defect local niche mechanics and healing outcomes. **(A)** subject-specific data column with low daily running distance. **(B)** subject-specific data column with near-optimal running distance. **(C)** subject-specific data column with high daily running distance. Subject-specific activity data is show via red dot on the response plot (Bone Volume vs Avg Daily Distance) across the top row. Histology scale bar = 1.5 mm.

Both the 2 and 3 mm defects exhibited relatively modest bridging rates of 29% and 43% which are expected since these segmental defects are close to previously established critically-sized femoral defects in Wistar rats [276,277]. Poser et al. found that 5 mm femoral mid-diaphyseal defect were critically-sized when stabilized with polyetherketone (PEEK) internal fixators for 15 week-old female Wistar rats (body weight ~184 g) [276]. The rats used in this study were lighter than the rats in our study. Although the authors did not list the axial stiffness of their PEEK fixation plates, we know that PEEK is a stiffer material than polyethylene so we can infer that the fixation plates used in our current study were less stiff. Harrison et al. found that 3 mm femoral mid-diaphyseal segmental defects were critically-sized when stabilized with external fixators for 12 month-old male Wistar rats (body weight 450-550 g) [277]. The rats used in their study were heavier

than the rats in our current study. The external fixator are also less stiff (~45-46 N/mm) than our fixation method (~145 N/mm). The size of a critically-sized defect has been shown to depend on the rat strain, weight, age, sex, and fixation method [278]. Since our internal fixation plates exhibit a stiffness in between these two studies, it is reasonable to expect the critical-size for our rodent model to fall somewhere between 3 and 5 mm. In fact, radiographs (captured at 40 kV with a 7 s exposure with a Faxitron MX-20) from a previous pilot study (n = 2-3) revealed that 2 and 3 mm defects resulted in a 100% and 33% of defects bridging within 8 weeks, respectively, while 0% of 4 mm defects bridged. For the current study, we utilized 2 and 3 mm defects because this model enables the detection of a potential improvement with rehabilitation without the use of biologics and their known confounding factors.

The linear regression analysis produced a model with a moderate goodness of fit (R2 = 0.524) and poor separation along both latent variables, suggesting that the influence of rehabilitation on bone healing cannot be adequately described with this approach (Fig. 18). Previous literature has suggested a nonlinear relationship between loading magnitude and bone healing, where moderate loading magnitude improved bone formation but high magnitude loading was severely detrimental [6,15]. This motivated a nonlinear modeling approach, allowing us to elucidate multifactorial, nonlinear relationships between additional rehabilitation parameters and bone healing.

Although comparisons of advantageous versus detrimental loading conditions for bone healing have been investigated, little work has looked beyond modulating the magnitude of cyclic loads. Previous studies by Rubin, Lanyon, and others have found that osteogenic responses are predominately influenced by strain magnitude, strain rate, and frequency [279–284]. Loading duration was also found to influence bone tissue, with extended periods of loading having a diminishing

effect [279]. However, these studies investigated adaptations of intact bones to loading since they did not involve an injury model. In addition, several groups have investigated interfragmentary motion and its clinical implication including rehabilitation regimens [191,258,262,263]. Both excessive and inadequate interfragmentary motion can negatively influence bone healing. The mechanical environment of a healing fracture is determined by the stiffness of fixation and weight bearing, suggesting that fracture healing requires a balance of both fixation and rehabilitation [192,196,216]. Flexible fixation strategies should not be paired with intense rehabilitation, just like rigid fixation strategies should not be paired with conservative rehabilitation. Although these studies, as well as others, have advanced mechanobiology principles, they did involve subject-specific tracking of multiple rehabilitation parameters to discern multifactorial relationships between rehabilitation parameters and bone healing. In our study, we were able to track subject-specific activity to calculate six rehabilitation parameters used as inputs into multivariate regression analyses. Our results revealed that daily running distance and rest were the most influential rehabilitation parameters on bone healing (Fig. 19B). Nonlinear regressions revealed a distant nonlinear relationship between average daily distance and endpoint bone formation, where a moderate amount of daily distance paired with longer rest correlated with improved bone formation (Fig. 19C-E). These results indicated that rehabilitation decisions must consider the importance of rest, especially since rehabilitation regimens with shorter rest periods resulted in 100% nonunion after larger bone injuries. Additional research to expand our multifactorial understanding of rehabilitation regimens influence on bone healing will be crucial to inform clinical rehabilitation decisions.

Based on mechanobiology principles, we hypothesize that adequate rest time is crucial for the underlying mechanisms of bone healing, especially during the first month after injury. Bone

healing consists of the inflammatory stage (0-7 days), followed by soft callus formation (2-3 weeks), hard callus formation (3-4 months), and eventual remodeling [259]. Our rehabilitation regimens started after the inflammatory stage (day 7), and our results found that daily rest throughout soft callus formation was crucial for larger defects. This stage of healing entails revascularization through angiogenesis and vasculogenesis, progenitor cells (e.g. MSCs) differentiating into fibroblasts and chondrocytes, recruitment of precursor cells, and ossification [259,285]. The importance of rest throughout these physiological processes is supported by literature that found osteogenic cells can become saturated with dynamic loading after only a few loads (60). The addition of rest in-between loading cycles has been shown to promote enhanced activation of osteoblasts and increased bone formation [286–289]. Srinivasan et al. investigated whether insertion of rest could make a non-osteogenic loading magnitude osteogenic. They found that inserting rest significantly increased bone formation (8-fold increase) compared to low-magnitude loading without rest [290]. Rest also improved osteogenic response in an aged, osteoporotic model [291]. These studies hypothesized that rest in-between loading cycles enhances the osteogenic response by maximizing transient fluid flow known to stimulate osteogenic cells [292]. Our results support the importance of rest in-between exercise sessions and further suggest that larger bone injuries may require more rest than smaller injuries.

Balancing activity and rest throughout early rehabilitation is also supported by literature that found excessive loads inhibited vascularization, progenitor cell differentiation, and bone formation [6,16,293,294]. Checa and Prendergast used a mechano-biological model to investigate vascular network development and tissue growth inside a bone scaffold under different loading conditions. They found that low levels of mechanical loading stimulated bone formation, while high levels inhibited capillary growth and bone formation [293]. Bratengeier also found that

progenitor cells exhibited an osteodestructive response with high amplitudes fluid flow compared to cells that underwent low amplitudes fluid [294]. Lastly, in a segmental defect model, Boerckel *et al.* found that excessive early loading significantly inhibited the vasculature and bone regenerative responses [6]. Building on these mechanobiology principles, our results suggest that rehabilitation must provide advantageous levels of activity while balancing adequate rest periods to improve bone healing. Our study revealed that the relative levels of activity and rest depended on injury severity since unrestricted rehabilitation resulted in 0% union for larger bone injuries but 80% union in smaller injuries. These results further suggest that bone injuries that are only one millimeter different in size exhibit different mechanosensitivity. Injuries of different sizes are known to heal through different mechanisms because of the different vessel regrowth requirements and local mechanics, which direct endochondral versus intramembranous ossification [262,295,296]. Larger bone injuries may be more mechanosensitive because of their increased instability and interfragmentary movement, reduced progenitor pool, and greater damage to the vasculature compared to smaller injuries [262,297–301]. It's also worth noting that daily rest is inversely related to the number of running bouts/day (i.e. as daily rest increased across the different rehabilitation profiles, the number of daily running bouts decreased). Therefore, larger defects, with greater mechanosensitivity, may benefit from greater rest because this rehabilitation regimen also ensures fewer running bouts each day. Conversely, the stability and smaller interfragmentary movement of smaller defects, may enable these defects to withstand and even benefit from more frequent loading.

Our multivariate nonlinear regression models support restricted early running distance and longer daily rest, however, a limitation of our dataset is that it is small for training a predictive model (N= 25). Instead, our model was intended to identify influential rehabilitation parameters

and their respective relationship to bone healing. To develop a robust predictive model, our dataset would require a larger sample size to better represent the entire range of daily running distance and rest time potentials. It is also worth noting that our work was performed in segmental bone defects not treated with biologics. Future work could investigate rehabilitation in larger bone injuries treated with growth factors or other secondary treatments to better simulate clinical treatment.

The novel finite element (FE) analysis pipeline employed in this research facilitated the application of subject-specific geometry and material assignment for both the defect and ectopic bone with a generic model of the proximal and distal femur and fixation plate. The irregular shape observed in the ectopic bone formation surrounding the defect (Fig. 20A) underscores the importance of utilizing a subject-specific defect geometry rather than a generic one (e.g. cylinder). Furthermore, by incorporating the trabecular bone and marrow regions, we enhanced the accuracy of the generic femur model compared to previous studies [302,303]. By accurately representing the geometry and material properties of the femur and healing region, we characterized the interaction between mineralization and the local mechanical environment and their influence on bone healing. Our observations suggest that relying solely on bone volume extracted from microCT may not suffice to characterize functional bridging and mechanical strength recovery. For instance, the low distance control subject with a 3 mm defect exhibited a two-fold increase in bone volume from week 2 to week 4 post-injury. Yet, no functional bridging occurred at the defect site, resulting in nonunion. However, analysis of strain distribution at these time points revealed a 20% increase, indicating the absence of bridging (Fig. 20C). This emphasizes the capacity of FE analysis to provide crucial insights essential for tailoring subject-specific rehabilitation activities that would be impossible to obtain from microCT scans or radiographs alone. Furthermore, our observations

indicate that subjects with larger defects are more prone to experiencing strain of larger magnitude at the defect site, often resulting in nonunion. Previous studies have highlighted that significant gaps or misalignment between the bone ends can impede long bone's endogenous ability to regenerate and hinder the restoration of mechanical strength (80–82). Given the complexities associated with large femoral defects, tailoring rehabilitation activities to each subject's specific needs, including injury severity, alignment issues, and potential constraints on bone ingrowth and mechanical strength recovery, is imperative. Generic rehabilitation protocols may fall short of adequately addressing the unique requirements of individuals with larger bone defects. Therefore, customizing the rehabilitation activity offers the opportunity to optimize patient recovery, mitigate risks, and enhance long-term functional outcomes.

Our previous study revealed that high compressive strain (~20%) at the defect site stimulates increased bone formation [142]. Notably, under comparable loading conditions, the sedentary subjects in this current study that experienced greater compressive strain at week 4 exhibited higher bone volume by week 8 (Fig. 21). However, our study findings also indicate that, despite similar loading magnitudes, the two subjects with the highest mean compressive and shear strain at the defect lacked bridging by week 8. This "goldilocks" phenomenon aligns with prior research demonstrating that inadequate strain can lead to bone resorption, while excessive strain may prompt cartilage and fibrous tissue formation instead of woven bone, potentially resulting in nonunion [233,234,236,304,305]. Across all subjects, a mean compressive strain ranging from 0.5% to 1.15% and a mean shear strain ranging from 0.35% to 0.85% at week 4 correlated with greater bone volume by week 8 (Fig. 20D and 21). However, subjects exhibited higher bone volume at week 8 when the mean compressive strain fell between 1.5% and 2.2% and the shear strain ranged from 1.1% to 1.5% during week 2. It is important to note that these observations assume that the

loads applied to these subjects were similar to the loading experienced by the two subjects selected as the reference. Nevertheless, our results corroborate experimental data, as the rehabilitation groups, represented by subjects within these strain ranges, achieved a higher bridging rate, exceeding 50% (Fig. 17C). With a larger subject cohort, it may be possible to pinpoint target strain thresholds throughout distinct weeks of recovery, thereby optimizing bone healing outcomes.

The results of the FE analyses quantified the influence of rehabilitation and defect size on strains experienced in the healing region of the defect and its evolution during the healing process. Our results suggest that the ideal rehabilitation strategy should be initially prescribed based on defect size and evolve during the healing period based on mineralization levels and local mechanical response to loading. The methods applied in this study contribute to the groundwork for subject-specific FE analysis to guide the development of custom rehabilitation regimens in the clinical setting.

Clinical prescriptions of rehabilitation that account for subject-specific factors have the potential to improve clinical efficacy. Evidence-based rehabilitation guidelines depend on technology and research that enables subject-specific analysis to better explore rehabilitation as a therapeutic for bone healing. Our study leveraged subject-specific FE modeling and multivariate models to reveal a holistic and longitudinal understanding of how rehabilitation conditions relate to healing status and niche mechanics (Fig. 23). It is also well known that the local mechanical environment is influenced by surgical stabilization parameters (e.g. fixation method, fixation plate material etc.) and rehabilitation parameters. However, technology to longitudinally track subject-specific local parameters have been limited. Our subject-specific FE modeling, based on in vivo microCT scans, provide a tool to further investigate how additional aspects of bone injuries impact healing outcomes such as stabilization method (e.g. external fixation versus internal fixation).

Continued investigation of ad lib post-injury rehabilitation across subjects that undergo various fracture stabilization methods could further elucidate the interaction between loading magnitude and the necessary levels of activity and rest to achieve improved bone healing.

Our results reveal the critical importance of data-informed and subject-specific rehabilitation decisions to improve the efficacy of rehabilitation regimens after bone injuries. Using our implantable sensor technology and subject-specific FE modeling, we have been investigating an overall hypothesis that bone healing can be improved by achieving local strains within a beneficial range that change as a function of time [15,175]. For this study, we further hypothesized that this beneficial window of strain would change as a function of injury severity. However, our results revealed a more complicated reality; bone healing depends on more than an advantageous magnitude of local strains. Instead, bone healing also depends on an adequate balance between activity and rest that changes as a function of injury severity. Subject-specific rehabilitation decisions for bone healing must consider subject-specific factors such as injury stabilization, injury severity, and healing status, while also enforcing adequate rest. Future work that leverages subject-specific approaches can help advance mechanobiology principles as well as evidence-based rehabilitation to improve clinical outcomes after musculoskeletal injuries.

CHAPTER 5: TREADMILL REHABILIITATION WITH INTERMITTENT REST MODULATES INFLAMMATION AND IMPROVES HEALING FOLLOWING BONE INJURY

5.1 Introduction

Traumatic femur fractures are a significant burden with an increasing annual incidence between 1.0 and 2.9 million worldwide [306]. The femur is the most fractured long bone in the body and often necessitates surgical fixation [307]. Injuries associated with femur shaft fractures are the major cause of morbidity in polytrauma patients [308,309]. Successful femur fracture healing necessitates the use of appropriate fixation devices and postoperative rehabilitation. Immediately after surgery, patients are given restricted weight-bearing protocols and suggested special rehabilitation exercises to facilitate fracture healing. However, the amounts and prescribed progression of loading are not well understood. In fact, little is known about how specific rehabilitative exercises influence the local mechanical environment at the fracture site. Technology to track real-time local strains around the fracture site could improve awareness of the appropriate forces for successful fracture healing and which exercise regimens achieve these forces.

In response to this need, Klosterhoff *et al.* developed an implantable strain sensor embedded on internal fixation plates used in a preclinical rodent segmental defect model [3]. He used this model to investigate how different fixation plate materials, with unique flexural stiffnesses, impacted the local mechanical environment during ambulatory loading and subsequent bone healing after 6 mm mid diaphyseal defects. They found that more compliant fixation plates (145.2 ± 10.6 N/mm) presented higher strains within the defect region and resulted in 60% more bone formation than defects stabilized with stiff fixation plates (232.4 ±

20.1 N/mm) [15]. Others have also found that too much loading, due to a lack in fixation stability, can significantly impair bone healing [6,65,310].

Compared to altering fixation plate designs, rehabilitative exercise provides a more dynamic strategy to modulate the mechanical environment following traumatic fractures. Using the compliant fixation plates and implantable strain sensors developed by Klosterhoff *et al.*, we have shown that rehabilitation of greater intensity increased local compressive and shear strains and significantly improved bone healing after 2 mm segmental bone defects as compared to subjects in sedentary conditions [175]. In fact, rehabilitation of greater intensity facilitated the regeneration of femurs that achieved intact femur strength. In a follow-up study we explored unique rehabilitation profiles comprised of six rehabilitation parameters to investigate the multifactorial effect of rehabilitation on bone healing. We found that postoperative rehabilitation needs to balance activity and rest time. The rehabilitation profile with a moderate amount of daily running distance and longer daily rest periods increased the incidence of union as compared to rehabilitation with the same daily running distance but shorter daily rest [246]. Further, we found that the beneficial levels of activity and rest depended on injury severity since the same rehabilitation regimen resulted in 0% union for larger, 3 mm, bone injuries but 80% union in smaller, 2 mm, bone injuries [246]. We hypothesize that rehabilitation influenced bone healing is an injury-size dependent manner due to the increased mechanosensitivity and interfragmentary movement experienced by larger injuries. Ultimately this study informed a multifactorial rehabilitation profile predicted to improve bone healing that involves a moderate amount of running distance paired with longer daily rest time.

Beyond exercise, literature has also explored dynamic loading strategies focused on dynamization, defined as increasing interfragmentary movement (IFM) between fracture ends by

reducing fixation stiffness from a rigid to a more flexible state [311]. This strategy has successfully promoted fracture healing in clinical and preclinical scenarios that often involve stabilization hardware with a locked (rigid) versus unlocked (flexible) state [6,192,196,311,312]. Studies have begun looking at the timing of dynamization, but support for early versus late dynamization remains controversial [202]. Comparing dynamization across experiments is challenged by the lack of standardization across studies. Studies often involve (1) diverse stabilization hardware with unique mechanical properties, (2) diverse subjects with different body weights, loading patterns, bone quality, etc, and (3) different fracture morphologies with unique mechanical and biological demands. These factors influence the local mechanical environment within the regenerative niche, making it hard to discern which loading strategies are optimal diverse fracture types and patient populations. Ultimately, it remains unclear how dynamization timing and magnitude affects bone healing and how rehabilitation should account for these changes to fixation plate stability.

In the current study, we wanted to explore a data-informed rehabilitation strategy using treadmills as an exercise platform that enables precise control of running distance, duration, and speed. Further, we wanted to implement adaptive rehabilitation that involved rehabilitation with gradually increasing intensity controlled by treadmill incline. For this study rodents underwent two weeks of pre-training on a flat treadmill and then underwent surgery to create a unilateral 3 mm segmental bone defect stabilized with compliant, internal fixation plates. Our implantable strain sensors were also implanted. Rodents were left to recovery for one week and then randomly allocated to different rehabilitation conditions: no incline control, gradual adaptive incline, and delayed adaptive incline (Fig. 24). The no incline control group ran on a flat treadmill throughout recovery. The gradual adaptive incline group ran on a treadmill with incline

that increased by 0.5% each week totaling to 3% incline by week 8 post-injury. The delayed adaptive incline group ran on a flat treadmill until week 4 post-injury and then they ran at a 1.5% incline for two week and finished the final two weeks at a 3% incline. All groups ran twice per week at a speed of 13 m/min for 12 minutes. These parameters were informed by our previous study that predicted improve bone healing with this rehabilitation regimen [246]. We longitudinally monitored bone healing with i*n vivo* radiographs and microCT scans. We also collected strain sensor data twice per week during treadmill running to monitor subject-specific strains throughout rehabilitation and healing. Due to previous support for higher intensity rehabilitation and dynamization principles, we hypothesized that adaptive rehabilitation with gradually increasing intensity would improve bone formation compared to no incline controls [175]. Further, we expected the timing of adaptation to matter. We hypothesized that delayed adaptations would result in low-magnitude loading throughout the callus consolidation stage, resulting in less bone formation than subjects that undergo rehabilitation with early adaptations.

5.2 Methods

5.2.1 Surgical Procedure

Unilateral 3 mm segmental defects were created in the left femur of 16-week old female Wistar (Envigo) rats that weighed between 242-314 grams (N = 15) [175]. Rats were anesthetized by isoflurane (Vet One Fluriso) throughout the entire surgical procedure with rodent toe pinch and respiratory checks every 10-15 minutes. Immediately prior to surgery rodents were shaved and the surgical area was cleaned with gauze soaked in alcohol (70% isopropyl) and chlorhexidine (Vet One). Rats were also subcutaneously given a dose of 1 mg/kg of Slow-Release Buprenorphine based on their preoperative weight at 1mg/mL concentration and 3 mL of Lactated-Ringer Solution (LRS, Vet One). Using aseptic techniques and sterile instruments,

surgery involved an anterolateral skin incision using a scalpel (blade #10). Tenotomy scissors were then used to separate the biceps femoralis and vastus lateralis muscle groups. Any remaining muscle tissue on the femur was lifted off the bone using periosteal elevators. With the femur exposed, we used an in-house clamping system to position the fixation plate on the dorsolateral side of the femur centered along the distal-proximal axis. The internal fixation plate was anchored to the femur using 000-120 stainless-steel screws (oval fillister, J.I Morris). Then the clamp system was removed, and a 3 mm defect was created in the mid-diaphyseal region using an oscillating saw (Halls). Defects were left empty to better discern the impact of exercise without biologic treatment as a confounding factor. Defect size was confirmed with a measuring device and a 3-layer closure approach was performed to close the muscle, subcutaneous tissue, and skin using 4-0 Vicryl suture, 4-0 Monocryl suture, and rat wound clips, respectively. Following closure, animals were transferred to a postoperative station to remove any remaining blood and apply a paste (metronidazole powder with NewSkin liquid bandage) to the wound clips to deter incision site chewing. Animals were randomly allocated to rehabilitation groups: no incline control, gradual adaptive incline, and delayed adaptive incline. Postoperative support included daily Clear H2O Boost Gel, Nutri-Cal gel, Cheez-its, 2-3 mL of LRS solution administered subcutaneously, and enrichment such as Nylabones, crinkled paper, and PVC tubes through day 5 post-injury. 48 hours after the surgery, standard buprenorphine at 0.3mg/mL was also given subcutaneous at approximately 0.03mg/kg for additional pain support. Animals were euthanized by CO_2 asphyxiation after 8 weeks of recovery. Rodents were singly housed in standard rodent cages (Techniplast) for the seven days following surgery and then doubly housed for the remainder of the study. These cages were equipped with bedding, various enrichment,

and provided ad lib access to food and water. All procedures were approved by the University of Oregon IACUC (20-32).

For the follow-up study, we created bilateral 2 and 3 mm defects in the femur of 16-week old female Wistar (Envigo) rats that weighed between 250-313 grams (N = 21 rates, 42 defects). For bilateral defects, two segmental defect surgeries were performed on a single rat with one surgery involving a 2 mm segmental bone defect to the right limb and a 3 mm segmental bone defect to the left limb. Bilateral surgeries were utilized for the follow-up study to eliminate the potential of limb shielding to minimize loading variability across subjects.

5.2.2 Treadmill Running Protocol

All rats underwent two weeks of treadmill running before surgery to support compliance post-injury. This training involved a gradual ramp up of both treadmill speed and running duration ranging from 8 m/min for 10 minutes to 16 m/min for 20 minutes. Then one week after surgery, and twice weekly thereafter, each animal ran for 12 minutes at a speed of 13 m/min. The total distance traveled loosely approximated the distance previously predicted to improve bone healing [246]. The training frequency of twice per week was selected based off a previous study that trained rodents twice a week for 20 minutes at a speed of 6.5 m/min [15]. Rodent running lanes were made in-house and enabled 8 rodents to simultaneously run. Our studies had an n = 5-7 per group, so rodents ran with their experimental group throughout postoperative rehabilitation. In the initial pilot study, the only difference in treadmill running protocols between groups was the treadmill incline (Fig. 24). The no incline control group ran on a flat (0%) incline treadmill throughout their 8 weeks of recovery. The gradual incline group ran on a flat treadmill for the first week of postoperative training. Their treadmill incline increased by 0.5% weekly thereafter, totaling to 3% of incline by week 8 post-injury. The delayed incline group ran on a flat treadmill

throughout the first four weeks of recovery and then ran on a 1.5% incline treadmill for two weeks and 3% incline for the remaining two weeks.

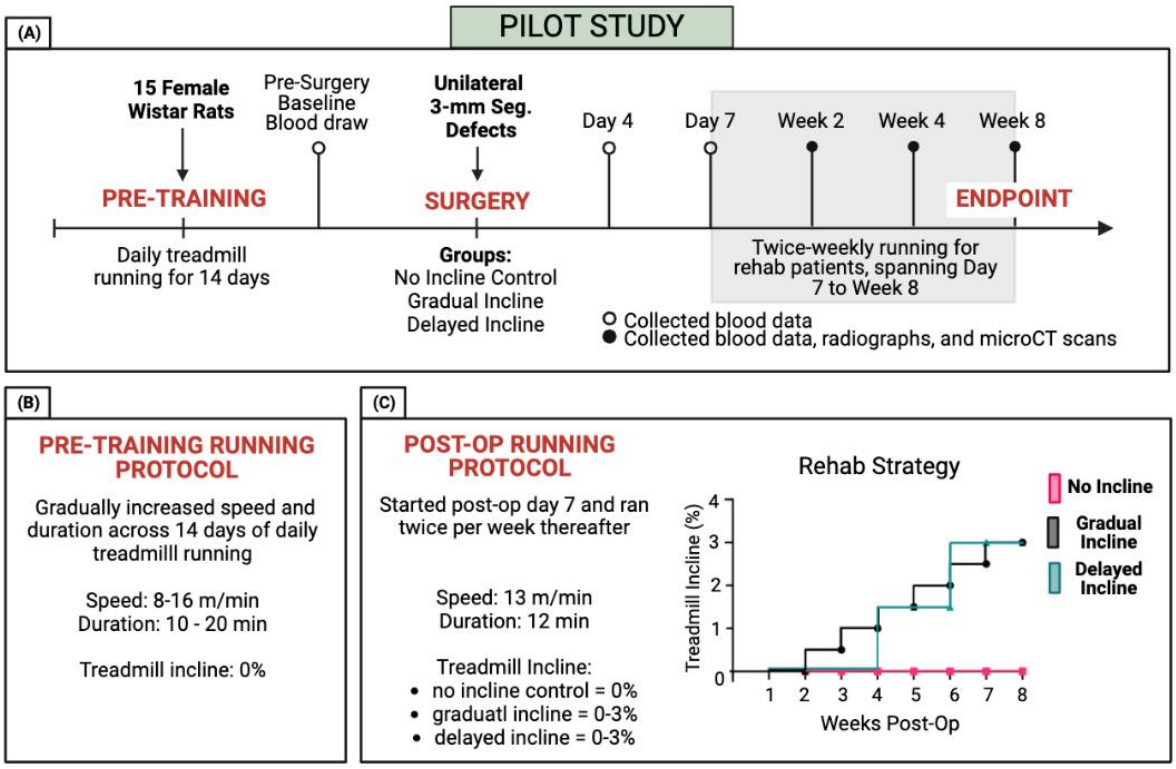

Figure 24. Pilot study design details. (**A**) Experimental timeline with data collection details. (**B**) Running protocol for pre-training prior to surgery. (**C**) Running protocol for after surgery training including a graph to show the temporal progression of treadmill incline for each experimental group.

For the follow up study, all rats underwent two weeks of preoperative treadmill running, identical to the pilot study pretraining outlined above. Starting one week after surgery, non-sedentary groups received treadmill running twice weekly on a treadmill that remained flat for the entire study. Both the rehabilitation with rest and the rehabilitation without rest groups ran at a speed of 13 m/min. The rehabilitation with rest group ran for one minute and then rested on the stationary treadmill for one minute. This group was on the treadmill for a total of 24 minutes but only ran for 12 of those minutes. The rehabilitation with no rest group ran for 12 minutes with no breaks. Similar to the pilot study, this speed and running duration was selected based on previously developed predictive models [246].

5.2.3 In Vivo Radiographs and microCT

To monitor bone formation, in vivo radiographs and microCT scans were acquired at 2, 4, and 8 weeks post-injury while rats were under anesthesia. Digital radiographs were captured at 40 kV with a 7 s exposure (Faxitron MX-20). MicroCT scans were performed using 48 μm voxels, 55 kVp, 145 mA, and 750 ms integration time (VivaCT 80, Scanco Medical). For the pilot study with unilateral segmental bone defects, bone formation was analyzed inside a standard 2.5 mm long cylindrical volume of interest (VOI) centered between the intact bone ends of 3 mm defects. For the follow up study with bilateral segmental bone defects, bone formation was evaluated inside standard 1.5 mm and 2.5 mm long cylindrical volumes of interest (VOI) that were centered between the intact bone ends of 2 mm and 3 mm defects, respectively. The results were reported as longitudinal bone volume (BV).

5.2.4 Immune Characterization

For both the pilot study and follow-up study, blood was drawn from the tail artery of rats using multiple use drawing needles (VACUETTE, 22G) at post-injury day 4, day 7, weeks 1, 2, 4, and 8 to monitor systemic immune cells over time. Baseline blood draws were also performed before surgery. The day 4 and day 7 timepoints were selected to observe the early immune response to traumatic bone injuries. The remaining timepoints were selected to observe the immune response return to baseline levels. Approximately 300 μL of blood was collected into lithium-heparin coated Microtainer tubes (BD) for flow cytometric analysis. After blood collection, red blood cells were lysed using RBC lysis buffer (1X, eBioscience) according to manufacturer's instructions. Cells were then fixed and resuspended in FACS buffer made of 2% FBS in PBS. Cells were then incubated with anti-rat CD32 to prevent non-specific antibody binding and subsequently stained for various immune cells including T cells (CD3+), cytotoxic T

cells (CD3+CD8+), helper T cells (CD3+CD4+FoxP3-), regulatory T cells (CD3+CD4FoxP3+), monocytes (CD11b+CD68+), and myleloid-derived suppressor cells (called MDSCs, CD11b+His48+). The BD Accuri C6 flow cytometer was used for data collection and FlowJo software was used for analysis with gates set based on FMO controls allowing <1% noise. Monocytes were excluded from the pilot study immune data and T regulatory cells were excluded from the follow up study immune data due to staining errors.

5.2.5 Statistical Analysis

All data were reported as mean ± standard deviation (SD). Significance was determined at $p < 0.05$. Two-way ANOVA with Tukey's multiple comparisons test was used to analyze *in vivo* bone formation as a function of rehabilitation conditions and time. Two-Way ANOVA with Sidak's multiple comparisons test was used to analyze longitudinal systemic immune cell populations as a function of rehabilitation conditions and time. GraphPad Prism 10 software was used to perform all statistical calculations and graphs.

5.3 Results

For this study, we explored treadmill running after traumatic bone injuries across two animal studies. For the first pilot study, our experimental groups involved (1) no incline control, (2) gradual incline, and (3) delayed incline to investigate how the progression of rehabilitation intensity impacts bone healing after unilateral 3 mm segmental bone defects. These groups

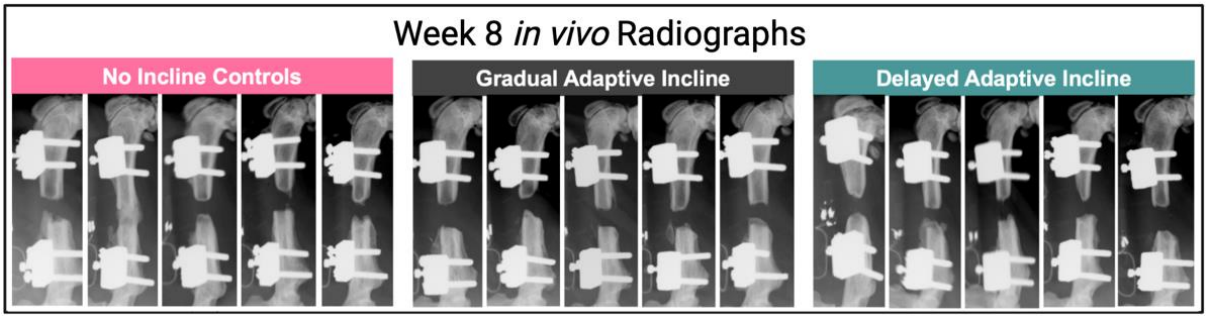

Figure 25. Endpoint radiographs from pilot study revealed 14/15 nonunions across all three rehabilitation groups with minimal bone formation within the defect region.

consist of rehabilitation with intensity that remained stagnantly low (no incline control), gradually increased (gradual incline), or increased only after week 4 which is after the callus stage of healing (delayed incline). All subjects ran twice weekly at a speed of 13 m/min for a total of 12 minutes based on previous studies that found these rehabilitation parameters to improve bone healing [246]. Across the rehabilitation groups, we examined longitudinal bone healing with *in vivo* radiographs and microCT scans as well as systemic immune cells with repeated blood collection, and flow cytometric analysis. After 8 weeks of recovery, we found a 93.4% nonunion rate across all subjects (Fig. 25). Based on the previous study used to inform our rehabilitation conditions, we expected bridging rates around 60%. Our previous study utilized rodent running wheels as opposed to treadmills. We selected treadmills as the rehabilitation platform because of the ability to precisely investigate a specific rehabilitation regimen predicted to improve bone healing. On running wheels rats ran an average of 10 seconds per running bout and ran roughly 60 to 160 bouts each day after injury [246]. Conversely, on treadmill rats ran for 12 consecutive minutes to achieve the distance predicted to improve bone healing. Although treadmills are a frequently used rehabilitation platform for both preclinical and

clinical research, steady-state running without intermittent rest may disrupt the callus formation stage of bone healing after a segmental bone defects that is close to critically-sized [313–316].

To further investigate our hypothesis that steady-state running disrupts bone healing, we performed a follow-up study that investigated whether rehabilitation with intermittent rest would improve bone healing. This study involved three groups: sedentary, rehabilitation with rest (1 minute running/1 minute rest), and rehabilitation with no rest (12 minutes running). The two rehabilitation groups ran on treadmills with the same running parameters as the pilot study (Fig. 24 and 27). We performed bilateral surgeries to create 2 and 3 mm segmental bone defects to minimizes potential off-loading of the injured limb. We evaluated longitudinal bone healing and systemic immune markers using the same techniques as the pilot study. In this follow-up study we found increased bone formation, both statistically and near-statistically, in 3 and 2 mm defects, respectively, when compared to rehabilitation without rest (Fig. 28A-B). We also found that rehabilitation with rest doubled the bridged rates for 2 mm defects compared to sedentary

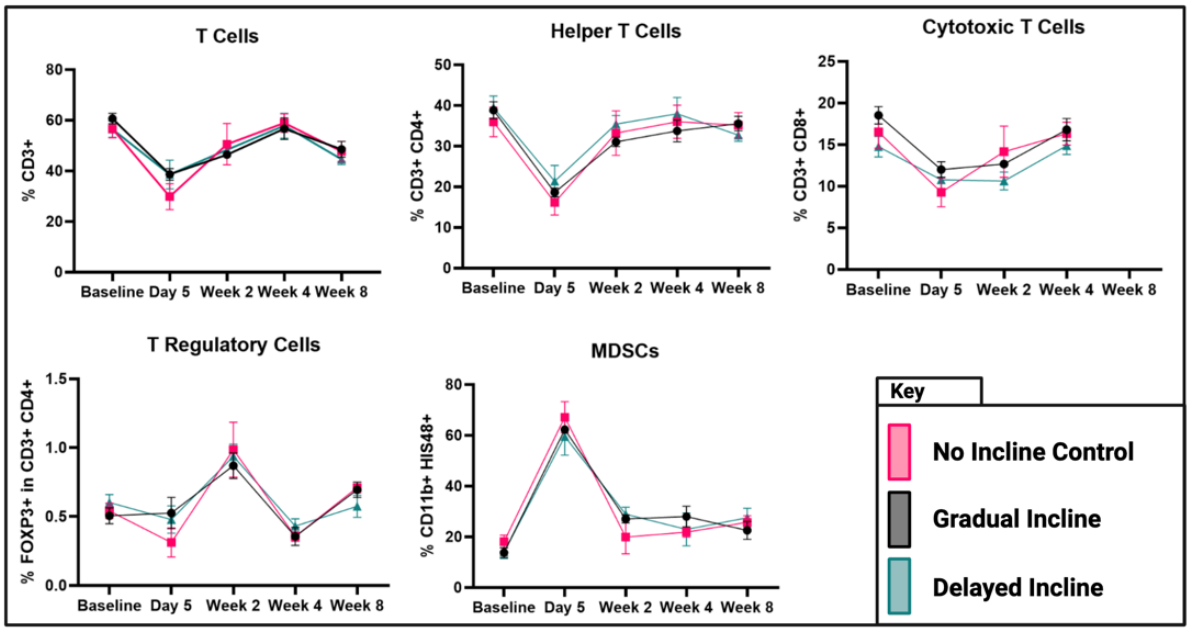

Figure 26. Pilot study systemic immune cell temporal characterization using flow cytometry across 5 different cell types (n = 5). Data are mean ± SD.

and rehabilitation without rest controls after 8 weeks of recovery (Fig. 28C). Lastly, we found that the introduction of rehabilitation with rest restored myeloid-derived cell types to baseline faster than subjects that were left in sedentary condition or introduced to rehabilitation without rest (Fig. 30).

5.3.1 Treadmill running resulted in 93.4% nonunion rates in unilateral 3 mm defects and systemic immune cell trends were consistent with previously characterized nonunion

Treadmill running that involved running twice per week at a speed of 13 m/min for a total duration of 12 minutes results in 14 out of 15 defects presenting with nonunion after 8 weeks of recovery (Fig. 25). Radiographic evidence revealed minimal bone formation within the defect region, suggesting that these defects failed to achieve a stable callus during early weeks of healing (Fig. 25). In addition, longitudinal blood draws and flow cytometric analysis investigated the systemic immune response to trauma and temporal resolution. After blood collection, cells were fixed and stained to differentiate different immune cells: T cells, cytotoxic T cells, helper T cells, regulatory T cells, and MDSCs. Longitudinal flow cytometry data revealed a pronounced inflammatory response observed immediately post-injury, followed by a compensatory anti-inflammatory response across all three rehabilitative protocols (Fig. 26). All cell types achieved baseline levels by week 4 post-injury (Fig. 26). No significant difference was seen across

experimental groups, which is expected since nearly all injuries resulted in nonunion after 8 weeks of recovery.

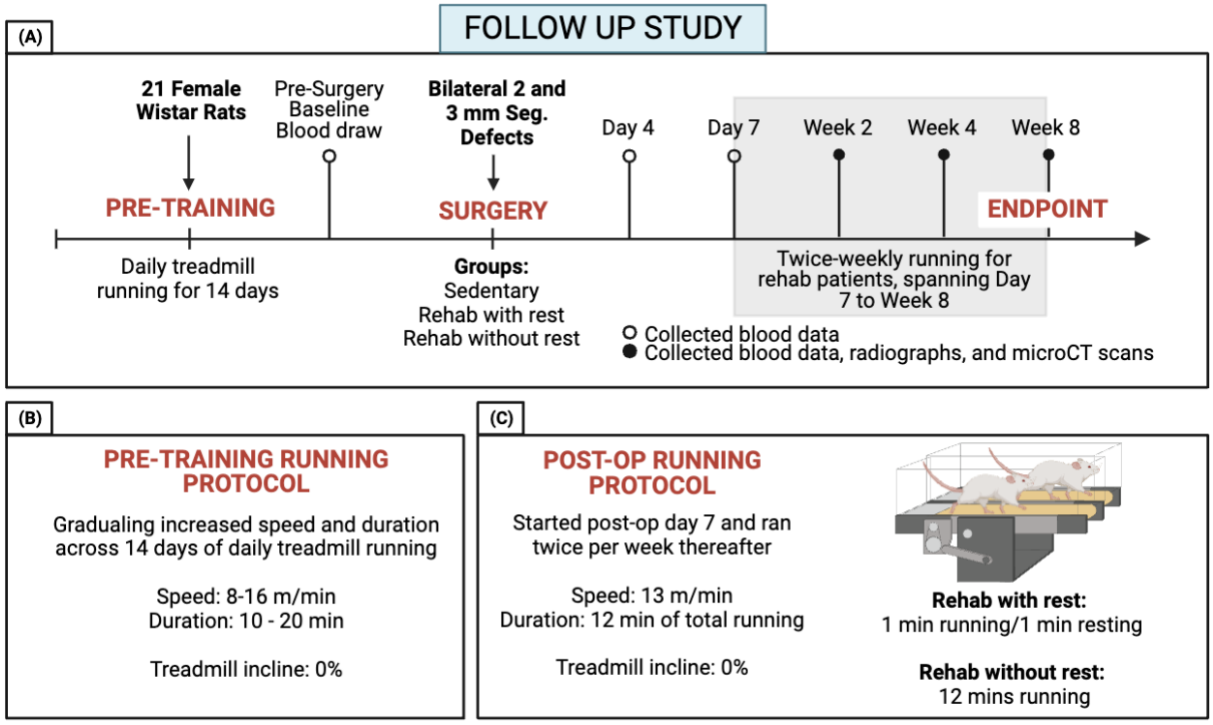

Figure 27. Follow up study design details. (**A**) Experimental timeline with data collection details. (**B**) Running protocol for pre-training prior to surgery. (**C**) Running protocol for after surgery training including details on the rehabilitation with rest versus rehabilitation without rest groups.

5.3.2 Introducing intermittent rest increased bone formation and endpoint bridging rates compared to rehabilitation without intermittent rest

For the follow-up study we investigated the influence of rehabilitation with intermittent rest versus rehabilitation without rest and sedentary controls on bone healing after bilateral bone injuries. Analysis of bone formation revealed an increase in endpoint bone volume in the rehabilitation with rest group compared to rehabilitation without rest for 2- and 3-mm defects

(Fig. 28A-B). For 2 mm defects, microCT quantifications revealed a near-significant increase in bone volume for subjects that underwent rehabilitation with rest compared to rehabilitation

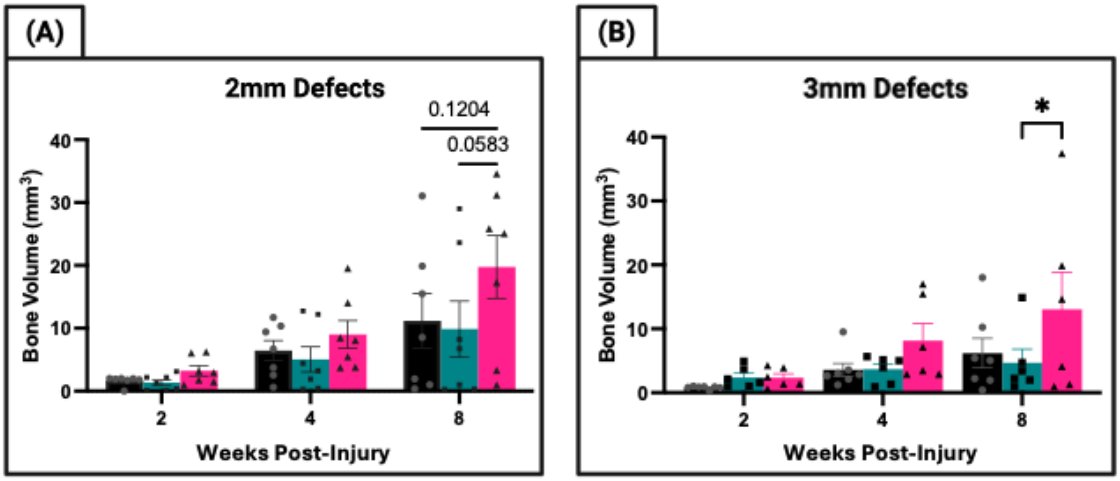

(C)

Week 8 Bridging Rates (%)		
Group	2mm Defects	3mm Defects
Sedentary	28.5 (2/7)	0.00 (0/7)
Rehab w/o Rest	28.5 (2/7)	0.00 (0/6)
Rehab w/ Rest	57.1 (4/7)	16.7 (1/6)

Figure 28. Rehabilitation with rest increase bone formation and endpoint bridging rates compared to rehabilitation without rest in 2 and 3 mm bone defects. (**A**) In vivo bone volume within centered 1.5 mm of 2 mm defects across 8 weeks of recovery (Two-Way Anova with Tukey's multiple comparisons, n = 7). (**B**) In vivo bone volume within centered 2.5 mm of 3 mm defects across 8 weeks of recovery (Two-Way Anova with Tukey's multiple comparisons: * p = 0.0455, n = 6-7). n = 1 subjects was excluded in the rehabilitation with rest and rehabilitation without rest because the defect was not 3 ± 0.5 mm. (**C**) Endpoint bridging rates after 8 weeks of recovery determined by radiographs and 3D microCT reconstructions. Data are Mean ± SD.

without rest and sedentary controls (Fig. 28A). For 3 mm defects, rehabilitation with rest significantly increased week 8 bone volume compared to rehabilitation without rest (Fig. 28B). In addition, the 2mm endpoint bridging rates for the rehabilitation rest group were double that of

sedentary and rehabilitation without rest controls (Fig. 28C). We continue to observe a persistent lack in union after 3 mm bone injuries with only 1/19 subjects achieving union by week 8 (Fig. 28C and 29).

5.3.3 Introduction of rehabilitation with rest restored myeloid-derived cell types back to baseline faster than sedentary and rehabilitation without rest controls

In addition to tracking longitudinal bone healing, we also collected arterial blood and performed subsequent flow cytometry to assess the systemic immune response to trauma at multiple timepoints (Fig. 27). We specifically investigated 5 different inflammatory and anti-inflammatory cell types including T cells, cytotoxic T cells, helper T cells, Monocytes, and MDSCs. Longitudinal flow cytometry data revealed an immediate inflammatory response to injury, followed by a compensatory anti-inflammatory response consistent with our pilot study (Fig. 30). The introduction of rehabilitation with rest significantly depleted monocyte populations in comparison to sedentary subjects at week 2, which is the first time point after the introduction of rehabilitation (Fig. 30B). Flow data also revealed a significant decrease in MDSC

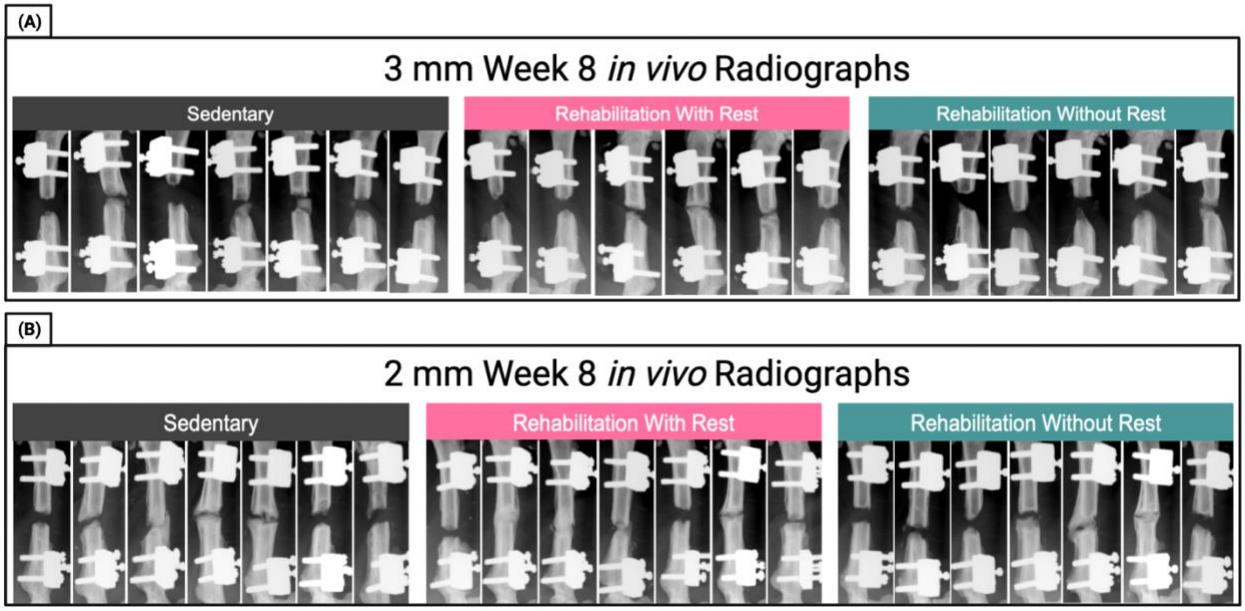

Figure 29. Endpoint radiographs from the follow up study. (**A**) Only 1/19 defects achieved union for 3 mm defects across all experimental groups. (**B**) 8/21 defects achieved union for 2 mm defects.

populations only in the rehabilitation with rest group between post-injury day 7 and week 2 (Fig. 30C). Time significantly influenced all cell types, but rehabilitation conditions only influenced cell types between day 7 and week 2 post-injury, which is immediately after the introduction of post-injury rehabilitation (Fig. 30).

5.4 Discussion

Many groups have found beneficial effects of treadmill exercise on bone tissue [313–315,317]. However, most of these studies investigated preclinical models of intact bone. Previously, Klosterhoff *et al.* investigated post-injury treadmill walking and its impact on bone healing of segmental bone defects stabilized with a stiff versus compliant fixation plate [15]. This study involved unilateral 6 mm segmental bone defects that were treated with Bone Morphogenetic Protein-2 (BMP-2), a potent bone forming biologic. They found that 20 minutes of treadmill walk at 6.5 m/min twice per week starting seven days post-injury significantly increased bone formation for defects stabilized with the compliant fixation plates compared to those fixed with stiff plates [15]. Suljevic *et al.*, also investigated post-injury treadmill exercise after a bi-cortical 1.6 mm hole through rodent femurs [318]. Their training program started two days post-injury and involved gradually increasing running time and speed across two weeks of training (5 days/week). Rodents ran at an initial speed of 10 m/min for 10 minutes and eventually ramped up to 16 m/min for 15 minutes. MicroCT data revealed significantly more newly formed bone within the regenerative niche for treadmill running group compared to sedentary controls [318]. Recent investigations of post-injury mechanical loading also revealed that too much rehabilitation too early can be deleterious. Boerckel *et al.* found that too much loading enabled by a fixation plate that was unlocked (making it more flexible) immediately after injury resulted in diminished bone formation after 8 mm segmental bone defects treated with BMP-2 [7].

Conversely, Boerckel *et al.*, also found that waiting to unlock the fixation plate until initial bridging occurred at week 4 significantly improved bone healing, suggesting a time-adaptive approach for mechanically-induced bone repair [6,7]. In our pilot study (n = 5) we wanted to implement a time-adaptive rehabilitation protocol by dynamically changing the intensity level across weeks of recovery. For this study, rodents underwent treadmill running twice per week at

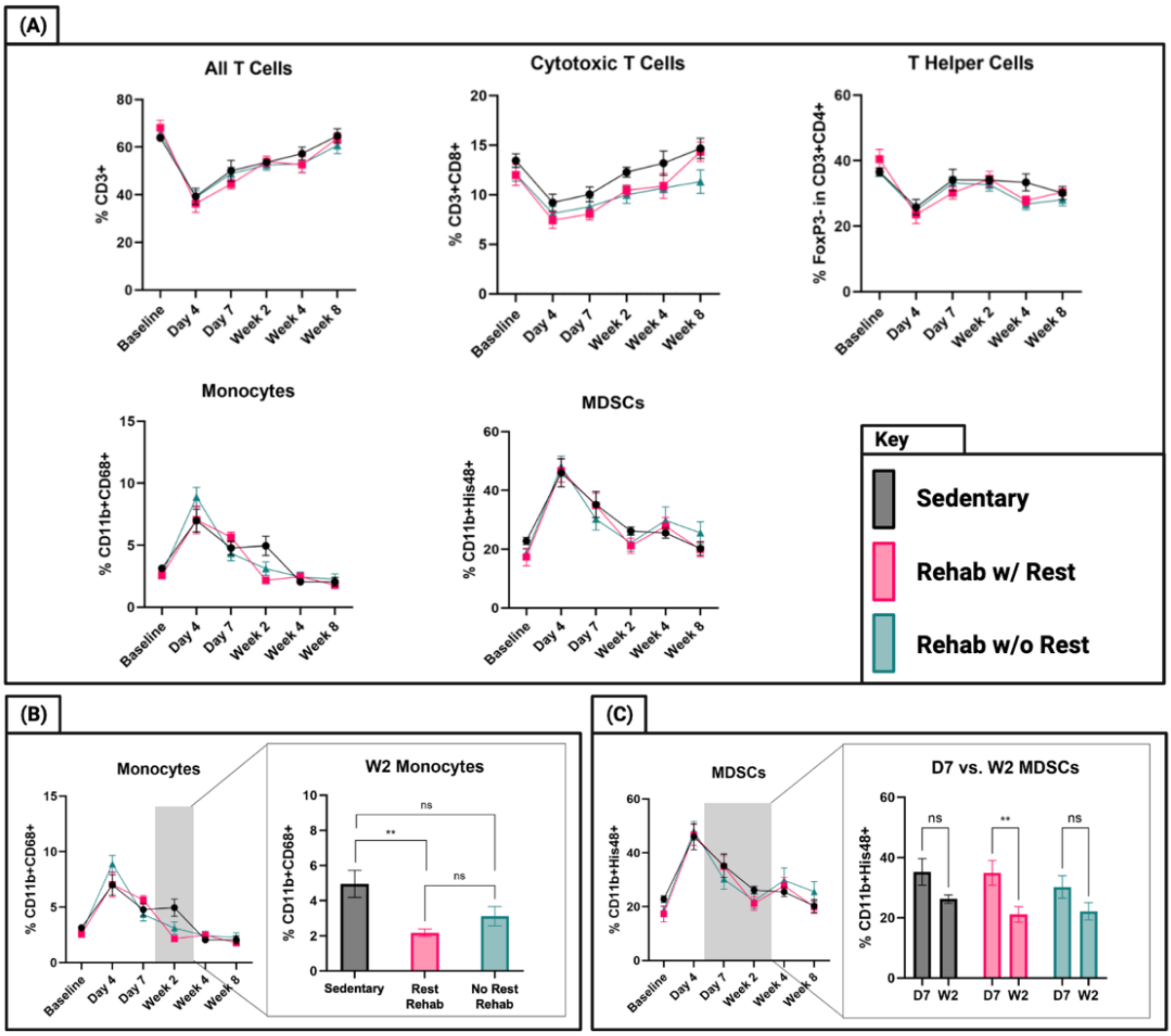

Figure 30. The introduction of rehabilitation with rest reduced systemic inflammation with myeloid-derived cell types restoring to baseline quicker than sedentary and rehabilitation with no rest controls. (**A**) Systemic immune cell temporal characterization using flow cytometry across 5 different cell types (n = 6-7). (**B**) Characterization of circulating monocytes, highlighting week 2 populations (Two-Way Anova with Sidak's multiple comparisons: ** p = 0.0013, n = 6-7); (**C**) Characterization of circulating MDSCs, highlighting a temporal change across day 7 and week 2 populations (Two-Way Anova with Sidak's multiple comparisons: ** p = 0.00185, n = 6-7). Data are Mean ± SD.

a speed of 13 m/min for 12 minutes with varying incline (between 0-3%) after unilateral 3 mm segmental bone defects not treated with biologics. We found that all treadmill rehabilitation regimens significantly impaired bone healing with only 1/15 defects achieving union within 8 weeks independent of time-adaptive changes to treadmill incline (Fig. 25). Previous studies with 2 and 3 mm defects achieved 30-80% bridging rates after 8 weeks of wheel running rehabilitation. Conversely, our pilot study that utilized treadmill running had 7% bridging rates. One difference between these studies was the use of running wheels versus treadmills as the rehabilitation platform. Previous studies revealed that on running wheels rodents run many (~50-200) short running bouts (~10 seconds) and achieved a 30-80% bridging rate after 3 mm bone injuries, but on treadmills rodents ran for 12 minutes without any breaks and achieved a 7% bridging rate after 3 mm bone injuries. These results suggest that running many short bouts with intermittent rest in between may provide a mechanical environment more conducive to bone repair. Therefore, in a follow up study, we investigated whether introducing intermittent rest periods throughout our treadmill running protocol would mitigate the consistent nonunion observed in the pilot study. We found that adding a one minute rest period between each minute of treadmill running improved bone formation and bridging rates after bilateral 2 and 3 mm defects when compared to treadmill running with no rest periods (Fig. 28). In fact, this rehabilitation regimen with intermittent rest doubled the bridging rates after 2 mm defects compared to sedentary and rehabilitation without rest controls (Fig. 28C).

The importance of intermittent rest between loading bouts is consistent with other literature that has found intermittent rest to enhance intact bone formation [286–291,319,320]. In fact, inserting rest periods within loading regimens has been shown to mitigate adaptive response saturation of mechanotransducive cell types crucial for bone health such as osteocytes [289]. Within

these studies, rest periods were short and long term. Robling *et al.* investigated long term rest periods by separating loading regimens into a discrete number of loading bouts. They found that separating 360 cyclic loads into multiple discrete bouts of 60, 90, or 180 loads enhanced osteogenesis. In fact, the number of discrete loading bouts was positively correlated with osteogenesis; 60 loading cycles, 6 times per day boosted bone formation rates 10-fold, while 180 cycles, 2 times per day only increased bone formation 4-fold compared to control bones [288]. With short term rest, Srinivasan *et al.* found that 10 second rest periods between sequential loading cycles enabled several loading regimen to become osteogenic that were previously shown to as not osteogenic [22–24]. They found a low-frequency loading regimen with intermittent rest improved periosteal osteogenesis in mice tibiae relative to tibiae loaded continually for the same total duration [286]. Additionally, Srinivasan also found that 10 seconds of rest between load cycles transformed low-magnitude loading into a potent osteogenic regimen [286]. In fact, they further validated these results by showing that 10 seconds of rest between loading cycles of low-magnitude can also increase osteogenic response in both adolescent and adult mice [291]. It is known that osteocytes and other bone cells are stimulated by shear stress induced by fluid flow within bone's lacunae network [321,322]. Therefore, it is hypothesized that inserting a rest period between repetitive loading cycles may enable repetitive maximal fluid flow, thereby enhancing the osteogenic potential of that regimen. Additionally, Rubin and Lanyon have observed a saturation of bone formation if repetitive loading regimens had more than 36 cycles per day [279]. Research also hypothesized that loading cycles with intermittent rest periods combats bone tissue saturation, thereby enhancing bone formation. It's important to note that these studies investigated the impact of loading with rest periods on intact bone. Conversely, our study investigated the translation of this concept into a traumatic bone injury model. We found

rehabilitation with rest significantly improved bone formation and bridging rates compared to rehabilitation without rest after 2 and 3 mm segmental bone defects.

Our lab has investigated the influence of rehabilitation on 2 and 3 mm segmental bone defects across several studies [175,246]. Radiographic evidence has consistently revealed two types of nonunion. One type happens when no callus tissue is present in the defect region by week 4, resulting in nonunion with distinct bone caps by week 8. Conversely, another type of nonunion has some newly formed tissue within the defect region by week 4 but this tissue fails to bridge the defect region by week 8. These nonunion phenotypes suggest that nonunion occurs due to inadequate conditions for the callus formation or callus consolidation phases of bone healing. We hypothesize that these unique stages of bone healing have distinct mechanical needs. Therefore, we wanted to investigate adaptive rehabilitation with gradually increasing intensity in our pilot study. Surprisingly, this study with unilateral 3 mm bone injuries and post-injury treadmill running resulted in nonunion in 14/15 defects (Fig. 25). Radiographs revealed nonunion with no callus tissue in the defect region across 14/15 subjects (Fig. 25). These results suggest that our experimental set up resulted in a mechanical environment not conducive to callus formation. Previous studies with bilateral 2 and 3 mm defects achieved 30-80% bridging rates after 8 weeks of wheel running rehabilitation. Conversely, our pilot study used unilateral defects susceptible to off-loading of their injured limb which likely reduced the load felt within the regenerative niche. Therefore, we hypothesized that the low-magnitude loading due to shielding of rodent's injured limb and the lack in intermittent rest were detrimental to healing.

To investigate this hypothesis, we performed a follow-up study that evaluated rehabilitation with rest on bone healing after bilateral 2 and 3 mm defects, compared to sedentary and rehabilitation without rest controls (Fig. 27). Analysis of bone formation revealed an

increase in endpoint bone volume in the rehabilitation with rest group compared to rehabilitation without rest for 2 and 3 mm defects (Fig. 28). After 3 mm bone injuries we observed a low bridging rate of 5% (1/19) across the three experimental groups. Unlike our previous pilot study, several of the nonunion had some bone formation within the defect regions but failed to bridge the defect (Fig. 29). The presence of callus tissue within the defect region suggests that these subjects had a mechanical environment more conducive to callus formation than our pilot study. Furthermore, bilateral defects, which minimize off-loading of the injured limb might facilitate a mechanical environment more supportive of callus formation in a 3 mm bone injury. As expected, bridging rates were lower in larger bone injuries, which have a reduced progenitor pool, greater damage to the vasculature, and experience more interfragmentary movement than smaller defects [262,300,301]. These factors, likely make larger defects more mechanosensitive. Without biological support, 3 mm injuries exhibit minimal bridging with treadmill running, suggesting that the induced mechanical environment was not enough to overcome limitations to the biological environment.

Previous studies have achieved a 60% bridging rate with 3 mm defects treated with post-injury rehabilitation. This study investigated in-cage rodent running wheels instead of treadmill running. Research has found that rats show signs of systemic stress after short term (1-5 days) of treadmill exercise [323]. Eight weeks of forced treadmill running also resulted in adaptations to neuroendocrine tissues and immune responses that are commonly associated with chronic stress [324]. Recent work has also found that psychosocial stress can negatively impact fracture healing, while free-running wheel access is highly rewarding to rodents [241–243]. In fact, literature has established that cage enrichment, like the in-cage running wheels, improves the mental and physical fitness of laboratory rats [324]. Therefore, the unexpectantly low bridging rates observed

in the current studies may be partially explained by the additional stress from post-injury treadmill running compared to wheel running.

Although our findings suggest a beneficial impact of rehabilitation with intermittent rest on bone healing, it's worth noting some limitations. Our study is slightly under powered with a sample size of 5 to 7 animals per group. Ideally, our study should investigate 8-10 rodents per group for robust statistical analyses. Future work is adding subjects that undergo identical bilateral surgeries and rehabilitation as our follow up study (n = 4) to increase our sample size to 10-11 per group. This study will also implant our strain sensors to detect local strains as a function of time and rehabilitation conditions. In addition, we only investigated one ratio of running to rest (1 min running/1 min rest). We selected this ratio of running to rest due to logistical constraints of our treadmill system. After the speed is set, the treadmill belt and rats take several seconds for both to achieve the desired speed. We selected a minimum running duration of one minute to ensure that rodents would achieve the desired running speed and distance based on previous work. We also selected an equivalent rest period duration for our initial investigation of intermittent rest with expectations to explore additional ratios in the future. Robling *et al*. found that rest periods of less than 7 seconds did not boost osteogenesis, while 14 seconds of rest significantly increased rat tibial bone formation rates, suggesting that further tuning our rehabilitation regimen may differentially impact bone healing [320]. Our bone healing results also achieved low bridging rates with nearly all groups achieving a bridging rate below 50%. These results reveal potential to improve bridging rates by continuing to optimize our rehabilitation regimen or investigating potential synergistic relationships between rehabilitation and local biologics such as BMP-2. Tuning of the rehabilitation regimen could investigate different durations of running and intermittent rest. Rats complied with our post-

injury rehabilitation after a unilateral or bilateral defect. Therefore, it'd also be reasonable to run rodents more frequently throughout the week to mimic previous studies that had better bridging rates after wheel running 5-7 days a week.

The immune system's dynamic response to factors such as injury and exercise necessitates longitudinal characterizations of blood biomarkers. In our pilot study we investigated the systemic immune response to rehabilitation regimens to explore potential correlations with endpoint bone healing. Blood was collected from rats at designated time points: baseline (prior to surgery), day 4, weeks 2, 4, and 8. Subsequent cell fixation and staining differentiated different immune cells (Fig. 26). Longitudinal flow cytometry data revealed a pronounced inflammatory response immediately post-injury, followed by a compensatory anti-inflammatory response that were not significantly different between experimental groups (Fig. 26). This result was not surprising since 93% of defects were a nonunion by week 8. The temporal trends of these inflammatory and anti-inflammatory cells were consistent with previously characterized nonunion after 8 mm segmental bone defects that were not treated with biologics within the first 8 weeks post-injury [325]. The dynamic modulation of these cell types underscores the complex interplay of immune cells throughout the healing process. Literature has previously established a relationship between systemic immune cells and endpoint bone regeneration in sedentary rats; however, the immune response to traumatic bone injury has not been well characterized in rats that undergo postoperative exercise [7,18]. It has also been shown that exercise influences immune cell types across several preclinical and clinical studies, however these studies do not involve traumatic bone injuries [326–330]. The segmental 2 and 3 mm defect models provide robust models to explore the temporal immune cells after trauma and throughout rehabilitation without the confounding factor of BMP-2 with known inflammatory

effects [331–333]. Our temporal characterization of the immune response in response to 2 and 3 mm traumatic bone injuries will enable future research to evaluate rehabilitation as a therapeutic treatment and its effects on immune cells, offering insights into intervention efficacy and recovery mechanisms.

In our follow-up study, longitudinal blood collections and flow cytometric analysis revealed that myeloid-derived cell types (monocytes and MDSCs) were differentially impacted by two different rehabilitation regimens. At the first time point after the introduction of rehabilitation post-injury, rehabilitation with rest significantly depleted the monocyte population compared to sedentary controls (Fig. 30). A significant decrease in MDSC populations was also only observed in the rehabilitation with rest group between post-injury day 7 and week 2, which is also the group with the highest bone volume and endpoint bridging rates (Fig. 30). Elevated MDSCs, within 2 weeks of traumatic bone injuries have been previously correlated to poor endpoint bone healing [275,325]. Exercise has a known anti-inflammatory effect, which is hypothesized to involve the release of several cytokines (IL-6, IL-10, IL-1, etc) that regulate T cell, monocyte, and macrophage functions [334]. Building on this work, we found only rehabilitation with rest to decrease systemic inflammatory by restoring myeloid-derived cell types to baseline levels faster than rehabilitation without rest and sedentary controls. Conversely rehabilitation without rest and sedentary controls had similar temporal trends in immune cells and diminished bone healing. In our experimental set up, the use of bilateral defects limited our ability to correlate systemic immune markers to bone healing. However, we were able to discern significant influences of different rehabilitation regimens on immune cells during early weeks of healing. Our findings ultimately suggest that rehabilitation could be utilized as a therapeutic to

not only increase bone formation, but also modulate the immune response in a manner conducive to bone healing.

In conclusion, we found that post-injury treadmill exercise must incorporate intermittent rest periods to improve bone healing after bilateral 2 and 3 mm bone defects with no biological augmentation treatment. A previous study also found that long term rest (> 10 hours/day) is crucial to bone healing [246]. Taken together, our findings support both long term and short term rest for bone formation, which is consistent with literature that found both types of rest crucial for intact bone health. Our blood analysis also revealed that only the introduction of rehabilitation with rest decreased systemic immune cell populations previously correlated with impaired bone healing [275,325]. Therefore, our results support rehabilitation, that balances a moderate amount of activity with both short and long term rest, as a therapeutic to not only produce beneficial mechanical loads, but also modulate the immune response to improve bone healing.

CHAPTER 6: CONCLUSIONS AND CLINICAL IMPACT

Content of this chapter are adapted from *Nash K.E., Ong K.G., Gebreyesus E.A., LaBella S.A., Weiss J.A., Harrer J.A., Willett N.J., Leucht P., and Guldberg R.E., (2022) Springer [1] as well as *Nash K.E., Ong K.G., and Guldberg R.E., (2022) Connective Tissue Research [2].

*Publication under maiden name: Kylie E. Nash

6.1 Primary Conclusions & Contributions to the Field

Altogether, the work conducted throughout this thesis provided 6 principal contributions:

1. Established a platform for data-informed rehabilitation regimens using tunable rehabilitation equipment, our implantable strain sensors, subject-specific finite element models, and longitudinal activity and bone healing data.
2. Validated that dynamic strains across bone defects change as a function of time and healing status.
3. Utilized rehabilitation to promote functional regeneration of segmental bone injuries to intact, unoperated strength without the use of biologics.
4. Challenged the longstanding focus of modulating the loading magnitude for optimized bone regeneration by revealing the importance of both long term and short term rest within post-injury rehabilitation protocols.
5. Developed a data-informed multifactorial rehabilitation regimen predicted to improve bone healing.
6. Demonstrated mechanosensitivity of the immune response following the introduction of post-injury rehabilitation.

Regenerative Rehabilitation

Several research groups have investigated the osteogenic potential of mechanical stimulation on bone tissue to inform regenerative medicine and rehabilitation strategies. These research groups have predominately utilized fixation plate stiffness or loading apparatuses to modulate the loading magnitude [6,15,27,65,191,279,335]. However, there's a finite number of fixation plate design modifications, and loading apparatuses do not exert physiological loading patterns representative of locomotion. Therefore, the studies described in this thesis utilized rehabilitative exercise as a clinically-relevant and dynamic strategy to modulating loading parameters.

In Aim 1, we investigated the influence of rehabilitative intensity on the local mechanical environment and bone healing. This aim integrated the strain sensor platform developed by Klosterhoff *et al.* that quantifies the *in vivo* mechanical environment throughout recovery [3]. This sensor technology demonstrated that local niche mechanics change as a function of time and rehabilitation. Rehabilitation of greater intensity significantly increased the local compressive and shear strains along the fixation plate and within the regenerative niche. Further, higher magnitude loads resulted in significantly improved bone healing. In contrast to the longstanding belief that 2-10% strains are advantageous to fracture healing, our results suggest that compressive strains ranging from 12-18% two weeks post-injury can also promote robust fracture healing [257,258]. In fact, rehabilitation that induced these high strains led to the regeneration of a 2 mm segmental bone defect, which achieved intact femur strength without the use of biologics. Although higher magnitude loading produced the best healing outcome for this study, our lab has also shown that too much loading too early can severely inhibit bone formation [6,7]. This previous study involved a fixation plate was either locked (rigid) or unlocked (flexible). Boerckel *et al.* found that unlocking the fixation plates immediate at time of injury resulted in consistent nonunion after an 8 mm bone injury. This study predated our preclinical

implantable strain sensor and thus does not provide quantifications of local strains within the regenerative niche. The lack in local strains quantifications highlights the need for more studies with our implantable sensor technology to quantify local strains in relation to time and healing status to determine the optimal strain conditions for bone healing as a function of time. Overall, this study supported rehabilitation as an influential therapeutic for fracture healing and validated the potential of the implantable sensor technology to continuously quantify the local mechanical environment and advance our understanding of mechanical environments conducive to bone healing.

Although many research groups have investigated advantageous versus detrimental loading conditions for bone healing, little work has looked beyond modulating the magnitude of cyclic loads. Rubin, Lanyon, and others have found that osteogenic responses can be influenced by strain magnitude, strain rate, frequency of loading, and loading duration [279–284]. However, these studies investigated the osteogenic potential of intact bones and did not utilize a bone injury model. Therefore, for Aim 2, we examined the multifactorial effect of six different rehabilitation parameters on bone healing after traumatic bone injuries. This study revealed that bone healing depended on an adequate balance between activity and rest which changed as a function of injury severity; more severe bone injuries required less daily activity and longer rest periods than smaller injuries. Machine learning was employed to produce nonlinear multivariate models, which revealed a "goldilocks" phenomenon for bone healing, where some rehabilitation is needed to stimulate bone formation, but too much can be severely detrimental. Furthermore, these models revealed that bone healing is maximized when a moderate amount of running is paired with longer rest periods. The findings throughout Aims 1 and 2, provided a data-informed rehabilitation protocol that was predicted to improve bone healing and accounted for

rehabilitation intensity, activity level, and rest periods. We hypothesized that rest is important to segmental bone injuries due to the known cellular response saturation of bone cells in the absence of rest periods [280,320].

In Aim 3, we wanted to further explore this data-informed rehabilitation protocol by utilizing treadmills that enabled precise control of factors such as running distance, duration, speed, rest, etc. Despite several research groups utilizing treadmill exercise for musculoskeletal research, we found that treadmill exercise after unilateral traumatic bone fracture resulted in nearly 100% nonunion [314,315,317]. Based on mechanobiology principles, we believe treadmill exercise was disruptive to bone healing because of the lack in short-term rest between loading bouts. Researchers have found that short-term rest between loading bouts improves the osteogenic potential of mechanical stimulation [286,287,289,291,292]. Researchers hypothesize that short-term rest minimizes the chance of mechanotransducive cells experiencing signal saturation and that the rest enables repetitive creation of maximal fluid flow, enhancing osteogenic potential. Motivated by these mechanobiology principles, Aim 3 investigated the importance of intermittent rest within rehabilitation protocol for bone healing. Consistent with literature, our results reveal that bone healing is improved when treadmill exercise incorporated intermittent rest. Therefore, this thesis revealed the importance of both long term and short term rest on bone healing. The novel insight into rest periods for bone healing revealed that rehabilitation strategies need to not only optimize the loading magnitude, but they also need to adequately balance activity levels with rest periods both in the short and long term.

Beyond loading and rehabilitation conditions, investigators have studied the effects of exercise on the inflammatory response. Several research groups have found that exercise modulates the immune response both in preclinical and clinical studies [12,223,313]. However, these

studies did not involve a traumatic injury. Therefore, in Aim 3, we investigated the systemic immune response to traumatic bone injuries and different post-injury rehabilitation conditions. While preliminary, our immune characterization revealed that rehabilitation can not only modulate the local mechanical environment but also the systemic immune response to trauma. Only the introduction of rehabilitation with rest depleted systemic myeloid-derived cells throughout early weeks of recovery as compared to sedentary and rehabilitation without rest subjects. Interestingly, the rehabilitation with rest group also had significantly improved bone healing, which is consistent with previous literature that found impaired bone healing with increased myeloid-derived cell types across early weeks of healing d[275,325]. Taken together, the results of this thesis support the use of local strains and systemic immune markers as potential feedback metrics to inform evidence-based rehabilitation decisions.

Translational Insight with Implantable Sensors

A major challenge facing surgeons and physical therapists seeking to treat complex fractures is defining and controlling the mechanical environment conducive to bone healing. Therefore, complex fractures are often treated with conservative and subjective surgical and rehabilitation approaches. Motivated to address this challenge, the studies described in this thesis continued utilizing an implantable strain sensor that provided objective quantification of the local mechanical environment in response to fixation plate stiffness, healing status, and rehabilitation. Previous work by Klosterhoff *et al.* developed this strain sensor platform and revealed that (1) fixation plate stiffness significantly impacted the local mechanical environment and fracture healing and (2) that strains data from early weeks of recovery can predict bone healing outcomes before radiographic evidence [15]. Building on this work, this thesis also revealed that (1) local strains only decrease if healing progresses and (2) that rehabilitation conditions can significantly

influence local strains and healing outcomes. These principles highlight our strains sensors as a technology with the capability to provide real-time, subject-specific strain data as a feedback indicator of healing status to inform adaptive rehabilitation decisions.

6.2 Future Directions

The findings of this thesis motivate the future exploration of rehabilitation-based treatments for improved bone healing. Future questions and research initiatives to advance this work can focus on four thrusts: (1) adaptive rehabilitation strategies that rely on immune and strain data as feedback indicators of healing status to inform personalized rehabilitation decisions, (2) potential synergies between biologics and rehabilitation for larger bone injuries, (3) the necessary balance between fixation plate stiffness and rehabilitative loading for improved bone healing, and (4) the translation of an implantable strain sensor embedded on clinical hardware used for complex fractures.

While this thesis investigated several aspects of rehabilitative loading on bone healing, all rehabilitation conditions remained unchanged throughout recovery. Dynamic loading strategies have been investigated by several research groups that incorporate dynamization or reverse dynamization strategies. Dynamization increases interfragmentary movement by reducing the fixation stiffness throughout recovery, while reverse dynamization decreases interfragmentary movement by increasing the fixation stiffness throughout recovery [187,193]. Research has yet to investigate dynamic rehabilitation strategies as a means to "dynamize" a healing fracture. Future work could utilize the resistance running wheels, locked versus unlocked treadwheels, or treadmill platform to explore adaptive rehabilitation that varies the amount of activity, intensity, speed, or rest periods over time. Furthermore, rehabilitation adaptations could be informed by subject-

specific strain or immune data to develop optimized rehabilitation regimens that adapt to subject-specific needs.

Traumatic bone fractures are often treated with biologics both in preclinical and clinical studies [336,337]. These biologics often involve growth factors or small molecules that are used to robustly form bone after large injuries. With the support of rehabilitative exercise as a promising therapeutic for bone regeneration, future work could investigate potential synergies between biologics and rehabilitation. More specifically, this thesis characterized a reliable rehabilitation-induced nonunion model: 3 mm segmental bone defect that was stabilized with compliant fixation plates and underwent post-injury treadmill exercise. Future work could utilize this model with a low dose of biologics to elucidate potential synergies between these strategies that target the biological and mechanical needs for bone healing.

Traumatic bone injuries often require the implantation of stabilization hardware that have unique mechanical properties. It is known that implant stiffness can significantly impact healing, and this thesis revealed that rehabilitation conditions can significantly impact the loads felt by implants and subsequent healing. Clinically, it is hypothesized that fractures stabilized with rigid implants can withstand earlier and greater limb loading than fractures stabilized with less rigid implants. However, the lack in technology to track the evolving local mechanical environment has limited the understanding of the interactions between implant stiffness and rehabilitation and their combined influence on bone healing. Therefore, future work could investigate the interaction and necessary balance between the implant stiffness and rehabilitative loading.

The mechanical environment is a known potent influencers of fracture healing, however a quantified understanding of the local mechanical environment throughout healing is limited. This motivates the commercialization of a clinical strains sensor that can integrate with surgical

hardware used to treat severe bone fractures. Data from these sensors have the potential to advance our understanding of the mechanical demands for improved fracture healing as well as optimize surgical and rehabilitation strategies utilized to treated clinical fractures.

6.3 Clinical Impact

6.3.1 Clinical Problem: Distal Femoral Fractures

An estimated 90,941 distal femoral fractures (DFF) occur annually in the United States and the incidence of these injuries has nearly doubled in the last twenty years as our population ages [338,339]. Each of these fractures incur up to $61k in surgical costs, totaling a $5.5B annual yearly burden on the US healthcare system [340–342]. The incidence of DFFs has a bimodal age distribution with nearly all patients being either young adults with a high energy trauma or elderly adults with a low-energy mechanism [343]. Treatment of DFFs is further complicated for geriatric patients who often have comorbidities, increasing the risk of nonunion or implant failure [344]. One-year mortality rates in geriatric patients associated with DFF are approximately 25%, highlighting the significant public health concern associated with these fractures [345].

Despite the significant and growing clinical burden of complex bone fractures, technology to improve surgical and postoperative care has been limited. Complication and mortality rates remain consistently high for DFF patients partially because surgical decisions on plate type, screw patterning, construct rigidity and postoperative weight bearing protocols are subjective and depend on expert opinions as opposed to objective data. Despite its growing prevalence, there is no consensus on surgical approach or implant hardware design for DFF fracture repairs. In addition, radiographs and clinical assessment, which often do not have enough temporal resolutions and specificity, are still the primary tools used to track healing status, leading to uncertainty in assessment of fracture healing progression and increasing the risk of nonunion and implant

hardware failure. A sensor technology that can measure forces *in situ* to inform intraoperative surgical decisions on fixation plate location, type, and screw pattern could help standardize surgical repairs. Further, sensor technology that is incorporated onto clinically-used lateral fixation plates would allow surgeons to maintain their surgical approach, minimizing potential risk to patients and supporting clinical adoption of the technology.

With the current available technology, surgeons struggle to identify at-risk patients after DFFs until postoperative complications occur. The most common postoperative complications for DFFs are nonunion or implant failure. Once these complications occur, surgeons are left with minimal options outside of revision surgery, which are significant emotional, financial, and physical burdens on patients. Sensor technology to enable proactive identification of at-risk patients could enable surgeons to intervene with nonunion therapeutics (e.g. bone stimulators) or adjust physical therapy protocols at an early timepoint and increase the chances of achieving union. Additionally, insurance providers continue to reduce coverage for postoperative physical therapy and the standard-of-care for DFFs struggle to keep up with this increasingly strict timeline.

6.3.2 Commercialization Potential to Help Complex Fractures

Favorable conditions for bone healing require precise control of longitudinal strains in the fracture gap, which are regulated by fixation stiffness and rehabilitation protocols. Research suggests that maintaining a 2–10% strain between fracture ends promotes fracture healing [234,346]. However, excessive or insufficient strain can lead to non-union or delayed union, as confirmed by both experimental and clinical studies [236,304,305,347,348]. In addition, despite the importance of early but safe weight-bearing for geriatric patients, the relationship between fixation rigidity, rehabilitation, and healing potential remains undefined in the distal femur largely because of technological deficits in the current standard of care. Optimal treatment of DFFs requires a delicate

balance between fixation stiffness and rehabilitation which could be achieved by tracking real-time fixation plate mechanics. Clinical sensors that provide noninvasive, quantitative readouts of fixation plate strains as a feedback indicator of implant stability and healing status have the potential to inform intraoperative and postoperative decisions. More specifically, sensors that read strains across internal fixation plate could provide data to inform intraoperative surgical decisions on fixation plate location, type, and screw pattern through intraoperative force testing to improve surgical outcomes and standardize surgical DFF repairs. In addition, these sensors could inform rehabilitation: for patients progressing within the 2-10% strain window, our sensor would enable faster advancement through rehabilitative exercises, minimizing recovery time and associated healthcare costs. Conversely, for patients with strains outside the 2-10% window, our sensor could identify these individuals as "at-risk" before a second operation is required due to nonunion or implant instability, ultimately reducing reoperation rates. Furthermore, this technology could provide new understanding of the dynamic strain environment involved in fracture healing that would advance our understanding of the fracture healing environment after DFF and other fractures throughout the body.

Other innovations for challenging fractures such as DFFs include modifications to surgical approaches and implant designs. These modifications have shown limited clinical impact. Orthopedic implant companies started making titanium fixation plates instead of stainless-steel plates in 1992, yet no clear advantage to postoperative outcomes have been found [349]. Furthermore, there has been a recent increase in DFF stabilized by two implants (plate and nail or two plates) with unclear impact on complications [350]. In addition, distal femoral replacement is a new surgical approach for DFF repairs. Distal femoral replacement surgeries cost roughly 26% more than the standard ORIF procedure (that use a fixation plate) and have shown increased rates of

postoperative complications following DFF repair compared to ORIF [342,351]. These examples illustrate the need for innovative technology, besides changing surgical approaches and implant design, to reduce the stagnant reoperation rates associated with DFF treatment.

Other sensor-based innovations include an auditory feedback devices to provide insight on postoperative weight bearing [352,353]. This device was found to be ineffective in preventing limb overloading due to a lag between auditory perception and motor response [353,354]. Subsequent iterations of the auditory feedback devices found that verbal feedback from the physical therapist remained more beneficial in achieving weight-bearing compliance [354,355]. Leveraging the beneficial oversight of physical therapists, a clinical sensor that measures real-time fixation plates strains would empower physical therapists with real-time patient-specific data to enable evidence-based rehabilitation.

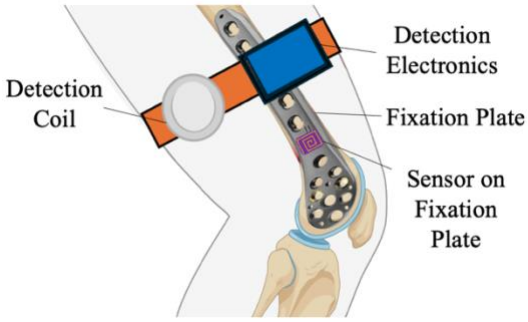

Figure 31. Illustration of an internal sensor fixation plate and wearable detection system. The wearable device is shown a few inches from the actual position to highlight the sensor.

With our preclinical sensor platform, we are one step closer to developing a clinical sensing system to monitor local strains along internal fixation plates. The sensing element would comprise a battery-free, wireless sensor embedded on an internal fixation plate that is already the standard of care for DFFs. The instrumented bone plate would be wirelessly monitored with a wearable device, allowing real-time, continuous biofeedback for surgeons and physical therapists to make informed intraoperative and postoperative decisions (Fig. 31). Our instrumented bone plate will enable surgeons to objectively confirm stable fixation intraoperatively and track whether each patient is staying within the established beneficial window of 2-10% strains throughout postoperative recovery to minimize complication rates, revisions surgeries, recovery time, and healthcare costs associated with DFFs.

This technology would be highly innovative as it allows surgeons to track patient-specific mechanics throughout surgery, healing, and postoperative physical therapy to objectively inform surgical implant decisions, nonunion management, and physical therapy.

REFERENCES

1. Nash, K. E. *et al.* Regenerative Rehabilitation Strategies for Complex Bone Injuries. in *Regenerative Rehabilitation: From Basic Science to the Clinic* (eds. Greising, S. M. & Call, J. A.) 251–289 (Springer International Publishing, Cham, 2022). doi:10.1007/978-3-030-95884-8_8.
2. Nash, K. E., Ong, K. G. & Guldberg, R. E. Implantable biosensors for musculoskeletal health. *Connective Tissue Research* **0**, 1–15 (2022).
3. Klosterhoff, B. S. *et al.* Wireless implantable sensor for noninvasive, longitudinal quantification of axial strain across rodent long bone defects. *Journal of Biomechanical Engineering* **139**, 111004 (2017).
4. Uhrig, B. A., Li, M.-T. A., Willett, N. J. & Guldberg, R. E. Models of composite bone and soft-tissue limb trauma. in *Biomaterials and Regenerative Medicine* (ed. Ma, P. X.) 534–554 (Cambridge University Press, Cambridge, 2013). doi:10.1017/CBO9780511997839.035.
5. Egol, K. A., Koval, K. J. & Zuckerman, J. D. *Handbook of Fractures*. (Lippincott Williams & Wilkins, Philadelphia, Pa., 2010).
6. Boerckel, J. D., Uhrig, B. A., Willett, N. J., Huebsch, N. & Guldberg, R. E. Mechanical regulation of vascular growth and tissue regeneration in vivo. *Proceedings of the National Academy of Sciences* **108**, E674–E680 (2011).
7. Boerckel, J. D. *et al.* Effects of in vivo mechanical loading on large bone defect regeneration. *Journal of Orthopaedic Research* **30**, 1067–1075 (2012).
8. Kalfas, I. H. Principles of bone healing. *FOC* **10**, 1–4 (2001).

9. McKibbin, B. The biology of fracture healing in long bones. *The Journal of Bone and Joint Surgery. British volume* **60-B**, 150–162 (1978).

10. Elliott, D. S. *et al.* A unified theory of bone healing and nonunion: BHN theory. *The Bone & Joint Journal* **98-B**, 884–891 (2016).

11. Kenwright, J. & Goodship, A. E. Controlled mechanical stimulation in the treatment of tibial fractures. *Clin Orthop Relat Res* 36–47 (1989).

12. Guder, C., Gravius, S., Burger, C., Wirtz, D. C. & Schildberg, F. A. Osteoimmunology: a current update of the interplay between bone and the immune system. *Frontiers in Immunology* **11**, 58 (2020).

13. Willett, N. J. *et al.* Attenuated human bone morphogenetic protein-2–mediated bone regeneration in a rat model of composite bone and muscle injury. *Tissue Engineering Part C: Methods* **19**, 316–325 (2013).

14. Ruehle, M. A. *et al.* Decorin-supplemented collagen hydrogels for the co-delivery of bone morphogenetic protein-2 and microvascular fragments to a composite bone-muscle injury model with impaired vascularization. *Acta Biomaterialia* **93**, 210–221 (2019).

15. Klosterhoff, B. S. *et al.* Wireless sensor enables longitudinal monitoring of regenerative niche mechanics during rehabilitation that enhance bone repair. *Bone* **135**, 115311 (2020).

16. Ruehle, M. A. *et al.* Extracellular matrix compression temporally regulates microvascular angiogenesis. *Sci. Adv.* **6**, eabb6351 (2020).

17. Lord, J. M. *et al.* The systemic immune response to trauma: an overview of pathophysiology and treatment. *Lancet* **384**, 1455–1465 (2014).

18. Rosenthal, M. D. & Moore, F. A. Persistent Inflammation, Immunosuppression, and Catabolism: Evolution of Multiple Organ Dysfunction. *Surg Infect (Larchmt)* **17**, 167–172 (2016).

19. Vantucci, C. E., Roy, K. & Guldberg, R. E. Immunomodulatory strategies for immune dysregulation following severe musculoskeletal trauma. *Journal of Immunology and Regenerative Medicine* **2**, 21–35 (2018).

20. Masquelet, A. C. Muscle reconstruction in reconstructive surgery: soft tissue repair and long bone reconstruction. *Langenbecks Arch Surg* **388**, 344–346 (2003).

21. Yazar, S., Lin, C.-H. & Wei, F.-C. One-stage reconstruction of composite bone and soft-tissue defects in traumatic lower extremities. *Plastic and Reconstructive Surgery* **114**, 1457–1466 (2004).

22. Nauth, A. *et al.* Managing bone defects. *Journal of Orthopaedic Trauma* **25**, 462–466 (2011).

23. Deramo, P. & Rose, J. Flaps, muscle and musculocutaneous. *StatPearls* (2020).

24. Wong, T. M. *et al.* Masquelet technique for treatment of posttraumatic bone defects. *ScientificWorldJournal* **2014**, 710302 (2014).

25. Uk, O. *et al.* The Masquelet technique of induced membrane for healing of bone defects. A review of 8 cases. *Injury* vol. 46 Suppl 8 https://pubmed.ncbi.nlm.nih.gov/26747918/ (2015).

26. Aronson, J. M. D. Experimental and clinical experience with distraction osteogenesis. *Cleft Palate-Craniofacial Journal* **31**, 473–482 (1994).

27. Claes, L. E. & Heigele, C. A. Magnitudes of local stress and strain along bony surfaces predict the course and type of fracture healing. *J Biomech* **32**, 255–266 (1999).

28. Compton, J., Fragomen, A. & Rozbruch, S. R. Skeletal repair in distraction osteogenesis: mechanisms and enhancements. *JBJS Reviews* **3**, 1 (2015).

29. Ai-Aql, Z. S., Alagl, A. S., Graves, D. T., Gerstenfeld, L. C. & Einhorn, T. A. Molecular mechanisms controlling bone formation during fracture healing and distraction osteogenesis. *J Dent Res* **87**, 107–118 (2008).

30. Hoyt, B. W., Pavey, G. J., Pasquina, P. F. & Potter, B. K. Rehabilitation of lower extremity trauma: a review of principles and military perspective on future directions. *Curr Trauma Rep* **1**, 50–60 (2015).

31. Bacon, S. *et al.* A retrospective analysis of comminuted intra-articular fractures of the tibial plafond: open reduction and internal fixation versus external ilizarov fixation. *Injury* **39**, 196–202 (2008).

32. Joslin, C. C., Eastaugh-Waring, S. J., Hardy, J. R. W. & Cunningham, J. L. Weight bearing after tibial fracture as a guide to healing. *Clin Biomech (Bristol, Avon)* **23**, 329–333 (2008).

33. Kershaw, C. J., Cunningham, J. L. & Kenwright, J. Tibial external fixation, weight bearing, and fracture movement. *Clin Orthop Relat Res* 28–36 (1993).

34. Taljanovic, M. S. *et al.* Fracture fixation. *RadioGraphics* **23**, 1569–1590 (2003).

35. Mitkovic, M. B., Bumbasirevic, M. Z., Lesic, A. & Golubovic, Z. Dynamic external fixation of comminuted intra-articular fractures of the distal tibia (type C pilon fractures). *Acta Orthop Belg* **68**, 508–514 (2002).

36. Sato, K., Kikuchi, S. & Yonezawa, T. In vivo intradiscal pressure measurement in healthy individuals and in patients with ongoing back problems. *Spine (Phila Pa 1976)* **24**, 2468–2474 (1999).

37. Zlowodzki, M., Vogt, D., Cole, P. A. & Kregor, P. J. Plating of femoral shaft fractures: open reduction and internal fixation versus submuscular fixation. *Journal of Trauma and Acute Care Surgery* **63**, 1061–1065 (2007).

38. Arazi, M., Oğün, T. C., Oktar, M. N., Memik, R. & Kutlu, A. Early weight-bearing after statically locked reamed intramedullary nailing of comminuted femoral fractures: is it a safe procedure? *J Trauma* **50**, 711–716 (2001).

39. Lin, S.-J., Chen, C.-L., Peng, K.-T. & Hsu, W.-H. Effect of fragmentary displacement and morphology in the treatment of comminuted femoral shaft fractures with an intramedullary nail. *Injury* **45**, 752–756 (2014).

40. Rj, B., Jr, T. T., Ms, M.-Z., Vp, N. & Sm, B. Immediate weight-bearing after treatment of a comminuted fracture of the femoral shaft with a statically locked intramedullary nail. *J Bone Joint Surg Am* **81**, 1538–1544 (1999).

41. Greising, S. M., Corona, B. T. & Call, J. A. Musculoskeletal regeneration, rehabilitation, and plasticity following traumatic injury. *Int J Sports Med* **41**, 495–504 (2020).

42. Hurkmans, H. L. *et al.* The difference between actual and prescribed weight bearing of total hip patients with a trochanteric osteotomy: long-term vertical force measurements inside and outside the hospital. *Archives of Physical Medicine and Rehabilitation* **88**, 200–206 (2007).

43. Inverarity, L. Weight-bearing restrictions and activity after surgery. *Verywell Health* https://www.verywellhealth.com/weight-bearing-restrictions-2696668 (2020).

44. Stucky, F., Vesin, J.-M., Kayser, B. & Uva, B. The effect of lower-body positive pressure on the cardiorespiratory response at rest and during submaximal running exercise. *Front Physiol* **9**, (2018).

45. Latham, N. K. *et al.* Effect of a home-based exercise program on functional recovery following rehabilitation after hip fracture a randomized clinical trial. *JAMA* **311**, 700–708 (2014).

46. Ilfeld, B. M., Duke, K. B. & Donohue, M. C. The association between lower extremity continuous peripheral nerve blocks and patient falls after knee and hip arthroplasty. *Anesth Analg* **111**, 1552–1554 (2010).

47. Long, W. T. *et al.* Postoperative pain management following total knee arthroplasty: a randomized comparison of continuous epidural versus femoral nerve infusion. *J Knee Surg* **19**, 137–143 (2006).

48. Cheville, A. L., Smith, S. R. & Basford, J. R. Rehabilitation medicine approaches to pain management. *Hematology/Oncology Clinics of North America* **32**, 469–482 (2018).

49. Osterweis, M., Kleinman, A. & Mechanic, D. *Rehabilitation Approaches and Issues in Chronic Pain*. *Pain and Disability: Clinical, Behavioral, and Public Policy Perspectives* (National Academies Press (US), 1987).

50. Wolff, J. Das gesetz der transformation der knochen. *A Hirshwald* **1**, 1–152 (1892).

51. Brand, R. A. Biographical sketch: Julius Wolff, 1836–1902. *Clin Orthop Relat Res* **468**, 1047–1049 (2010).

52. Fyhrie, D. P. & Carter, D. R. A unifying principle relating stress to trabecular bone morphology. *Journal of Orthopaedic Research* **4**, 304–317 (1986).

53. Carter, D. R., Fyhrie, D. P. & Whalen, R. T. Trabecular bone density and loading history: Regulation of connective tissue biology by mechanical energy. *Journal of Biomechanics* **20**, 785–794 (1987).

54. Beaupré, G. S., Orr, T. E. & Carter, D. R. An approach for time-dependent bone modeling and remodeling—theoretical development. *Journal of Orthopaedic Research* **8**, 651–661 (1990).

55. Levenston, M. E., Beaupré, G. S., Schurman, D. J. & Carter, D. R. Computer simulations of stress-related bone remodeling around noncemented acetabular components. *The Journal of Arthroplasty* **8**, 595–605 (1993).

56. Huiskes, R., Driel, W. D. V., Prendergast, P. J. & Søballe, K. A biomechanical regulatory model for periprosthetic fibrous-tissue differentiation. *Journal of Materials Science: Materials in Medicine* **8**, 785–788 (1997).

57. Loboa, E. G., Wren, T. A. L., Beaupré, G. S. & Carter, D. R. Mechanobiology of soft skeletal tissue differentiation—a computational approach of a fiber-reinforced poroelastic model based on homogeneous and isotropic simplifications. *Biomech Model Mechanobiol* **2**, 83–96 (2003).

58. Wren, T. A., Beaupré, G. S. & Carter, D. R. Tendon and ligament adaptation to exercise, immobilization, and remobilization. *Journal of rehabilitation research and development* **37**, 217–24 (2000).

59. Stevens, S. S., Beaupré, G. S. & Carter, D. R. Computer model of endochondral growth and ossification in long bones: Biological and mechanobiological influences. *Journal of Orthopaedic Research* **17**, 646–653 (1999).

60. Hernandez, C. J. A model of mechanobiologic and metabolic influences on bone adaptation. 10.

61. Ament, C. & Hofer, E. P. A fuzzy logic model of fracture healing. *J Biomech* **33**, 961–968 (2000).

62. Zadeh, L. A. Fuzzy sets. *Information and Control* **8**, 338–353 (1965).

63. Shefelbine, S. J., Augat, P., Claes, L. & Simon, U. Trabecular bone fracture healing simulation with finite element analysis and fuzzy logic. *Journal of Biomechanics* **38**, 2440–2450 (2005).

64. Bailón-Plaza, A. & van der Meulen, M. C. A mathematical framework to study the effects of growth factor influences on fracture healing. *J Theor Biol* **212**, 191–209 (2001).

65. Bailón-Plaza, A. & van der Meulen, M. C. H. Beneficial effects of moderate, early loading and adverse effects of delayed or excessive loading on bone healing. *Journal of Biomechanics* **36**, 1069–1077 (2003).

66. Geris, L., Gerisch, A., Sloten, J. V., Weiner, R. & Oosterwyck, H. V. Angiogenesis in bone fracture healing: A bioregulatory model. *Journal of Theoretical Biology* **251**, 137–158 (2008).

67. Geris, L., Sloten, J. V. & Oosterwyck, H. V. Connecting biology and mechanics in fracture healing: an integrated mathematical modeling framework for the study of nonunions. *Biomech Model Mechanobiol* **9**, 713–724 (2010).

68. Checa, S. & Prendergast, P. J. A mechanobiological model for tissue differentiation that includes angiogenesis: a lattice-based modeling approach. *Ann Biomed Eng* **37**, 129–145 (2009).

69. Gardner, T. N., Stoll, T., Marks, L., Mishra, S. & Knothe Tate, M. The influence of mechanical stimulus on the pattern of tissue differentiation in a long bone fracture — an FEM study. *Journal of Biomechanics* **33**, 415–425 (2000).

70. Liu, R. W. *et al.* Computational simulation of axial dynamization on long bone fractures. *Clinical Biomechanics* **20**, 83–90 (2005).

71. Byrne, D. P., Lacroix, D. & Prendergast, P. J. Simulation of fracture healing in the tibia: Mechanoregulation of cell activity using a lattice modeling approach. *Journal of Orthopaedic Research* **29**, 1496–1503 (2011).

72. Alierta, J. A., Pérez, M. A. & García-Aznar, J. M. An interface finite element model can be used to predict healing outcome of bone fractures. *Journal of the Mechanical Behavior of Biomedical Materials* **29**, 328–338 (2014).

73. Wilson, C. J., Schütz, M. A. & Epari, D. R. Computational simulation of bone fracture healing under inverse dynamization. *Biomech Model Mechanobiol* **16**, 5–14 (2017).

74. Ganadhiepan, G. *et al.* The effects of dynamic loading on bone fracture healing under ilizarov circular fixators. *Journal of Biomechanical Engineering* **141**, (2019).

75. Mehboob, A. & Chang, S.-H. Biomechanical simulation of healing process of fractured femoral shaft applied by composite intramedullary nails according to fracture configuration. *Composite Structures* **185**, 81–93 (2018).

76. O'Connor, C. & Kiourti, A. Wireless sensors for smart orthopedic implants. *J Bio Tribo Corros* **3**, 20 (2017).

77. Karipott, S. S., Nelson, B. D., Guldberg, R. E. & Ong, K. G. Clinical potential of implantable wireless sensors for orthopedic treatments. *Expert Review of Medical Devices* **15**, 255–264 (2018).

78. Ledet, E. H., Liddle, B., Kradinova, K. & Harper, S. Smart implants in orthopedic surgery, improving patient outcomes: a review. *Innov Entrep Health* **5**, 41–51 (2018).

79. Rydell, N. W. Forces acting on the femoral head-prosthesis: a study on strain gauge supplied prostheses in living persons. *Acta Orthopaedica Scandinavica* **37**, 1–132 (1966).

80. Burny, F. *et al.* Concept, design and fabrication of smart orthopedic implants. *Med Eng Phys* **22**, 469–479 (2000).

81. Nelson, B. D., Karipott, S. S., Wang, Y. & Ong, K. G. Wireless technologies for implantable devices. *Sensors* **20**, 4604 (2020).

82. Ledet, E. H. *et al.* Implantable sensor technology: from research to clinical practice. *J Am Acad Orthop Surg* **20**, 383–392 (2012).

83. Rohlmann, A., Schwachmeyer, V., Graichen, F. & Bergmann, G. Spinal loads during post-operative physiotherapeutic exercises. *PLoS One* **9**, e102005 (2014).

84. Szivek, J. A., Roberto, R. F. & Margolis, D. S. In vivo strain measurements from hardware and lamina during spine fusion. *J Biomed Mater Res B Appl Biomater* **75**, 243–250 (2005).

85. Soares dos Santos, M. P. *et al.* Instrumented hip implants: Electric supply systems. *Journal of Biomechanics* **46**, 2561–2571 (2013).

86. Borchani, W., Aono, K., Lajnef, N. & Chakrabartty, S. Monitoring of postoperative bone healing using smart trauma-fixation device with integrated self-powered piezo-floating-gate sensors. *IEEE Trans Biomed Eng* **63**, 1463–1472 (2016).

87. Graichen, F., Arnold, R., Rohlmann, A. & Bergmann, G. Implantable 9-channel telemetry system for in vivo load measurements with orthopedic implants. *IEEE Trans Biomed Eng* **54**, 253–261 (2007).

88. Pacella, N., DeRouin, A., Pereles, B. & Ong, K. G. Geometrical modification of magnetoelastic sensors to enhance sensitivity. *Smart Mater. Struct.* **24**, 025018 (2014).

89. DeRouin, A. J., Pacella, N., Zhao, C., An, K. & Ong, K. G. A wireless sensor for real-time monitoring of tensile force on sutured wound sites. *IEEE Transactions on Biomedical Engineering* (2016) doi:10.1109/TBME.2015.2470248.

90. Oess, N. P., Weisse, B. & Nelson, B. Magnetoelastic strain sensor for optimized assessment of bone fracture fixation. *IEEE Sensors Journal* (2009) doi:10.1109/JSEN.2009.2025575.

91. Vlaisavljevich, E. *et al.* Magnetoelastic vibrational biomaterials for real-time monitoring and modulation of the host response. *J Mater Sci: Mater Med* **24**, 1093–1104 (2013).

92. Karipott, S. S., Veetil, P. M., Nelson, B. D., Guldberg, R. E. & Ong, K. G. An embedded wireless temperature sensor for orthopedic implants. *IEEE Sensors Journal* **18**, 1265–1272 (2018).

93. Bergmann, G. *et al.* In vivo glenohumeral contact forces--measurements in the first patient 7 months postoperatively. *J Biomech* **40**, 2139–2149 (2007).

94. Ledet, E. H., Tymeson, M. P., Dirisio, D. J., Cohen, B. & Uhl, R. L. Direct real-time measurement of in vivo forces in the lumbar spine. *The Spine Journal* **5**, 85–94 (2005).

95. Gustke, K. A., Golladay, G. J., Roche, M. W., Elson, L. C. & Anderson, C. R. A targeted approach to ligament balancing using kinetic sensors. *J Arthroplasty* **32**, 2127–2132 (2017).

96. Clausen, I. & Glott, T. Development of clinically relevant implantable pressure sensors: perspectives and challenges. *Sensors (Basel)* **14**, 17686–17702 (2014).

97. Kannan, R. Y., Salacinski, H. J., Sales, K., Butler, P. & Seifalian, A. M. The roles of tissue engineering and vascularisation in the development of micro-vascular networks: a review. *Biomaterials* **26**, 1857–1875 (2005).

98. Koike, N. *et al.* Creation of long-lasting blood vessels. *Nature* **428**, 138–139 (2004).

99. Guldberg, R. E. *et al.* Mechanical stimulation of tissue repair in the hydraulic bone chamber. *J Bone Miner Res* **12**, 1295–1302 (1997).

100. Klosterhoff, B. S. *et al.* Implantable Sensors for Regenerative Medicine. *Journal of Biomechanical Engineering* **139**, 021009 (2017).

101. Kolambkar, Y. M. *et al.* An alginate-based hybrid system for growth factor delivery in the functional repair of large bone defects. *Biomaterials* **32**, 65–74 (2011).

102. Koydemir, H. C. & Ozcan, A. Wearable and implantable sensors for biomedical applications. *Annual Review of Analytical Chemistry* **11**, 127–146 (2018).

103. Ben Amar, A., Kouki, A. B. & Cao, H. Power approaches for implantable medical devices. *Sensors (Basel)* **15**, 28889–28914 (2015).

104. Shah, J. P., Phillips, T. M., Danoff, J. V. & Gerber, L. H. An in vivo microanalytical technique for measuring the local biochemical milieu of human skeletal muscle. *Journal of Applied Physiology* **99**, 1977–1984 (2005).

105. Gerdle, B., Ghafouri, B., Ernberg, M. & Larsson, B. Chronic musculoskeletal pain: review of mechanisms and biochemical biomarkers as assessed by the microdialysis technique. *J Pain Res* **7**, 313–326 (2014).

106. Nyein, H. Y. Y. *et al.* A wearable patch for continuous analysis of thermoregulatory sweat at rest. *Nat Commun* **12**, 1823 (2021).

107. Nyein, H. Y. Y. *et al.* Regional and correlative sweat analysis using high-throughput microfluidic sensing patches toward decoding sweat. *Science Advances* **5**, eaaw9906 (2019).

108. Peake, J. M., Kerr, G. & Sullivan, J. P. A Critical Review of Consumer Wearables, Mobile Applications, and Equipment for Providing Biofeedback, Monitoring Stress, and Sleep in Physically Active Populations. *Front. Physiol.* **9**, (2018).

109. Zhu, R. Real-time monitoring of the athlete's musculoskeletal health based on an embedded processor. *Microprocessors and Microsystems* **81**, 103742 (2021).

110. Klosterhoff, B. S. *et al.* Real-time monitoring of mechanical cues in the regenerative niche reveal dynamic strain magnitudes that enhance bone repair. *bioRxiv* 663278 (2019) doi:10.1101/663278.

111. Yang, J. C. *et al.* Electronic Skin: Recent Progress and Future Prospects for Skin-Attachable Devices for Health Monitoring, Robotics, and Prosthetics. *Advanced Materials* **31**, 1904765 (2019).

112. Armitage, L., Rajan, G., Kark, L., Simmons, A. & Prusty, B. G. Simultaneous Measurement of Normal and Shear Stress Using Fiber Bragg Grating Sensors in Prosthetic Applications. *IEEE Sensors Journal* **19**, 7383–7390 (2019).

113. Sanders, J. E., Zachariah, S. G., Baker, A. B., Greve, J. M. & Clinton, C. Effects of changes in cadence, prosthetic componentry, and time on interface pressures and shear stresses of three trans-tibial amputees. *Clinical Biomechanics* **15**, 684–694 (2000).

114. Laszczak, P., Jiang, L., Bader, D. L., Moser, D. & Zahedi, S. Development and validation of a 3D-printed interfacial stress sensor for prosthetic applications. *Medical Engineering & Physics* **37**, 132–137 (2015).

115. Laszczak, P. *et al.* A pressure and shear sensor system for stress measurement at lower limb residuum/socket interface. *Medical Engineering & Physics* **38**, 695–700 (2016).

116. Longo, U. G. *et al.* Biosensors for Detection of Biochemical Markers Relevant to Osteoarthritis. *Biosensors* **11**, 31 (2021).

117. Bernotiene, E. *et al.* Emerging technologies and platforms for the immunodetection of multiple biochemical markers in osteoarthritis research and therapy. *Front Med (Lausanne)* **7**, (2020).

118. Song, S. Y. *et al.* Chip-based cartilage oligomeric matrix protein detection in serum and synovial fluid for osteoarthritis diagnosis. *Analytical Biochemistry* **420**, 139–146 (2012).

119. Huang, Y.-C. *et al.* Quantification of tumor necrosis factor-α and matrix metalloproteinases-3 in synovial fluid by a fiber-optic particle plasmon resonance sensor. *Analyst* **138**, 4599–4606 (2013).

120. Chiang, C.-Y. *et al.* Fiber-optic particle plasmon resonance sensor for detection of interleukin-1β in synovial fluids. *Biosensors and Bioelectronics* **26**, 1036–1042 (2010).

121. Thévenot, D. R., Toth, K., Durst, R. A. & Wilson, G. S. Electrochemical biosensors: recommended definitions and classification1International Union of Pure and Applied Chemistry: Physical Chemistry Division, Commission I.7 (Biophysical Chemistry); Analytical Chemistry Division, Commission V.5 (Electroanalytical Chemistry).1. *Biosensors and Bioelectronics* **16**, 121–131 (2001).

122. Honjol, Y. *et al.* Current view and prospect: Implantable pressure sensors for health and surgical care. *Medical Devices & Sensors* **3**, e10068 (2020).

123. Chiang, C.-C., K. Lin, C.-C. & Ju, M.-S. An implantable capacitive pressure sensor for biomedical applications. *Sensors and Actuators A: Physical* **134**, 382–388 (2007).

124. Tan, E. L. *et al.* Implantable biosensors for real-time strain and pressure monitoring. *Sensors* **8**, 6396–6406 (2008).

125. Grieshaber, D., MacKenzie, R., Vörös, J. & Reimhult, E. Electrochemical biosensors - sensor principles and architectures. *Sensors* **8**, 1400–1458 (2008).

126. Ferguson, J. E. & Redish, A. D. Wireless communication with implanted medical devices using the conductive properties of the body. *Expert Rev Med Devices* **8**, 427–433 (2011).

127. Polikov, V. S., Block, M. L., Fellous, J.-M., Hong, J.-S. & Reichert, W. M. In vitro model of glial scarring around neuroelectrodes chronically implanted in the CNS. *Biomaterials* **27**, 5368–5376 (2006).

128. Turner, J. N. *et al.* Cerebral astrocyte response to micromachined silicon implants. *Exp Neurol* **156**, 33–49 (1999).

129. Major, M. R., Wong, V. W., Nelson, E. R., Longaker, M. T. & Gurtner, G. C. The foreign body response: at the interface of surgery and bioengineering. *Plastic and Reconstructive Surgery* **135**, 1489–1498 (2015).

130. Morais, J. M., Papadimitrakopoulos, F. & Burgess, D. J. Biomaterials/tissue interactions: possible solutions to overcome foreign body response. *AAPS J* **12**, 188–196 (2010).

131. Onuki, Y., Bhardwaj, U., Papadimitrakopoulos, F. & Burgess, D. J. A review of the biocompatibility of implantable devices: current challenges to overcome foreign body response. *J Diabetes Sci Technol* **2**, 1003–1015 (2008).

132. Kim, S.-J. *et al.* Evaluation of the biocompatibility of a coating material for an implantable bladder volume sensor. *The Kaohsiung Journal of Medical Sciences* **28**, 123–129 (2012).

133. Koschwanez, H. E., Yap, F. Y., Klitzman, B. & Reichert, W. M. In vitro and in vivo characterization of porous poly-L-lactic acid coatings for subcutaneously implanted glucose sensors. *J Biomed Mater Res A* **87**, 792–807 (2008).

134. Hickey, T., Kreutzer, D., Burgess, D. J. & Moussy, F. In vivo evaluation of a dexamethasone/PLGA microsphere system designed to suppress the inflammatory tissue response to implantable medical devices. *J Biomed Mater Res* **61**, 180–187 (2002).

135. Tipnis, N. P. & Burgess, D. J. Sterilization of implantable polymer-based medical devices: A review. *International Journal of Pharmaceutics* **544**, 455–460 (2018).

136. Lanyon, L. E., Hampson, W. G., Goodship, A. E. & Shah, J. S. Bone deformation recorded in vivo from strain gauges attached to the human tibial shaft. *Acta Orthop Scand* **46**, 256–268 (1975).

137. D'Lima, D. D., Fregly, B. J. & Colwell, C. W. Implantable sensor technology: measuring bone and joint biomechanics of daily life in vivo. *Arthritis Research & Therapy* **15**, 203 (2013).

138. Ledet, E. H., Liddle, B., Kradinova, K. & Harper, S. Smart implants in orthopedic surgery, improving patient outcomes: a review. *IEH* **5**, 41–51 (2018).

139. Burny, F., Donkerwolcke, M., Bourgois, R., Domb, M. & Saric, O. Twenty years experience in fracture healing measurement with strain gauges. *Orthopedics* **7**, 1823–1826 (1984).

140. Schneider, E. *et al.* Loads acting in an intramedullary nail during fracture healing in the human femur. *J Biomech* **34**, 849–857 (2001).

141. Klosterhoff, B. S. *et al. Effects of Osteogenic Ambulatory Mechanical Stimulation on Early Stages of BMP-2 Mediated Bone Repair*. http://biorxiv.org/lookup/doi/10.1101/2020.07.28.225870 (2020) doi:10.1101/2020.07.28.225870.

142. Klosterhoff, B. S. *et al.* Effects of osteogenic ambulatory mechanical stimulation on early stages of BMP-2 mediated bone repair. *Connect Tissue Res* 1–12 (2021) doi:10.1080/03008207.2021.1897582.

143. Mavrogenis, A. & Parvizi, J. Biology of Implant Osseointegration. *Journal of Musculoskeletal & Neuronal Interactions* 61–71 (2009).

144. Burton, A. R., Sun, P. & Lynch, J. P. Bio-compatible wireless inductive thin-film strain sensor for monitoring the growth and strain response of bone in osseointegrated prostheses. *Structural Health Monitoring* 1475921719831452 (2019) doi:10.1177/1475921719831452.

145. Frossard, L. *et al.* Apparatus for monitoring load bearing rehabilitation exercises of a transfemoral amputee fitted with an osseointegrated fixation: A proof-of-concept study. *Gait & Posture* **31**, 223–228 (2010).

146. Frossard, L. *et al.* Monitoring of the load regime applied on the osseointegrated fixation of a trans-femoral amputee: A tool for evidence-based practice. *Prosthet Orthot Int* **32**, 68–78 (2008).

147. Cole, C. P. & Navarro, R. R. eDisc: The First Artificial Spinal Disc With Integral Force-Sensing Microelectronics. in 49–50 (American Society of Mechanical Engineers Digital Collection, 2009). doi:10.1115/BioMed2007-38052.

148. Cushner, F., Schiller, P., Gross, J., Mueller, J. k. & Hunter, W. A total knee arthroplasty prosthesis capable of remote patient monitoring. *Orthopaedic Proceedings* **103-B**, 18–18 (2021).

149. Mancipe Castro, L. M., Sequeira, A., García, A. J. & Guldberg, R. E. Articular Cartilage- and Synoviocyte-Binding Poly(ethylene glycol) Nanocomposite Microgels as Intra-Articular Drug Delivery Vehicles for the Treatment of Osteoarthritis. *ACS Biomater. Sci. Eng.* **6**, 5084–5095 (2020).

150. Afsarimanesh, N., Mukhopadhyay, S. C. & Kruger, M. Molecularly imprinted polymer-based electrochemical biosensor for bone loss detection. *IEEE Transactions on Biomedical Engineering* **65**, 1264–1271 (2018).

151. Tadano, S., Takeda, R., Sasaki, K., Fujisawa, T. & Tohyama, H. Gait characterization for osteoarthritis patients using wearable gait sensors (H-Gait systems). *Journal of Biomechanics* **49**, 684–690 (2016).

152. Ismailidis, P. *et al.* Measuring gait kinematics in patients with severe hip osteoarthritis using wearable sensors. *Gait & Posture* **81**, 49–55 (2020).

153. Kobsar, D., Osis, S. T., Boyd, J. E., Hettinga, B. A. & Ferber, R. Wearable sensors to predict improvement following an exercise intervention in patients with knee osteoarthritis. *Journal of NeuroEngineering and Rehabilitation* **14**, 94 (2017).

154. Revzin, A., Maverakis, E. & Chang, H.-C. Biosensors for immune cell analysis—A perspective. *Biomicrofluidics* **6**, 021301-021301–13 (2012).

155. Alonso, B. *et al.* Osteoarthritis-related biomarkers profile in chronic anterior cruciate ligament injured knee. *The Knee* **27**, 51–60 (2020).

156. Bullen, R. A., Arnot, T. C., Lakeman, J. B. & Walsh, F. C. Biofuel cells and their development. *Biosensors and Bioelectronics* **21**, 2015–2045 (2006).

157. Nguyen, M. Q. *et al.* Field distribution models of spiral coil for misalignment analysis of wireless power transfer systems. *IEEE Transaction on Microwave Theory and Techniques* **62**, 920–930 (2014).

158. Pereles, B. D., DeRouin, A. J. & Ong, K. G. Partially Loaded Magnetoelastic Sensors With Customizable Sensitivities for Large Force Measurements. *IEEE Sensors Journal* **15**, 591–597 (2015).

159. Ernst, M., Richards, R. G. & Windolf, M. Smart implants in fracture care – only buzzword or real opportunity? *Injury* **52**, S101–S105 (2021).

160. Dinis, H. & Mendes, P. M. A comprehensive review of powering methods used in state-of-the-art miniaturized implantable electronic devices. *Biosensors and Bioelectronics* **172**, 112781 (2021).

161. Lee, S., Shi, Q. & Lee, C. From flexible electronics technology in the era of IoT and artificial intelligence toward future implanted body sensor networks. *APL Materials* **7**, 031302 (2019).

162. Phan, H.-P. Implanted Flexible Electronics: Set Device Lifetime with Smart Nanomaterials. *Micromachines* **12**, 157 (2021).

163. Bashir, R. BioMEMS: state-of-the-art in detection, opportunities and prospects. *Adv Drug Deliv Rev* **56**, 1565–1586 (2004).

164. Gilleo, K. MEMS in medicine. *Circuit Assembly* **16**, 32–33 (2005).

165. Ashammakhi, N. *et al.* Biodegradable Implantable Sensors: Materials Design, Fabrication, and Applications. *Advanced Functional Materials* **31**, 2104149 (2021).

166. Luo, M., Martinez, A. W., Song, C., Herrault, F. & Allen, M. G. A microfabricated wireless rf pressure sensor made completely of biodegradable materials. *Journal of Microelectromechanical Systems* **23**, 4–13 (2014).

167. Tsang, M., Armutlulu, A., Martinez, A. W., Allen, S. A. & Allen, M. Biodegradable magnesium/iron batteries with polycaprolactone encapsulation: A microfabricated power source for transient implantable devices. (2015) doi:10.1038/MICRONANO.2015.24.

168. Yin, L. *et al.* Materials, designs, and operational characteristics for fully biodegradable primary batteries. *Adv Mater* **26**, 3879–3884 (2014).

169. Kim, D.-H. *et al.* Dissolvable films of silk fibroin for ultrathin conformal bio-integrated electronics. *Nat Mater* **9**, 511–517 (2010).

170. Pizzolato, C. *et al.* Bioinspired Technologies to Connect Musculoskeletal Mechanobiology to the Person for Training and Rehabilitation. *Frontiers in Computational Neuroscience* **11**, 96 (2017).

171. Krouskop, T. A., Dougherty, D. R. & Vinson, F. S. A pulsed Doppler ultrasonic system for making noninvasive measurements of the mechanical properties of soft tissue. *J Rehabil Res Dev* **24**, 1–8 (1987).

172. Rando, T. A. & Ambrosio, F. Regenerative Rehabilitation: Applied Biophysics Meets Stem Cell Therapeutics. *Cell Stem Cell* **22**, 306–309 (2018).

173. Boutry, C. M. *et al.* A stretchable and biodegradable strain and pressure sensor for orthopaedic application. *Nat Electron* **1**, 314–321 (2018).

174. Ashley, E. A. *et al.* Clinical evaluation incorporating a personal genome. *Lancet* **375**, 1525–1535 (2010).

175. Williams, K. E. *et al.* Early Resistance Rehabilitation Improves Functional Regeneration Following Segmental Bone Defect Injury. *npj Regenerative Medicine* (2024).

176. Calori, G. M., Mazza, E., Colombo, M., Ripamonti, C. & Tagliabue, L. Treatment of long bone non-unions with polytherapy: Indications and clinical results. *Injury* **42**, 587–590 (2011).

177. Keating, J. F., Simpson, A. H. R. W. & Robinson, C. M. The management of fractures with bone loss. *The Journal of Bone and Joint Surgery. British volume* **87-B**, 142–150 (2005).

178. Hoit, G., Bonyun, M. & Nauth, A. Hardware considerations in infection and nonunion management. *OTA Int* **3**, e055 (2020).

179. Houben, I. B., Raaben, M., Van Basten Batenburg, M. & Blokhuis, T. J. Delay in weight bearing in surgically treated tibial shaft fractures is associated with impaired healing: a cohort analysis of 166 tibial fractures. *Eur J Orthop Surg Traumatol* **28**, 1429–1436 (2018).

180. Hurkmans, H. L. *et al.* The Difference Between Actual and Prescribed Weight Bearing of Total Hip Patients With a Trochanteric Osteotomy: Long-Term Vertical Force Measurements Inside and Outside the Hospital. *Archives of Physical Medicine and Rehabilitation* **88**, 200–206 (2007).

181. Giangregorio, L. & Blimkie, C. J. R. Skeletal Adaptations to Alterations in Weight-Bearing Activity. *Sports Med* **32**, 459–476 (2002).

182. Vandenborne, K. *et al.* Longitudinal study of skeletal muscle adaptations during immobilization and rehabilitation. *Muscle & Nerve* **21**, 1006–1012 (1998).

183. Yoshiko, A. *et al.* Effects of post-fracture non-weight-bearing immobilization on muscle atrophy, intramuscular and intermuscular adipose tissues in the thigh and calf. *Skeletal Radiol* **47**, 1541–1549 (2018).

184. Herrador Colmenero, L. *et al.* Effectiveness of mirror therapy, motor imagery, and virtual feedback on phantom limb pain following amputation: A systematic review. *Prosthet Orthot Int* **42**, 288–298 (2018).

185. Argentati, C. *et al.* Insight into Mechanobiology: How Stem Cells Feel Mechanical Forces and Orchestrate Biological Functions. *International Journal of Molecular Sciences* **20**, 5337 (2019).

186. Cowin, S. C. Wolff's Law of Trabecular Architecture at Remodeling Equilibrium. *Journal of Biomechanical Engineering* **108**, 83–88 (1986).

187. Glatt, V., Tepic, S. & Evans, C. Reverse Dynamization: A Novel Approach to Bone Healing. *J Am Acad Orthop Surg* **24**, e60-61 (2016).

188. Barcik, J. & Epari, D. R. Can Optimizing the Mechanical Environment Deliver a Clinically Significant Reduction in Fracture Healing Time? *Biomedicines* **9**, 691 (2021).

189. Duda, G. N. *et al.* The decisive early phase of bone regeneration. *Nat Rev Rheumatol* **19**, 78–95 (2023).

190. Thompson, W. R., Scott, A., Loghmani, M. T., Ward, S. R. & Warden, S. J. Understanding Mechanobiology: Physical Therapists as a Force in Mechanotherapy and Musculoskeletal Regenerative Rehabilitation. *Physical Therapy* **96**, 560–569 (2016).

191. Bartnikowski, N. *et al.* Modulation of fixation stiffness from flexible to stiff in a rat model of bone healing. *Acta Orthopaedica* **88**, 217–222 (2017).

192. Claes, L. *et al.* Late Dynamization by Reduced Fixation Stiffness Enhances Fracture Healing in a Rat Femoral Osteotomy Model. *Journal of Orthopaedic Trauma* **25**, 169 (2011).

193. Claes, L., Wilke, H.-J., Augat, P., Rübenacker, S. & Margevicius, K. Effect of dynamization on gap healing of diaphyseal fractures under external fixation. *Clinical Biomechanics* **10**, 227–234 (1995).

194. Epari, D. R., Schell, H., Bail, H. J. & Duda, G. N. Instability prolongs the chondral phase during bone healing in sheep. *Bone* **38**, 864–870 (2006).

195. Glatt, V., Samchukov, M., Cherkashin, A. & Iobst, C. Reverse Dynamization Accelerates Bone-Healing in a Large-Animal Osteotomy Model. *JBJS* **103**, 257–263 (2021).

196. Claes, L. *et al.* Early dynamization by reduced fixation stiffness does not improve fracture healing in a rat femoral osteotomy model. *Journal of Orthopaedic Research* **27**, 22–27 (2009).

197. Fu, R., Feng, Y., Liu, Y., Willie, B. M. & Yang, H. The combined effects of dynamization time and degree on bone healing. *Journal of Orthopaedic Research* **40**, 634–643 (2022).

198. Boerckel, J. D., Dupont, K. M., Kolambkar, Y. M., Lin, A. S. P. & Guldberg, R. E. In Vivo Model for Evaluating the Effects of Mechanical Stimulation on Tissue-Engineered Bone Repair. *Journal of Biomechanical Engineering* **131**, (2009).

199. Epari, D. R., Wehner, T., Ignatius, A., Schuetz, M. A. & Claes, L. E. A case for optimising fracture healing through inverse dynamization. *Medical Hypotheses* **81**, 225–227 (2013).

200. Tufekci, P. *et al.* Early mechanical stimulation only permits timely bone healing in sheep. *Journal of Orthopaedic Research* **36**, 1790–1796 (2018).

201. Schmidt, I., Albert, J., Ritthaler, M., Papastavrou, A. & Steinmann, P. Bone fracture healing within a continuum bone remodelling framework. *Computer Methods in Biomechanics and Biomedical Engineering* **25**, 1040–1050 (2022).

202. Schultz, B. J., Koval, K., Salehi, P. P., Gardner, M. J. & Cerynik, D. L. Controversies in Fracture Healing: Early Versus Late Dynamization. *Orthopedics* **43**, e125–e133 (2020).

203. Verrier, S. *et al.* Tissue engineering and regenerative approaches to improving the healing of large bone defects. *European cells & materials* **32**, 87–110 (2016).

204. Windolf, M. *et al.* A Biofeedback System for Continuous Monitoring of Bone Healing. in *Proceedings of the International Joint Conference on Biomedical Engineering Systems and Technologies - Volume 1* 243–248 (SCITEPRESS - Science and Technology Publications, Lda, Setubal, PRT, 2014). doi:10.5220/0004913002430248.

205. Windolf, M. *et al.* Continuous Rod Load Monitoring to Assess Spinal Fusion Status–Pilot In Vivo Data in Sheep. *Medicina* **58**, 899 (2022).

206. Barcik, J. *et al.* Short-Term Bone Healing Response to Mechanical Stimulation—A Case Series Conducted on Sheep. *Biomedicines* **9**, 988 (2021).

207. Hettiaratchi, M. H. *et al.* Heparin-mediated delivery of bone morphogenetic protein-2 improves spatial localization of bone regeneration. *Science advances* **6**, eaay1240 (2020).

208. Krishnan, L. *et al.* Delivery vehicle effects on bone regeneration and heterotopic ossification induced by high dose BMP-2. *Acta Biomaterialia* **49**, 101–112 (2017).

209. Maas, S. A., Ellis, B. J., Ateshian, G. A. & Weiss, J. A. FEBio: Finite Elements for Biomechanics. *Journal of Biomechanical Engineering* **134**, (2012).

210. Lacroix, D., Prendergast, P. J., Li, G. & Marsh, D. Biomechanical model to simulate tissue differentiation and bone regeneration: Application to fracture healing. *Med. Biol. Eng. Comput.* **40**, 14–21 (2002).

211. Mehboob, A., Mehboob, H., Chang, S.-H. & Tarlochan, F. Effect of composite intramedullary nails (IM) on healing of long bone fractures by means of reamed and unreamed methods. *Composite Structures* **167**, 76–87 (2017).

212. Wehner, T. *et al.* Internal forces and moments in the femur of the rat during gait. *Journal of Biomechanics* **43**, 2473–2479 (2010).

213. Miyamoto, S., Yoshikawa, H. & Nakata, K. Axial mechanical loading to *ex vivo* mouse long bone regulates endochondral ossification and endosteal mineralization through activation of the BMP-Smad pathway during postnatal growth. *Bone Reports* **15**, 101088 (2021).

214. Carroll, S. F., Buckley, C. T. & Kelly, D. J. Cyclic Tensile Strain Can Play a Role in Directing both Intramembranous and Endochondral Ossification of Mesenchymal Stem Cells. *Front. Bioeng. Biotechnol.* **5**, (2017).

215. Carter, D. R. & Wong, M. Mechanical stresses and endochondral ossification in the chondroepiphysis. *Journal of Orthopaedic Research* **6**, 148–154 (1988).

216. Augat, P. *et al.* Early, full weightbearing with flexible fixation delays fracture healing. *Clin Orthop Relat Res* 194–202 (1996) doi:10.1097/00003086-199607000-00031.

217. Yang, C., Liu, Y., Wang, Z., Lin, M. & Liu, C. Controlled mechanical loading improves bone regeneration by regulating type H vessels in a S1Pr1-dependent manner. *The FASEB Journal* **36**, e22530 (2022).

218. He, S. *et al.* Low-frequency vibration treatment of bone marrow stromal cells induces bone repair in vivo. *Iran J Basic Med Sci* **20**, 23–28 (2017).

219. Hadjiargyrou, M., McLeod, K., Ryaby, J. P. & Rubin, C. Enhancement of fracture healing by low intensity ultrasound. *Clin Orthop Relat Res* S216-229 (1998) doi:10.1097/00003086-199810001-00022.

220. Duarte, L. R. The stimulation of bone growth by ultrasound. *Arch Orthop Trauma Surg (1978)* **101**, 153–159 (1983).

221. Ng, J. L., Kersh, M. E., Kilbreath, S. & Knothe Tate, M. Establishing the Basis for Mechanobiology-Based Physical Therapy Protocols to Potentiate Cellular Healing and Tissue Regeneration. *Front. Physiol.* **8**, (2017).

222. Chow, C. H. T. *et al.* Risk and protective factors in predicting pediatric acute postsurgical pain: A systematic review and meta-analysis. *Health Psychology* **42**, 723–734 (2023).

223. McKay, A. K. A., McCormick, R., Tee, N. & Peeling, P. Exercise and Heat Stress: Inflammation and the Iron Regulatory Response. *International Journal of Sport Nutrition and Exercise Metabolism* **31**, 460–465 (2021).

224. Frost, H. M. A 2003 Update of Bone Physiology and Wolff's Law for Clinicians. *The Angle Orthodontist* **74**, 3–15 (2004).

225. Goodship, A. & Kenwright, J. The influence of induced micromovement upon the healing of experimental tibial fractures. *The Journal of Bone and Joint Surgery. British volume* **67-B**, 650–655 (1985).

226. Goodship, A. E., Cunningham, J. L. & Kenwright, J. Strain Rate and Timing of Stimulation in Mechanical Modulation of Fracture Healing. *Clinical Orthopaedics and Related Research®* **355**, S105 (1998).

227. Kenwright, J. & Goodship, A. E. Controlled mechanical stimulation in the treatment of tibial fractures. *Clin Orthop Relat Res* 36–47 (1989).

228. Glatt, V. *et al.* Improved Healing of Large Segmental Defects in the Rat Femur by Reverse Dynamization in the Presence of Bone Morphogenetic Protein-2. *J Bone Joint Surg Am* **94**, 2063–2073 (2012).

229. Tsuji, K. *et al.* BMP2 activity, although dispensable for bone formation, is required for the initiation of fracture healing. *Nat Genet* **38**, 1424–1429 (2006).

230. Boerckel, J. D. *et al.* Effects of protein dose and delivery system on BMP-mediated bone regeneration. *Biomaterials* **32**, 5241–5251 (2011).

231. Kenwright, J. & Gardner, T. Mechanical Influences on Tibial Fracture Healing. *Clinical Orthopaedics and Related Research (1976-2007)* **355**, S179 (1998).

232. Claes, L. E. *et al.* Effects of Mechanical Factors on the Fracture Healing Process. *Clinical Orthopaedics and Related Research®* **355**, S132 (1998).

233. Duan, Z. & Lu, H. Effect of Mechanical Strain on Cells Involved in Fracture Healing. *Orthopaedic Surgery* **13**, 369–375 (2021).

234. Egol, K. A., Kubiak, E. N., Fulkerson, E., Kummer, F. J. & Koval, K. J. Biomechanics of locked plates and screws. *J Orthop Trauma* **18**, 488–493 (2004).

235. Perren, S. M. Physical and biological aspects of fracture healing with special reference to internal fixation. *Clin Orthop Relat Res* 175–196 (1979).

236. Aro, H. T. & Chao, E. Y. Biomechanics and biology of fracture repair under external fixation. *Hand Clin* **9**, 531–542 (1993).

237. Kenwright, J. *et al.* Effect of controlled axial micromovement on healing of tibial fractures. *Lancet* **2**, 1185–1187 (1986).

238. Carlier, A., Geris, L., Lammens, J. & Oosterwyck, H. V. Bringing computational models of bone regeneration to the clinic. *WIREs Systems Biology and Medicine* **7**, 183–194 (2015).

239. Carlier, A., Lammens, J., Van Oosterwyck, H. & Geris, L. Computational modeling of bone fracture non-unions: four clinically relevant case studies. *In silico cell tissue sci* **2**, 1 (2015).

240. Smith, B. L. *et al.* Behavioral and physiological consequences of enrichment loss in rats. *Psychoneuroendocrinology* **77**, 37–46 (2017).

241. Haffner-Luntzer, M. *et al.* Chronic psychosocial stress compromises the immune response and endochondral ossification during bone fracture healing via β-AR signaling. *Proceedings of the National Academy of Sciences* **116**, 8615–8622 (2019).

242. Beleza, J. *et al.* Self-Paced Free-Running Wheel Mimics High-Intensity Interval Training Impact on Rats' Functional, Physiological, Biochemical, and Morphological Features. *Front Physiol* **10**, 593 (2019).

243. Greenwood, B. N. *et al.* Long-term voluntary wheel running is rewarding and produces plasticity in the mesolimbic reward pathway. *Behav Brain Res* **217**, 354–362 (2011).

244. Nims, R. J. & Ateshian, G. A. Reactive Constrained Mixtures for Modeling the Solid Matrix of Biological Tissues. *J Elast* **129**, 69–105 (2017).

245. Huiskes, R. *et al.* Adaptive bone-remodeling theory applied to prosthetic-design analysis. *J Biomech* **20**, 1135–1150 (1987).

246. Williams, K. E. *et al.* Patient-Specific Multivariate Modeling for Regenerative Rehabilitation of Bone Healing. *Science Advances* (2024).

247. Kubiak, E. N., Beebe, M. J., North, K., Hitchcock, R. & Potter, M. Q. Early Weight Bearing After Lower Extremity Fractures in Adults. *JAAOS - Journal of the American Academy of Orthopaedic Surgeons* **21**, 727–738 (2013).

248. Wolff, J. *The Law of Bone Remodelling*. (Springer, Berlin, Heidelberg, 1986). doi:10.1007/978-3-642-71031-5.

249. Meade, J. B., Cowin, S. C., Klawitter, J. J., Van Buskirk, W. C. & Skinner, H. B. Bone remodeling due to continuously applied loads. *Calcif Tissue Int* **36**, S25–S30 (1984).

250. Noble, B. S. *et al.* Mechanical loading: biphasic osteocyte survival and targeting of osteoclasts for bone destruction in rat cortical bone. *American Journal of Physiology-Cell Physiology* **284**, C934–C943 (2003).

251. De Smet, E. *et al.* Effect of controlled early implant loading on bone healing and bone mass in guinea pigs, as assessed by micro-CT and histology. *Eur J Oral Sci* **114**, 232–242 (2006).

252. Gardner, M. J., Ricciardi, B. F., Wright, T. M., Bostrom, M. P. & van der Meulen, M. C. H. Pause insertions during cyclic in vivo loading affect bone healing. *Clin Orthop Relat Res* **466**, 1232–1238 (2008).

253. Hente, R., Füchtmeier, B., Schlegel, U., Ernstberger, A. & Perren, S. M. The influence of cyclic compression and distraction on the healing of experimental tibial fractures. *J Orthop Res* **22**, 709–715 (2004).

254. Wehrle, E., Paul, G. R., Tourolle né Betts, D. C., Kuhn, G. A. & Müller, R. Individualized cyclic mechanical loading improves callus properties during the remodelling phase of fracture healing in mice as assessed from time-lapsed in vivo imaging. *Sci Rep* **11**, 23037 (2021).

255. Grundnes, O. & Reikerås, O. Mechanical effects of function on bone healing. Nonweight bearing and exercise in osteotomized rats. *Acta Orthop Scand* **62**, 163–165 (1991).

256. Hente, R. & Perren, S. M. Mechanical Stimulation of Fracture Healing - Stimulation of Callus by Improved Recovery. *Acta Chir Orthop Traumatol Cech* **85**, 385–391 (2018).

257. Halvachizadeh, S. & Pape, H.-C. Perren's Strain Theory and Fracture Healing. in *Essential Biomechanics for Orthopedic Trauma: A Case-Based Guide* (eds. Crist, B. D., Borrelli Jr., J. & Harvey, E. J.) 17–25 (Springer International Publishing, Cham, 2020). doi:10.1007/978-3-030-36990-3_2.

258. Perren, S. M. Evolution of the internal fixation of long bone fractures. The scientific basis of biological internal fixation: choosing a new balance between stability and biology. *J Bone Joint Surg Br* **84**, 1093–1110 (2002).

259. Foster, A. L. *et al.* The influence of biomechanical stability on bone healing and fracture-related infection: *the legacy of Stephan Perren. Injury* **52**, 43–52 (2021).

260. Claes, L. *et al.* The mode of interfragmentary movement affects bone formation and revascularization after callus distraction. *PLoS One* **13**, e0202702 (2018).

261. Carter, D. R., Blenman, P. R. & Beaupré, G. S. Correlations between mechanical stress history and tissue differentiation in initial fracture healing. *Journal of Orthopaedic Research* **6**, 736–748 (1988).

262. Claes, L., Augat, P., Suger, G. & Wilke, H. J. Influence of size and stability of the osteotomy gap on the success of fracture healing. *J Orthop Res* **15**, 577–584 (1997).

263. Miramini, S. *et al.* The relationship between interfragmentary movement and cell differentiation in early fracture healing under locking plate fixation. *Australas Phys Eng Sci Med* **39**, 123–133 (2016).

264. Märdian, S., Schaser, K.-D., Duda, G. N. & Heyland, M. Working length of locking plates determines interfragmentary movement in distal femur fractures under physiological loading. *Clinical Biomechanics* **30**, 391–396 (2015).

265. Aalto, K. *et al.* Fracture repair during external fixation. Torsion tests of rabbit osteotomies. *Acta Orthop Scand* **58**, 66–70 (1987).

266. Chao, E. Y., Aro, H. T., Lewallen, D. G. & Kelly, P. J. The effect of rigidity on fracture healing in external fixation. *Clin Orthop Relat Res* 24–35 (1989).

267. Gautschi, O. P., Frey, S. P. & Zellweger, R. Bone Morphogenetic Proteins in Clinical Applications. *ANZ Journal of Surgery* **77**, 626–631 (2007).

268. Hu, K., Besschetnova, T. Y. & Olsen, B. R. Soluble VEGFR1 reverses BMP2 inhibition of intramembranous ossification during healing of cortical bone defects. *Journal of Orthopaedic Research* **35**, 1461–1469 (2017).

269. Stoeger, T. *et al.* In Situ Gene Expression Analysis During BMP2-induced Ectopic Bone Formation in Mice Shows Simultaneous Endochondral and Intramembranous Ossification. *Growth Factors* **20**, 197–210 (2003).

270. Kawai, M., Bessho, K., Maruyama, H., Miyazaki, J.-I. & Yamamoto, T. Human BMP-2 gene transfer using transcutaneous in vivo electroporation induced both intramembranous and endochondral ossification. *The Anatomical Record Part A: Discoveries in Molecular, Cellular, and Evolutionary Biology* **287A**, 1264–1271 (2005).

271. FEBio User Manual. *FEBio User Manual* https://help.febio.org/docs/FEBioUser-4-5/UM45.html.

272. 3.13 Contact Section. *FEBio User Manual* https://help.febio.org/docs/FEBioUser-3-6/UM36-Section-3.13.html.

273. Cory, E. *et al.* Compressive axial mechanical properties of rat bone as functions of bone volume fraction, apparent density and micro-ct based mineral density. *Journal of Biomechanics* **43**, 953–960 (2010).

274. 3.9.4.13 Image Map. *FEBio Studio Manual* https://help.febio.org/docs/FEBioStudio-2-5/FSM25-3.9.4.13.html.

275. Cheng, A. *et al.* Early systemic immune biomarkers predict bone regeneration after trauma. *PNAS* **118**, (2021).

276. Poser, L. *et al.* A Standardized Critical Size Defect Model in Normal and Osteoporotic Rats to Evaluate Bone Tissue Engineered Constructs. *BioMed Research International* **2014**, 348635 (2014).

277. Harrison, L. J., Cunningham, J. L., Strömberg, L. & Goodship, A. E. Controlled induction of a pseudarthrosis: a study using a rodent model. *J Orthop Trauma* **17**, 11–21 (2003).

278. Jäger, M., Sager, M., Lensing-Höhn, S. & Krauspe, R. The critical size bony defect in a small animal for bone healing studies (II): Implant evolution and surgical technique on a rat's femur / Der kritische Knochendefekt am Kleintier zur Untersuchung der Knochenheilung (II): Implantatentwicklung und Operationstechnik am Rattenfemur. **50**, 137–142 (2005).

279. Rubin, C. T. & Lanyon, L. E. Regulation of bone formation by applied dynamic loads. *J Bone Joint Surg Am* **66**, 397–402 (1984).

280. Lanyon, L. E. & Rubin, C. T. Static vs dynamic loads as an influence on bone remodelling. *Journal of Biomechanics* **17**, 897–905 (1984).

281. Rubin, C. T. & Mcleod, K. J. Promotion of Bony Ingrowth by Frequency-Specific, Low-Amplitude Mechanical Strain. *Clinical Orthopaedics and Related Research®* **298**, 165 (1994).

282. Turner, C. H. Three rules for bone adaptation to mechanical stimuli. *Bone* **23**, 399–407 (1998).

283. Heinonen, A. *et al.* Bone mineral density in female athletes representing sports with different loading characteristics of the skeleton. *Bone* **17**, 197–203 (1995).

284. Judex, S. & Zernicke, R. F. High-impact exercise and growing bone: relation between high strain rates and enhanced bone formation. *J Appl Physiol (1985)* **88**, 2183–2191 (2000).

285. Bruder, S. P., Fink, D. J. & Caplan, A. I. Mesenchymal stem cells in bone development, bone repair, and skeletal regenaration therapy. *Journal of Cellular Biochemistry* **56**, 283–294 (1994).

286. Srinivasan, S. *et al.* Rest-inserted loading rapidly amplifies the response of bone to small increases in strain and load cycles. *Journal of Applied Physiology* **102**, 1945–1952 (2007).

287. Srinivasan, S. *et al.* Rest Intervals Reduce the Number of Loading Bouts Required to Enhance Bone Formation. *Med Sci Sports Exerc* **47**, 1095–1103 (2015).

288. Robling, A. G., Burr, D. B. & Turner, C. H. Partitioning a Daily Mechanical Stimulus into Discrete Loading Bouts Improves the Osteogenic Response to Loading. *Journal of Bone and Mineral Research* **15**, 1596–1602 (2000).

289. LaMothe, J. M. & Zernicke, R. F. Rest insertion combined with high-frequency loading enhances osteogenesis. *Journal of Applied Physiology* **96**, 1788–1793 (2004).

290. Srinivasan, S., Weimer, D. A., Agans, S. C., Bain, S. D. & Gross, T. S. Low-Magnitude Mechanical Loading Becomes Osteogenic When Rest Is Inserted Between Each Load Cycle*. *Journal of Bone and Mineral Research* **17**, 1613–1620 (2002).

291. Srinivasan, S. *et al.* Enabling bone formation in the aged skeleton via rest-inserted mechanical loading. *Bone* **33**, 946–955 (2003).

292. Gross, T. S. *et al.* Why Rest Stimulates Bone Formation: A Hypothesis Based on Complex Adaptive Phenomenon. *Exercise and Sport Sciences Reviews* **32**, 9 (2004).

293. Checa, S. & Prendergast, P. J. Effect of cell seeding and mechanical loading on vascularization and tissue formation inside a scaffold: A mechano-biological model using a lattice approach to simulate cell activity. *Journal of Biomechanics* **43**, 961–968 (2010).

294. Bratengeier, C., Liszka, A., Hoffman, J., Bakker, A. D. & Fahlgren, A. High shear stress amplitude in combination with prolonged stimulus duration determine induction of osteoclast formation by hematopoietic progenitor cells. *The FASEB Journal* **34**, 3755–3772 (2020).

295. Schell, H. *et al.* Mechanical induction of critically delayed bone healing in sheep: radiological and biomechanical results. *J Biomech* **41**, 3066–3072 (2008).

296. Gómez-Benito, M. J., García-Aznar, J. M., Kuiper, J. H. & Doblaré, M. Influence of fracture gap size on the pattern of long bone healing: a computational study. *Journal of Theoretical Biology* **235**, 105–119 (2005).

297. Lewis, R. H. J., Perkins, M., Fischer, P. E., Beebe, M. J. & Magnotti, L. J. Timing is everything: Impact of combined long bone fracture and major arterial injury on outcomes. *Journal of Trauma and Acute Care Surgery* **92**, 21 (2022).

298. Hu, M. *et al.* Fixators dynamization for delayed union and non-union of femur and tibial fractures: a review of techniques, timing and influence factors. *J Orthop Surg Res* **18**, 577 (2023).

299. Marsell, R. & Einhorn, T. A. The biology of fracture healing. *Injury* **42**, 551–555 (2011).

300. Lippuner, K. *et al.* Effect of animal species and age on plate-induced vascular damage in cortical bone. *Arch Orthop Trauma Surg* **111**, 78–84 (1992).

301. Jeffery, E. C., Mann, T. L. A., Pool, J. A., Zhao, Z. & Morrison, S. J. Bone marrow and periosteal skeletal stem/progenitor cells make distinct contributions to bone maintenance and repair. *Cell Stem Cell* **29**, 1547-1561.e6 (2022).

302. Comiskey, D., MacDonald, B. J., McCartney, W. T., Synnott, K. & O'Byrne, J. Predicting the external formation of callus tissues in oblique bone fractures: idealised and clinical case studies. *Biomech Model Mechanobiol* **12**, 1277–1282 (2013).

303. Fan, R., Liu, J. & Jia, Z. Effects of different running intensities on the micro-level failure strain of rat femoral cortical bone structures: a finite element investigation. *BioMed Eng OnLine* **22**, 89 (2023).

304. Cheal, E. J., Hayes, W. C., White, A. A. & Perren, S. M. Stress analysis of compression plate fixation and its effects on long bone remodeling. *Journal of Biomechanics* **18**, 141–150 (1985).

305. Lewallen, D. G., Chao, E. Y., Kasman, R. A. & Kelly, P. J. Comparison of the effects of compression plates and external fixators on early bone-healing. *JBJS* **66**, 1084 (1984).

306. Agarwal-Harding, K. J. *et al.* Estimating the Global Incidence of Femoral Fracture from Road Traffic Collisions: A Literature Review. *JBJS* **97**, e31 (2015).

307. Anyaehie, U. E., Ejimofor, O. C., Akpuaka, F. C. & Nwadinigwe, C. U. Pattern of femoral fractures and associated injuries in a Nigerian tertiary trauma centre. *Nigerian Journal of Clinical Practice* **18**, 462 (2015).

308. Yoon, R. S. & Liporace, F. A. Impact of Intramedullary Nailing in the Treatment of Femur Fractures An Evolutionary Perspective. *Bull Hosp Jt Dis (2013)* **76**, 9–13 (2018).

309. O'Brien, P. J. Fracture fixation in patients having multiple injuries. *Can J Surg* **46**, 124–128 (2003).

310. Augat, P. *et al.* Early, Full Weightbearing With Flexible Fixation Delays Fracture Healing. *Clinical Orthopaedics and Related Research (1976-2007)* **328**, 194–202 (1996).

311. Fu, R. *et al.* Effects of dynamization timing and degree on bone healing of different fracture types. *Journal of Orthopaedic Research* **41**, 2394–2404 (2023).

312. Foxworthy, M. & Pringle, R. M. Dynamization timing and its effect on bone healing when using the Orthofix Dynamic Axial Fixator. *Injury* **26**, 117–119 (1995).

313. Smith, T. T. G. *et al.* Forced treadmill running reduces systemic inflammation yet worsens upper limb discomfort in a rat model of work-related musculoskeletal disorders. *BMC Musculoskelet Disord* **21**, 57 (2020).

314. Zhang, L. *et al.* Medium-Intensity Treadmill Exercise Exerts Beneficial Effects on Bone Modeling Through Bone Marrow Mesenchymal Stromal Cells. *Front. Cell Dev. Biol.* **8**, (2020).

315. Gao, L. *et al.* Treadmill exercise promotes bone tissue recovery in rats subjected to high + Gz loads. *J Bone Miner Metab* **42**, 302–315 (2024).

316. Palke, L. *et al.* Anti-gravity treadmill rehabilitation improves gait and muscle atrophy in patients with surgically treated ankle and tibial plateau fractures after one year: A randomised clinical trial. *Clin Rehabil* **36**, 87–98 (2022).

317. Gardinier, J. D., Rostami, N., Juliano, L. & Zhang, C. Bone adaptation in response to treadmill exercise in young and adult mice. *Bone Reports* **8**, 29–37 (2018).

318. Suljevic, O. *et al.* Does early post-operative exercise influence bone healing kinetics? Preclinical evaluation of non-critical sized femur defect healing. *Bone* **176**, 116869 (2023).

319. Yang, H., Embry, R. E. & Main, R. P. Effects of Loading Duration and Short Rest Insertion on Cancellous and Cortical Bone Adaptation in the Mouse Tibia. *PLOS ONE* **12**, e0169519 (2017).

320. Robling, A. G., Burr, D. B. & Turner, C. H. Recovery periods restore mechanosensitivity to dynamically loaded bone. *J Exp Biol* **204**, 3389–3399 (2001).

321. Moriishi, T. & Komori, T. Osteocytes: Their Lacunocanalicular Structure and Mechanoresponses. *Int J Mol Sci* **23**, 4373 (2022).

322. Turner, C. H., Forwood, M. R. & Otter, M. W. Mechanotransduction in bone: do bone cells act as sensors of fluid flow? *The FASEB Journal* **8**, 875–878 (1994).

323. Brown, D. A. *et al.* Short-term treadmill running in the rat: what kind of stressor is it? *Journal of Applied Physiology* **103**, 1979–1985 (2007).

324. Moraska, A., Deak, T., Spencer, R. L., Roth, D. & Fleshner, M. Treadmill running produces both positive and negative physiological adaptations in Sprague-Dawley rats. *American Journal of Physiology-Regulatory, Integrative and Comparative Physiology* **279**, R1321–R1329 (2000).

325. Vantucci, C. E. *et al.* Systemic Immune Modulation Alters Local Bone Regeneration in a Delayed Treatment Composite Model of Non-Union Extremity Trauma. *Front. Surg.* **9**, (2022).

326. Estruel-Amades, S., Camps-Bossacoma, M., Massot-Cladera, M., Pérez-Cano, F. J. & Castell, M. Alterations in the innate immune system due to exhausting exercise in intensively trained rats. *Sci Rep* **10**, 967 (2020).

327. Gholamnezhad, Z., Boskabady, M. H., Hosseini, M., Sankian, M. & Khajavi Rad, A. Evaluation of immune response after moderate and overtraining exercise in wistar rat. *Iran J Basic Med Sci* **17**, 1–8 (2014).

328. Baker, C., Hunt, J., Piasecki, J. & Hough, J. Lymphocyte and dendritic cell response to a period of intensified training in young healthy humans and rodents: A systematic review and meta-analysis. *Front Physiol* **13**, 998925 (2022).

329. Jonsdottir, I. H. & Hoffmann, P. The significance of intensity and duration of exercise on natural immunity in rats. *Med Sci Sports Exerc* **32**, 1908–1912 (2000).

330. Navarro, F. *et al.* Moderate exercise increases the metabolism and immune function of lymphocytes in rats. *Eur J Appl Physiol* **113**, 1343–1352 (2013).

331. Lee, K.-B. *et al.* BMP induced inflammation: A comparison of rhBMP-7 and rhBMP-2. *Journal of Orthopaedic Research* **30**, 1985–1994 (2012).

332. Wei, F., Zhou, Y., Wang, J., Liu, C. & Xiao, Y. The Immunomodulatory Role of BMP-2 on Macrophages to Accelerate Osteogenesis. *Tissue Engineering Part A* **24**, 584–594 (2018).

333. Nguyen, V. *et al.* BMP-2-induced bone formation and neural inflammation. *Journal of Orthopaedics* **14**, 252–256 (2017).

334. Gleeson, M. *et al.* The anti-inflammatory effects of exercise: mechanisms and implications for the prevention and treatment of disease. *Nat Rev Immunol* **11**, 607–615 (2011).

335. Nelson, B. D., Karipott, S. S., Guldberg, R. E. & Ong, K. G. A piezoelectric bone fixation plate for in vivo application and monitoring of mechanical loading during fracture healing. *Meas. Sci. Technol.* **31**, 095703 (2020).

336. Biase, P. D. & Capanna, R. Clinical applications of BMPs. *Injury* **36**, S43–S46 (2005).

337. Zhou, L., Wang, J. & Mu, W. BMP-2 promotes fracture healing by facilitating osteoblast differentiation and bone defect osteogenesis. *Am J Transl Res* **15**, 6751–6759 (2023).

338. DeKeyser, G. J., Thorne, T., Martin, B. & Haller, J. Changing Epidemiology of Distal Femur Fractures: Increase in Geriatric Fractures and Rates of Distal Femur Replacement. *Journal of American Academy of Orthopaedic Surgeons*.

339. Court-Brown, C. M. & McQueen, M. M. Global Forum: Fractures in the Elderly. *JBJS* **98**, e36 (2016).

340. Brodke, D. J., Devana, S. K., Upfill-Brown, A. & Lee, C. Cost-effectiveness of fixation versus arthroplasty for geriatric distal femur fractures. *Injury* **53**, 661–668 (2022).

341. Elsoe, R., Ceccotti, A. A. & Larsen, P. Population-based epidemiology and incidence of distal femur fractures. *Int Orthop* **42**, 191–196 (2018).

342. Caines, A., Adamczyk, A., Mahaffey, R. & Pickell, M. Open Reduction Internal Fixation Versus Distal Femoral Replacement (DFR) for Treatment of OTA/AO 33C Fractures in the Elderly: A Review of Functional Outcomes and Cost Analysis. *J Orthop Trauma* **37**, 14–18 (2023).

343. Hake, M. E., Davis, M. E., Perdue, A. M. & Goulet, J. A. Modern Implant Options for the Treatment of Distal Femur Fractures. *JAAOS - Journal of the American Academy of Orthopaedic Surgeons* **27**, e867 (2019).

344. Ricci, W. M. *et al.* Risk Factors for Failure of Locked Plate Fixation of Distal Femur Fractures: An Analysis of 335 Cases. *Journal of Orthopaedic Trauma* **28**, 83 (2014).

345. Myers, P. *et al.* Patient Mortality in Geriatric Distal Femur Fractures. *Journal of Orthopaedic Trauma* **32**, 111 (2018).

346. Perren, S. M. Physical and Biological Aspects of Fracture Healing with Special Reference to Internal Fixation. *Clinical Orthopaedics and Related Research (1976-2007)* **138**, 175 (1979).

347. Saunders, M. M. & Lee, J. S. The Influence of Mechanical Environment on Bone Healing and Distraction Osteogenesis. *Atlas of the Oral and Maxillofacial Surgery Clinics of North America* **16**, 147–158 (2008).

348. Holmström, T., Paavolainen, P., Slätis, P. & Karaharju, E. Effect of compression on fracture healing: Plate fixation studied in rabbits. *Acta Orthopaedica Scandinavica* **57**, 368–372 (1986).

349. Banovetz, J. M., Sharp, R., Probe, R. A. & Anglen, J. O. Titanium plate fixation: a review of implant failures. *J Orthop Trauma* **10**, 389–394 (1996).

350. O'Neill, D. C. *et al.* Medial and lateral dual plating of native distal femur fractures: a systematic literature review. *OTA Int* **6**, e227 (2023).

351. Dekeyser, G. J. *et al.* Geriatric Distal Femur Fractures Treated With Distal Femoral Replacement Are Associated With Higher Rates of Readmissions and Complications. *Journal of Orthopaedic Trauma* **37**, 485 (2023).

352. Hustedt, J. W., Blizzard, D. J., Baumgaertner, M. R., Leslie, M. P. & Grauer, J. N. Is It Possible to Train Patients to Limit Weight Bearing on a Lower Extremity? *Orthopedics* **35**, e31–e37 (2012).

353. Warren, C. G. & Lehmann, J. F. Training procedures and biofeedback methods to achieve controlled partial weight bearing: an assessment. *Arch Phys Med Rehabil* **56**, 449–455 (1975).

354. Hurkmans, H. L., Bussmann, J. B., Benda, E., Verhaar, J. A. & Stam, H. J. Effectiveness of Audio Feedback for Partial Weight-Bearing in and Outside the Hospital: A Randomized Controlled Trial. *Archives of Physical Medicine and Rehabilitation* **93**, 565–570 (2012).

355. Winstein, C. J. *et al.* Learning a Partial-Weight-Bearing Skill: Effectiveness of Two Forms of Feedback. *Physical Therapy* **76**, 985–993 (1996).